Hydrochemistry, hydrogen and oxygen isotopes, and radon in waters of the greater Timbavati catchment, South Africa

UNIVERSITEIT VAN PRETORIA
UNIVERSITY OF PRETORIA
YUNIBESITHI YA PRETORIA
Denkleiers • Leading Minds • Dikgopolo tša Dihlalefi

Submitted in fulfilment of the requirements for the degree
MSc Hydrogeology

Submitted to:

Department of Geology
School of Physical Sciences
Faculty of Natural and Agricultural Sciences
University of Pretoria

Submitted by:

Kirsten Raible
16005466

Date of Final Version:
16 May 2024

ABSTRACT:
A baseline study was conducted to gain a better understanding of the relationship between groundwater, geology, and geography of the Greater Timbavati Area, to advance the knowledge of hydrostratigraphical settings affected by various socioeconomic and environmental factors. Samples were collected from both surface water and groundwater and were taken in both nature reserves and rural communities for comparison. An Aquaread AP-5000 probe was used to measure basic water chemistry parameters as well as nitrates, ammonium, and ammonia in the field. Samples were also taken and analysed for radon using a Durridge RAD7. Rainwater samples were also collected from two sites for hydrogen and oxygen isotope analysis using a Los Gatos Research (LGR) Liquid Water Isotope Analyzer. There are noticeable differences between the surface water and groundwater chemistry and isotopic signatures. Groundwater samples have a mean TDS of 1217 mg/l and pH of 7.5 while surface water samples have a mean TDS of 332 mg/l and pH of 8.3. A close correlation between land use and nitrate concentrations is observed with higher values being found in groundwater in the more developed areas, over 500 mg/l, suggesting human and agricultural contamination. Unfortunately, there also appears to be no relationship between radon concentration and the underlying geology with mean values in groundwater ranging from 188 Bq/m^3 to 51400 Bq/m^3.

KEYWORDS:
Nitrates; radon; environmental isotopes; hydrogeology; basement aquifers

DECLARATION:

I, the undersigned, declare that the thesis, which I hereby submit for the degree MSc at the University of Pretoria, is my own work and has not previously been submitted by me for a degree at this or any other tertiary institution. I, the undersigned, furthermore, declare that:

- I understand what plagiarism is and am aware of the University's policy in this regard.
- I declare that this assignment (e.g. essay, report, project, assignment, dissertation, thesis, etc.) is my own original work. Where other people's work has been used (either from a printed source, Internet, or any other source), this has been properly acknowledged and referenced in accordance with Departmental requirements.
- I have not used work previously produced by another student or any other person to hand in as my own.
- I have not allowed, and will not allow anyone, to copy my work with the intention of passing it off as his or her own work.
- I understand the Department of Geology's policy on plagiarism and the criteria set for using Turnitin by the Department.
- I acknowledge that I am allowed to use Turnitin to evaluate my own work prior to submission.

Full names:	Kirsten Raible
Student number:	16005466
Date submitted:	16 May 2024
Degree:	M.Sc. Hydrogeology
Topic of work:	Hydrochemistry, hydrogen and oxygen isotopes, and radon in waters of the greater Timbavati catchment, South Africa
Supervisor(s):	Prof Matthys Dippenaar, Department of Geology
Co-supervisor(s):	Dr Roger Diamond, BIOGRIP
Signature:	

ACKNOWLEDGEMENTS:

This endeavour would not have been possible without the financial support of the Water Research Commission and the National Nuclear Regulator.

I would like to express my deepest appreciation to my supervisors Dr Roger Diamond and Prof Matthys Dippenaar for all your support and guidance. I shall always treasure the memories of our adventures in the field. Also, a special thanks to Meyer de Kock and Dr Ilana van Wyk for your support and assistance with the fieldwork.

I would like to extend my sincere gratitude to Acorn to Oaks, Andover Nature Reserve, Baobab, Hans Hoheisen Wildlife Research Station, Hluvukani Animal Clinic, Honeyguide, Kruger to Canyons, Manyeleti Game Reserve, Mpumalanga Tourism and Parks Agency, Nourish Eco Village, Sandringham Private Nature Reserve, Sigagula Childrens Centre, South African Wildlife College, Thorneybush Private Game Reserve, Wits Rural Campus and the community leaders of Welverdiend for allowing me to sample on their land.

Lastly, I'd like to thank my family, especially my parents and Wayne, for putting up with me during all the emotional ups and downs. Thank you for your emotional support and encouragement, I could not have done it without you.

TABLE OF CONTENTS

LIST OF FIGURES

LIST OF TABLES

LIST OF ABBREVIATIONS

BMP - Beneficial Management Practices
DO - Dissolved Oxygen
DWAF - Department of Water Affairs and Forestry
EC - Electric Conductivity
EIL - Environmental Isotope Laboratory
EOCs - Emerging Organic Contaminants
GIS - Geographic Information System
GMWL - Global Meteoric Water Line
GNIP - Global Network of Isotopes in Precipitation
ICP - Inductively Coupled Plasma
LEL - Local Evaporation Line
LGR - Los Gatos Research
LMWL - Local Meteoric Water Line
ORO - Oxidation Reduction Potential
PET - Polyethylene Terephthalate
PVC - Polyvinyl Chloride
SABS - South African Bureau of Standards
SAL - Salinity
SMOW - Standard Mean Ocean Water
TDS - Total Dissolved Solids
USA – United States of America
USGS - United States Geological Survey
WHO - World Health Organisation

1 Introduction

1.1 Aim

The aim of the study is to assess hydrostratigraphic systems in a fairly undisturbed area underlain by intrusive igneous and metamorphic rocks where no such data has yet been recorded. Groundwater geochemistry will give an insight into the hydrogeological and hydrostratigraphic baseline conditions in the greater Timbavati area, providing a foundation, and highlighting areas of importance, for further hydrogeological investigations in the area.

1.2 Objectives

The objectives of the project were to:

- Conduct a baseline study of the hydrochemistry of the greater Timbavati area.
- Gain a better understanding of the relationship between the groundwater, surface water and local geology in the area.
- Investigate the impact of the surrounding geography on the water geochemistry and quality.

1.3 Rationale

The main source of water for human use in the greater Timbavati area is groundwater. Information about the quantity and quality of groundwater is needed for planning and management of the resource to ensure sustainable use (Baloyi and Diamond, 2019).

Oxygen and hydrogen isotopes in water can provide information about the transportation and interconnectivity of water resources and reserves, as water in specific environments can obtain isotopic signatures that can be traced back along flow paths (Abiye, et al., 2013). This is because the mass variations in isotopes result in them behaving differently under the same physical, chemical, and biological processes (Appelo & Postma, 2005). When water evaporates from a body of liquid water, the lighter isotopes e.g., $^{1}H_2{}^{16}O$ will evaporate first, resulting in water vapour that is isotopically lighter than the remaining liquid water (Diamond, 2022). On the other hand, when water vapour condenses the heavier molecules such as $^{2}H_2{}^{18}O$ will condense before the lighter molecules, resulting in liquid water that is isotopically heavier than the water vapour. Moving inland the isotopic composition of rainwater becomes lighter due to the continental effect and the progressively lower temperatures required for rainout as well as the kinetic processes that lighten the water vapour (Appelo & Postma, 2005).

Groundwater chemistry is used to interpret the hydrogeological conditions within an aquifer and can be used as a basis for characterising groundwater within hydrogeological units. As water is a polar solvent it can easily dissolve ionic crystalline solids into a solution of separately charged ions, therefore, as water interacts with the geology of an area it acquires a distinct chemical composition (Hiscock & Bense, 2014; Sen, 2015). Stiff Plots show the ionic composition of the water samples, with the left-hand side of the diagram representing the cation concentrations and the right-hand side of the diagram showing the anion concentrations. The top axis has, Na^+ and Cl^- and reflects any possible marine influences, as the dominant salt in seawater is NaCl. The Ca^{2+} and HCO_3^- axis is meant to reflect the dissolution of $CaCO_3$ and rocks in general. Mg^{2+} and SO_4^+ are the remaining two major groundwater ion components (Appelo and Postma, 2005).

When detrital silicates such as amphiboles, biotite and clay minerals undergo chemical weathering, they can release trace metals into the environment (Edmunds et al., 1992). Atmospheric input is another possible source of trace metals in the water cycle (Appelo & Postma, 2005).

The main source of nitrate pollution in southern Africa is from on-site sanitation (Tredoux et al., 2009). The source of the pollution needs to be understood in order to put regulations and policies in place to reduce the amount of nitrate contamination. Pollution sources can be classified as either point-source or nonpoint source. Redox reactions occur when an electron is transferred from one atom to another. Redox processes in groundwater occur when an oxidant such as O_2 or NO_3^- is added to an aquifer that contains a reductant, or with the addition of a reductant such as dissolved organic matter to an aquifer that contains an oxidant. These processes are an important control of the concentrations of O_2, Fe, SO_4, H_2S, CH_4 etc in groundwater and determine the fate of pollutants like nitrate that have leached into the groundwater (Appelo and Postma, 2005).

The mineralogy and structure of rock units influence the amount of radon found in groundwater (Litt, et al., 1992). Radon enters the groundwater via emanation and diffusion from radium-bearing minerals (Hoehn and Von Gunten, 1989). Therefore, radon can be used as an indicator or tracer of groundwater discharge into surface waters (Vital, et al., 2022).

2 Literature Study

2.1 Hard Rock Aquifers

Aquifers developed within the fractured bedrock and weathered overburden of crystalline rocks are commonly referred to as basement-, hard rock-, bedrock- or weathered-fractured rock aquifers (Holland, 2011).

Large parts of Africa, South America, Asia, and Australia are reliant on groundwater from hard rock aquifers, especially in areas where surface water resources are seasonal and limited (Lachassagne et al., 2021). The groundwater quality from hard rock aquifers is also usually better than the surface water. However, the groundwater resources in hard rock aquifers are small in terms of sustainable discharge, with productive boreholes producing between 0.1 m^3/h to a few tens of m^3/h when compared to porous and karstic aquifers and are therefore classified as low-yielding (Lachassagne et al., 2021; Wright, 1992).

The hydraulic conductivity of hard rock aquifers relies on secondary fracture permeability due to weathering processes. Hard rock aquifers are composite aquifers comprised of two layers. The transmissive layer, which is a stratiform fractured or fissured layer forms the main part of the aquifer. This is overlain by the unconsolidated superficial zone. The unconsolidated layer is not pervious enough to deliver a significant discharge to most boreholes but has significant enough porosity to enable leakage towards the underlying fractured layer (Lachassagne et al., 2021). A conceptual model can be seen in Figure 1 below.

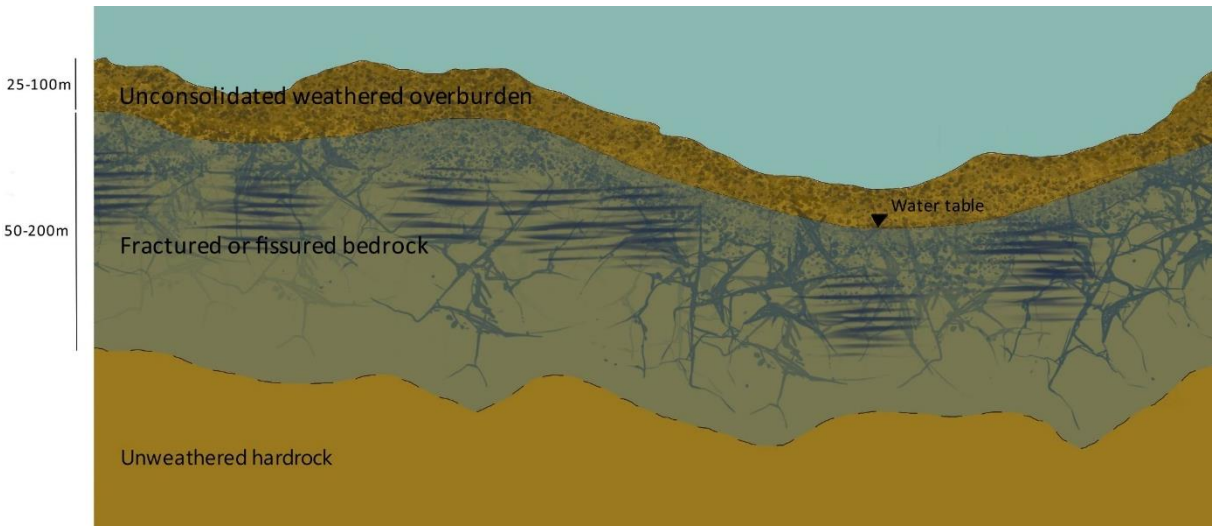

FIGURE 1: CONCEPTUAL MODEL OF HARD ROCK AQUIFER MODIFIED FROM LACHASSAGNE ET AL. (2021).

Rainfall is the dominant control to recharge and while they are directly related, they do not have a linear relationship (Holland, 2011; Wright, 1992). According to Harde & Winter (1996), the other main factors influencing recharge are relief, hydraulic conductivity, local topographic features, and stratigraphy.

While hard rock aquifers are essentially phreatic in character they may respond to localised abstraction in a semi-confined manner if the rest water level occurs in a low permeability horizon. They also respond to abstraction in a discontinuous fashion, despite being regional in occurrence, because of discontinuities or barrier boundaries within the fracture system and the low permeability of the regolith (Wright, 1992). Unweathered and unfractured hard crystalline rocks have low primary

porosity and low hydraulic conductivity, below 10^{-8} m/s (Lachassagne et al., 2021). The aquifer's hydraulic parameters are controlled by a fractured-weathered layer that has a fracture density which decreases with depth (Muchingami et al., 2019).

There are a few issues associated with hard rock aquifers. They are susceptible to surface pollution due to their shallow occurrence and recharge is sensitive to land use changes. Boreholes drilled into hard rock aquifers often have a high failure rate, in the range of 10 to 40%, with higher rates occurring in drier regions and regions with thin weathered overburdens. Storativity is low and aquifers can therefore be significantly depleted during sustained periods of drought (Wright, 1992).

2.1.1 Formation of Hard Rock Aquifers

Hard rock aquifers develop within the weathered overburden and fractured bedrock of crystalline rocks of igneous or metamorphic origin, generally of Precambrian age. The occurrence and characteristics of hard rock aquifers are largely due to the interaction of weathering processes related to recharge and groundwater throughflow (Wright, 1992) and the flow of groundwater in these aquifers is governed by the hydraulic gradient and hydraulic conductivity in the regolith and the underlying fractured bedrock (Muchingami et al., 2019).

Reviews and research by Dewandel et al. (2006), Lachassagne et al. (2011, 2014) and Worthington et al. (2016) showed that weathering is the main process that drives the development of significant groundwater resources in hard rock formations. The fracture layer is believed to be the result of the stress induced by chemical weathering and the swelling of minerals such as biotite, olivine, and pyroxene, resulting in volume changes increasing the stress in the rock and the eventual fracturing of the rock. The fractures then locally increase the transport and exportation of water through the rock, accelerating the weathering process. Other genetic hypotheses such as tectonics, unloading processes and the emplacement and cooling of plutonic rocks have also been formulated to explain the development of the fracture layer, however, Lachassagne et al. (2011, 2014 and 2021) demonstrated that this hypothesis is not relevant to explain the development of hard rock aquifers as there are no scientific demonstrations of their validity.

2.1.2 The Weathering Profile

The weathering profile above crystalline basement rocks has been divided into several zones' groupings based on physical, chemical, or mineralogical features. The schematic weathered profile above crystalline basement rocks can be seen in Figure 2 and is described below (Wright, 1992):

1. The collapsed zone may show marked lateral variation but is generally sandy on watershed areas with illuviated clay near the base and sometimes a 'stone line', on valley slopes where colluvial material accumulates and in valley bottoms, secondary clay minerals predominate. Slope bottom laterites may also occur which can result in perched water tables. Permeabilities vary in accordance with lithology although on watersheds the collapsed zone normally occurs above the water table.
2. Saprolite is derived by in situ weathering from the bedrock but is disaggregated. Permeability commonly increases at lower levels due to a lesser development of secondary clay minerals".
3. Saprock is weathered bedrock with fracture permeability generally increased as a result of weathering (as compared with fresh bedrock) unless infilled by illuviated clay minerals.
4. Bedrock – includes variably fractured fresh or weathered bedrock.

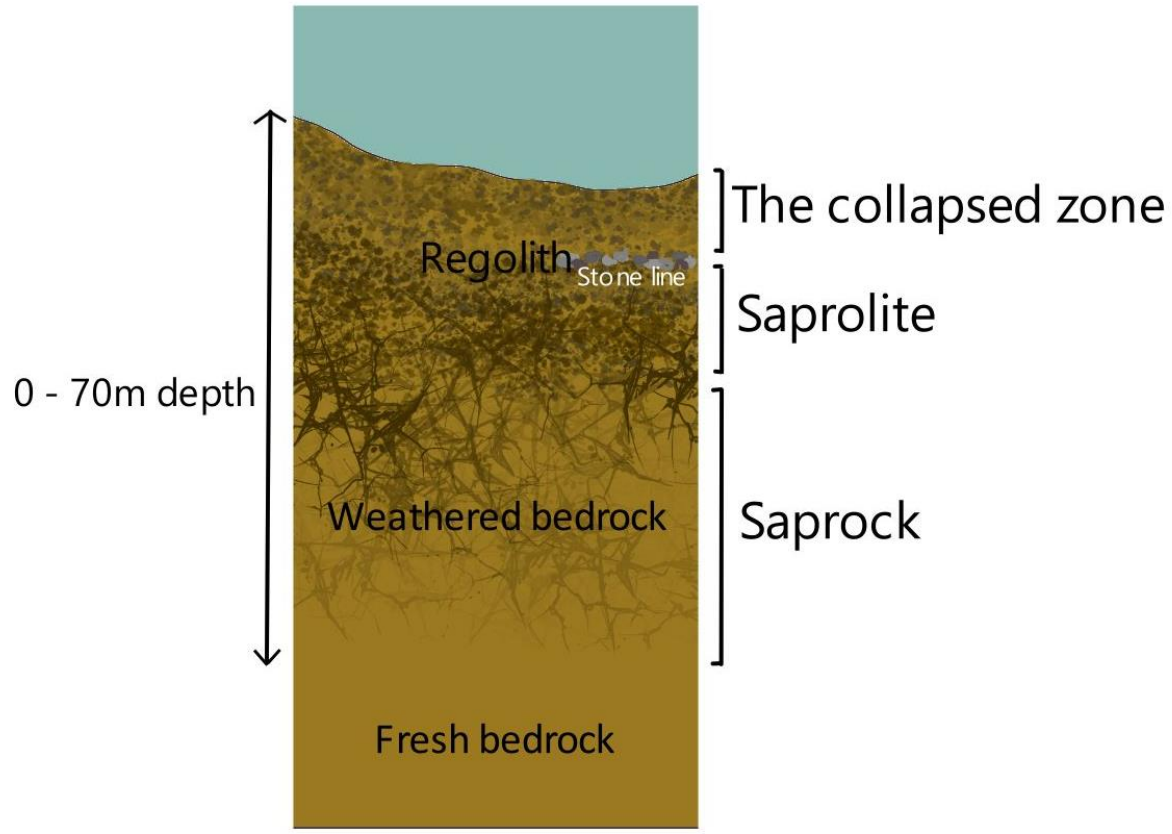

FIGURE 2: SCHEMATIC WEATHERED PROFILE ABOVE CRYSTALLINE BASEMENT ROCKS MODIFIED FROM WRIGHT (1992).

2.2 Environmental Isotopes

Hydrogen and oxygen both have three naturally occurring isotopes. Hydrogen occurs as a mixture of ^{1}H, ^{2}H (deuterium) and ^{3}H (tritium) and oxygen occurs as a mixture of ^{16}O, ^{17}O and ^{18}O. ^{1}H, ^{2}H, ^{16}O, ^{17}O and ^{18}O are stable isotopes and do not undergo nuclear transformation. Tritium (^{3}H) is not a stable isotope and has a half-life of 12.3 years; it can therefore be used for dating (Appelo and Postma, 2005).

The isotopic compositions of groundwater systems can give us information about the transportation and interconnectivity of water resources and reservoirs as well as the climate conditions at the point of infiltration (Yeh and Lee, 2018). Different isotopes of the same element behave differently under the same physical, chemical, and biological processes because of differences in their masses, and this results in fractionation. Due to isotope fractionation, meteoric water in different regions has different compositions of stable hydrogen and oxygen isotopes. When meteoric water seeps into the groundwater, its isotopic label is recorded in the groundwater and can be traced along flow paths and used as a basis for detecting groundwater sources (Ding et al., 2013; Liu and Yamanaka, 2012; Peng et al., 2016; Yeh et al., 2011).

2.2.1 Isotopic ratios and δ notation

Stable isotope concentrations are normally given as the ratio of the least abundant isotope over the most abundant isotope and expressed relative to a standard. This is because stable isotope ratio variations in nature are very small. The ratio of $^{18}O/^{16}O$ is represented by $\delta^{18}O$ and $^{2}H/^{1}H$ by $\delta^{2}H$ or more commonly δD. This is known as δ notation and expresses the deviation of the isotopic ratio (R) with respect to the ratio of the standards as seen in Equation 1.

$$\delta_{sample} = \frac{R_{sample} - R_{standard}}{R_{standard}} \cdot 1000$$

EQUATION 1

$$\text{Where } R = \frac{^{18}O}{^{16}O} \; or \; \frac{^{2}H}{^{1}H}$$

The internationally agreed standard for water is the "Vienna Standard Mean Ocean Water" or VSMOW, with the isotopes present in the ratios $^{18}O/^{16}O = 2.005x10^{-3}$ and $^{2}H/^{1}H = 1.56x10^{-4}$ (Appelo and Postma, 2005).

2.2.2 Meteoric Water Lines

The Global Meteoric Water Line (GMWL) represents the average global relationship between $\delta^{18}O$ and δD in precipitation (Putman et al., 2019). Craig (1961) first proposed a specific relationship between hydrogen and oxygen isotope distribution in atmospheric precipitation due to continuous fractionation caused by evaporation and precipitation, as seen in Figure 3 bellow. Craig (1961) analysed the $\delta^{18}O$ and δD isotope compositions of rain, snow, and river water samples from around the world and used linear regression to obtain the GMWL, with an equation of $\delta D = 8\delta^{18}O + 10‰$ (Yeh and Lee, 2018).

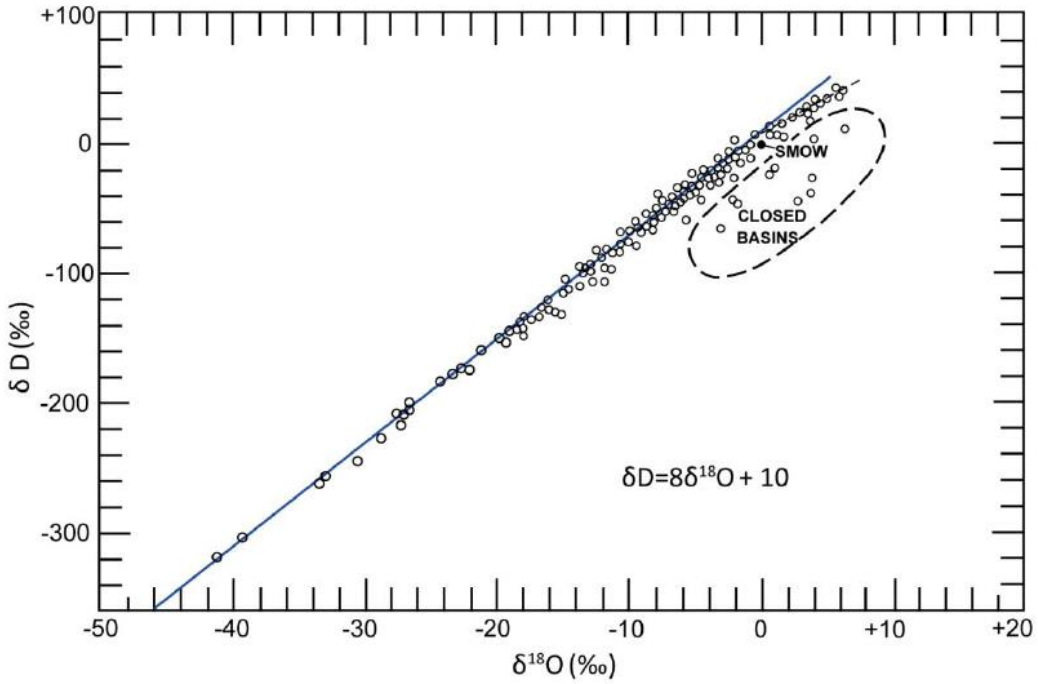

FIGURE 3: THE GLOBAL METEORIC WATER LINE, TAKEN FROM CRAIG (1961)

Rozanski et al. (1993) looked at the variability of Local Meteoric Water Lines (LMWL) by comparing the relationship between $\delta^{18}O$ and δD of monthly precipitation samples at selected Global Network of Isotopes in Precipitation (GNIP) sites. LMWLs are simplified representations of average $\delta^{18}O$ and δD relationships at a site and are often evaluated based on their deviation from the GMWL, they can be used to provide a reference framework for interpreting isotope ratios measured in terrestrial waters (Putman et al., 2019).

2.2.3 Deuterium excess

Deuterium excess is calculated as d (‰) = $\delta^2H - 8\delta^{18}O$ and correlates with the physical conditions such as humidity, air temperature and sea surface temperature of the oceanic source area of the precipitation (Froehlich et al., 2002; Merlivat and Jouzel, 1979). This is because the rate of ^2H depletion and ^{18}O depletion changes with the degree of saturation or relative humidity. ^2H is not affected by evaporation as much as ^{18}O at lower humidities and a sample will therefore plot further from the GMWL. As the humidity increases, the closer the system will come to equilibrium fractionation (Clark, 1997; Diamond, 2022).

2.2.4 Hydrogen and Oxygen Isotopes in Groundwater

Many hydrogeological studies (e.g. West et al. 2014; Peng et al. 2016; Yeh and Lee 2018; Hao et al. 2019; Zhu et al. 2019) use stable hydrogen and oxygen isotopes as natural tracers for identifying groundwater sources, unlike artificial tracers they are naturally occurring in the groundwater and do not need to be added.

Zhu et al. (2019) used the hydrochemical and isotopic characteristics to identify the recharge sources and water pathways for the Ebinur Lake Watershed as well as identify mechanisms of water pollution transfer.

Peng et al. (2016) used stable hydrogen and oxygen isotopes to identify the groundwater sources of the Taipei Basin by comparing precipitation, catchment surface water, reservoir water and Taipei Basin groundwater samples. According to Peng, et al. (2016), some of the advantages of using natural isotope tracers are "(1) Their ability to better reflect natural water behaviour, as most artificial tracers are solutes dissolved in water (Clark, 1997; Criss, 1999), (2) the conservation of hydrogen and oxygen isotopes as water's δ values are not greatly affected by water-rock reactions in normal low-temperature, low-circulation systems (McCarthy et al., 1992) and (3) the uniqueness of δ values to the origin of waters originating from different environments due to isotopic fractionation effects (Criss, 1999; Dansgaard, 1964; Yurtsever and Gat, 1981)."

Abiye et al. (2021) conducted an overview of aquifer physiognomies and the distribution of stable isotopes of hydrogen and oxygen in South African groundwaters and found distinct spatial variations due to recharge and mixing with existing groundwater. Mixing trends were confirmed by the observed alignment of the isotopic data along the GMWL, with closely clustered data suggesting the possibility of similar sources and the uniform mixing of water. The impact of moisture, with depleted isotopic signatures, from the southern polar region on the isotopic composition in various parts of the country is shown in the data. In the interior areas and western arid zones, the isotopic compositions of recharging waters mostly showed depletion, which was attributed to the depleted isotopic composition of the moisture source.

Harkness et al. (2018) used stable water isotopes to look at groundwater geochemistry in the Karoo Basin. They found that shallow groundwater was controlled by evaporation in arid conditions, while the saline waters were diluted by apparently fossil meteoric water that originated under wetter climatic conditions.

Diamond and Harris (2019) looked at stable isotope constraints on the hydrostratigraphy and aquifer connectivity in the Table Mountain group. They found that the isotopic compositions of groundwater at several locations had compositions like that of rainfall at higher altitudes in adjacent mountains rather than that of the ambient rainfall. The more negative delta values of the groundwater when compared to the weighted means for precipitation in likely recharge areas indicate that recharge takes place during heavy rainfall events or seasons with very negative delta values.

Petersen et al. (2023) used stable isotopes to investigate the surface and groundwater interactions in the Kruger National Park and found that the rainfall in the area is evaporatively enriched and the LMWL plots below the GMWL. They found that the groundwater across the entire area exhibited similar values and that the similarity between the perennial rivers and groundwater indicated a high interchange of water between the systems.

Mirzavand et al. (2020) showed that stable isotopes could be used in determining the source of groundwater salinization by comparing TDS with $\delta^{18}O$. Salem et al. (2022) was able to determine that the origin of salinity in the shallow groundwater of the Central Nile Delta Quaternary aquifer was due to evaporation, while the salinity of the deeper groundwater was from seawater intrusion.

2.3 Radon

Radon is a noble gas with atomic number 86. It has 3 naturally occurring isotopes known as actinon (^{219}Rn), thoron (^{220}Rn) and radon (^{222}Rn). Therefore, the term radon can refer either to the element with atomic number 86 or its isotope with an atomic mass of 222. The half-lives of the isotopes are 3.825 days for ^{222}Rn, 55.6 s for ^{220}Rn and 3.96 s for ^{219}Rn. As radon is a noble gas it is colourless, odourless, and mostly chemically inert. It is the most soluble noble gas and is also the heaviest and has the highest melting and boiling points as well as critical temperature and pressure. During the decay of radium, a radon atom and its alpha particle sibling recoil from one another when brought into existence; this is a violent process that propels them in opposite directions and can result in them being set free from a solid (Baskaran, 2016), as seen in Figure 4 bellow.

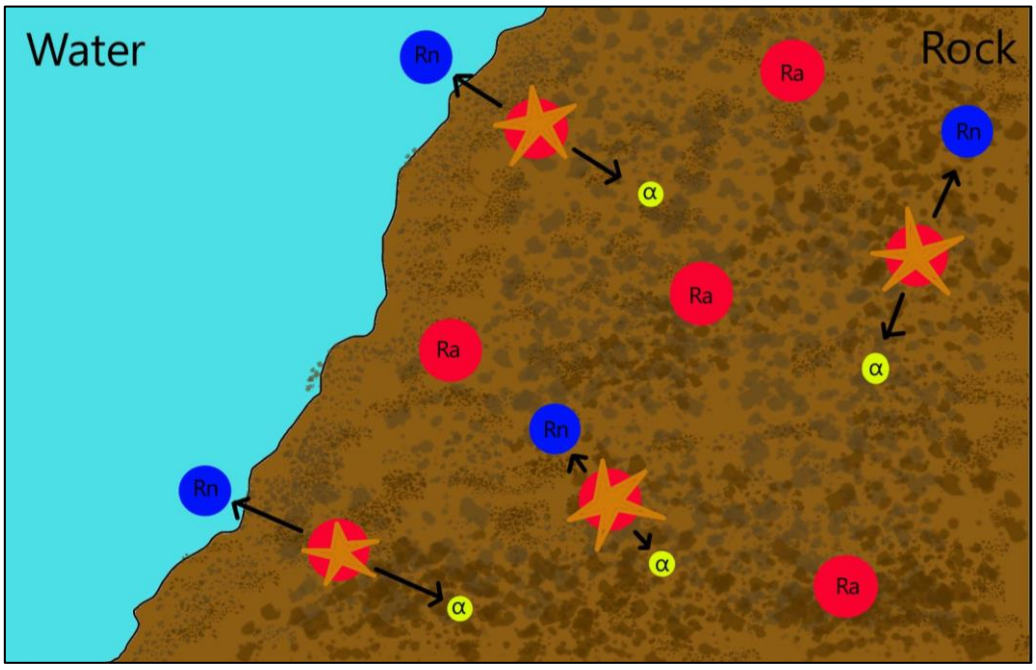

FIGURE 4: RADON ATOMS AND ALPHA PARTICLES RECOIL IN OPPOSITE DIRECTIONS AS A RESULT OF THE RADIUM DECAY PROCESS.

Radon is most soluble in organic liquids and moderately soluble in water. It can therefore dissolve into water flowing through rocks and oil containing radon. In a multiphase system at around 20 – 22 °C radon will concentrate the most in the organic liquid, then the gas phase and then the water. The colder the temperature the more soluble the radon, so as the temperature increases the concentration of radon in the gas phase increases at the expense of the liquid phase. Therefore, for

measuring purposes, radon in water can easily be extracted by bubbling air through the water or by extraction with an organic liquid scintillator (Tommasino, 2005).

2.3.1 Health Effects of Radon

The decay products of radon typically have short half-lives and when they decay, they emit highly energetic alpha particles. These alpha particles have the potential to initiate carcinogenesis (Esan et al., 2020). According to the United States Environmental Protection Agency (2014), the two main sources of radon exposure are radon in the air of your home and drinking water. Radon gas can seep from the soil into any type of building and build up to high levels in the air inside that building, or the radon gas can dissolve and accumulate in the groundwater. When this water is used within a building, the gas escapes from the water and goes into the air. Some radon does however remain in the water. Though most radon gas is exhaled again when breathing, some of the radon atoms decay along the respiratory tract. The decayed product then gets attached to the respiratory tract and can cause carcinogenesis. Radon in drinking water presents a risk for the development of internal organ cancer. This risk is however lower than that of developing lung cancer from breathing in radon gas (Esan et al., 2020).

2.3.2 Geology of Radon

Uranium and radium are the precursors to radon and are present in virtually all types of rocks and soil, with amounts varying from site to site and different geological materials. Soil uranium concentrations are affected by factors such as the source rock, porosity, precipitation, leaching etc. and therefore differ from uranium concentrations in the earth's crust. Uranium has a chemical affinity for phosphates. Phosphatic rocks therefore often contain elevated levels of uranium (Tommasino, 2005). According to Tommasino (2005), uranium tends to concentrate in magmas that form granites, and in shales that formed from marine mud high in organic matter. Fracturing and faulting can be sites for the deposition of uranium by uranium-bearing fluids. When a rock containing uranium is heated in the presence of a fluid, the uranium tends to move with the fluid until conditions change and the uranium then becomes concentrated. Therefore, even within the same rock formation/rock type, there can be a wide variety of uranium concentrations.

Adepelumi, et al. (2005) investigated the use of radon as a geological mapping tool in Ile-Ife, Nigeria. They found that the soil-gas radon concentrations found in the residual regolith soils reflected the geochemistry of the underlying crystalline bedrock. The radon concentrations in the soil overlying three rock types varied from 1100 Bq/m^3 to 79200 Bq/m^3 for granite gneiss, 1100 Bq/m^3 to 64900 Bq/m^3 for the grey gneiss, and from 1100 Bq/m^3 to 33000 Bq/m^3 for mica schist. The radon maps overlain with the geological map showed a good correlation, as the soils are the weathered products of the bedrock. It was therefore concluded that "the information obtained from radon studies can be used to supplement other geophysical methods for both local and regional geologic mapping" (Adepelumi et al., 2005).

2.3.3 Radon in Groundwater

As radon is a daughter product of radium and uranium, it is logical that radon will be found in aquifers within formations containing uranium-bearing minerals. Water penetrates voids in uranium-rich rocks and dissolves the uranium and radon that is present (Tommasino, 2005). However, uranium and radium are solutes, while radon is a gas, and they therefore are transported by different mechanisms within the groundwater (Skeppström and Olofsson, 2007). When radon is in contact with water it forms a clathrate-hydrate, $Rn.6H_2O$, and is trapped inside a lattice of water molecules (Grolander, 2009). Statistical analysis conducted by Cho & Choo (2019) on the geochemical behaviour of uranium and radon in groundwater revealed no close correlations between uranium and radon, they appeared to behave independently. Radon, unlike uranium, appeared to migrate independently with respect to most geochemical parameters. Radon can be transported substantial distances by carrier gases and

liquids such as CO_2 and H_2O (Tommasino, 2005) and according to Le Druillennec et al. (2010) in aquifers where the flow rate of groundwater is fast or variable, such as in fractured aquifers, it is unlikely that radon levels remain constant (Cho et al., 2015). These factors can even lead to high radon and uranium concentrations in bedrock with a low uranium content (Skeppström and Olofsson, 2007). Choubey and Ramola (1997) suggested that radon concentrations therefore primarily depend on the lithology, structural attributes, and presence of uranium-bearing minerals in rocks. Cho et al. (2015) also noted that radon concentrations did however correlate with hydrogeological components such as Eh, EC and depth. These components were consistent with the interaction of groundwater and granitic rocks. This is consistent with other sources, such as Knutsson & Olofsson (2002), Tommasino (2005), Cho et al. (2007), Prat et al. (2009), Yun et al (2017), Cho et al. (2019), Cho & Choo (2019) and Esan, et al. (2020), that have reported high uranium and radon concentrations in granitic areas.

Litt et al. (1992) looked at the influence of geology on radon in groundwater supplies of the New Jersey Highlands and found that both the mineralogy of the rock unit as well as the geological structure were important factors in controlling the groundwater radon concentrations. Groundwater radon concentrations ranged from 1332 Bq/m^3 to 888000 Bq/m^3 with a mean of 59200 Bq/m^3 in the region sampled. While different rock units had significantly different groundwater radon distributions, all units had some overlapping levels. Units that were previously identified as being uraniferous by Volkert (1989) yielded the highest radon concentrations while units that were non-uraniferous had low mean groundwater radon concentrations. High radon concentrations in a quartz-oligoclase gneiss unit were revealed to be due to thin localised veins and seams of microperthite alaskite intrusions. This shows that migmatites, alaskites and pegmatites that do not necessarily appear on geological maps can affect radioactivity on a local scale. Cho et al. (2015) analysed the relationships between radon in groundwater and related topographical, geological, and geochemical factors using probabilistic methods in a geographical information system to predict radon levels where radon is not yet surveyed or measured. Alabdula'aly (2014) collected water samples from 1025 wells supplying drinking water to the 13 regions of Saudi Arabia and analysed them for radon. The minimum value was 60 Bq/m^3 with a max value of 67400 Bq/m^3 and a median of 4620 Bq/m^3. Wells drilled into aquifers comprising predominantly sandstone with significant shale layers showed median values of 10500 Bq/m^3 compared to wells drilled into an aquifer comprising predominantly limestone and sandstone rocks which had a median value of 2360 Bq/m^3. A study in Sweden conducted by Knutsson and Olofsson (2002) noted a positive correlation between high radon concentrations in drilled wells and granites, pegmatites, felsic volcanics and some felsic gneisses.

The concentration of radon and uranium in groundwater is likely affected by several factors such as rock material properties, faulting, fracture systems, emanation, leaching, precipitation, redox conditions, and transport mechanisms (Skeppström and Olofsson, 2007; Tommasino, 2005). Another big influence on radon concentrations is how long it has been since the radon was dissolved into the groundwater, due to the short half-life of radon. It is also difficult to know how much radon released from radiogenic source material dissolved into the groundwater and how much of it degassed into the air. Radon levels can decrease due to diffusion towards the surface as well as due to the mixing of waters that have little to no radon (Kronfeld et al., 2004). Alabdula'aly (2014) and Cho et al. (2015) found that the radon levels in shallow aquifers were generally higher than those in deep aquifers, as dissolved radon tends to move upwards along fractures with the decrease in hydrostatic pressure. On the other hand, Cho et al. (2019) found that the average radon concentration was higher when sampling deeper wells in South Korea when compared to earlier studies, such as Cho et al. (2007). Cho et al. (2019) believed that this was due to radon in the shallow wells being able to escape more easily than the radon in the deep wells.

Hoehn et al. (1992) conducted a laboratory study to determine residence times and velocities of water flowing through an open-topped sandbox using naturally occurring ^{222}Rn. Radon was three times in

the interstitial water of the sandbox at seven outlets under steady-flow conditions. Results showed "that the ingrowth of radon in a flowing water system can be adequately described and that the radon method might be applied to field studies in sandy aquifers with groundwaters of a relatively slow flow velocity i.e., ≥ 0.2 m/day." The pore velocities obtained in the experiment were compared to and agreed with those from NaCl tracer tests.

Radon concentrations in groundwater are generally higher than that in surface water because surface water is not in contact with as much solid material and the input of radon is therefore lower. The radon found in surface water is mostly from the inflow of radon-rich groundwater, but it is quickly lost into the atmosphere via outgassing. Measuring radon concentrations in surface water and groundwater at different sites along a stream can be used to detect and quantify groundwater inflow. Radon can also be used to locate hydraulically active fractures in boreholes (Grolander, 2009).

According to Baskaran (2016), the major sources of radon in groundwater include:

i) Production from dissolved ^{226}Ra.
ii) Input from weathering resulting in congruent dissolution of U-bearing host rocks (leaching and incongruent breakdown of host rocks also could contribute ^{222}Rn to the surrounding waters).
iii) Input by recoil.
iv) Input from the production of sorbed ^{226}Ra when ^{230}Th in host rock undergoes alpha decay.

The major sinks of radon in groundwater are:

v) Radioactive decay.

The mass balance of radon in groundwater can be summarized as follows:
Rate of change of molar concentration of ^{222}Rn in a groundwater system = advection input + weathering input + recoil input + production from ^{226}Ra - radioactive decay.

2.4 Nitrates

2.4.1 Nitrogen Cycle

A visual representation of the nitrogen cycle can be seen in Figure 5. Nitrogen is a key component in plant nucleic or amino acids and chlorophyll. Plants are the base source of dietary N or protein for animals (McNeill and Unkovich, 2007). Plants acquire nitrogen from the soil, however, for plants to be able to use the nitrogen, it needs to be available in an inorganic form such as NH_3 (ammonia), NH_4^+ (ammonium), NO_2^- (nitrite) or NO_3^{2-} (nitrate). Microbes break down organic matter into these forms to produce much of the available nitrogen in soils. As cultivated crops have a higher nutrient uptake than natural plant growth, chemical fertilizers and manures are required to supply additional nitrogen to the soil as the mineralization capabilities of the soils are generally insufficient (Widdlson and Burt, 2008).

Approximately 78% of the Earth's atmosphere is comprised of N_2 (dinitrogen) gas. This makes up around 90% of the global nitrogen reservoir with the remaining 10% found in the earth's crustal reservoir. These reservoirs of nitrogen are relatively inactive while a small amount of biologically active nitrogen is found in the biomass and soils of the terrestrial nitrogen cycle (McNeill and Unkovich, 2007; Widdlson and Burt, 2008). The movement of nitrogen through the terrestrial cycle is dominated by soil nitrogen cycling. Surface applications, such as fertilizers and manure, provide most of the nitrogen inputs. When nitrogen is in inorganic form, mineralization, immobilization, nitrification, nitrate leaching, denitrification and plant uptake can take place. The movement of

nitrogen through the soil can occur upwards by crop uptake or gaseous loss, downwards via leaching into the groundwater or laterally via surface and subsurface into surface waters. Nitrate is vulnerable to being leached out of the soil by percolating rainfall and irrigation water as it is completely soluble in water. Anthropogenic activities such as intensive agriculture, over-fertilization, deforestation, biomass burning, combustion of fossil fuels, industrial activities and energy production have altered the natural biogeochemical cycling of nitrogen and increased the movement from one store to another (Widdlson and Burt, 2008). Denitrification is a naturally occurring microbial process that removes nitrates from soil and groundwater through the reduction of NO_3^- to N_2 (Appelo and Postma, 2005; McGill and Villholth, 2019). Organic carbon and pyrite (FeS_2), to a lesser extent, are the primary source of electrons for the reduction process in aquifers. However, reduced groundwater components, such as Fe^{2+}, H_2S and CH_4, also act as electron donors as they are thermodynamically favoured (Appelo and Postma, 2005). Denitrification can be used to combat groundwater pollution from nitrates (McGill and Villholth, 2019). NO_2^- and N_2O are intermediates of the denitrification process; when found in trace levels they can be evidence of ongoing denitrification (Appelo and Postma, 2005).

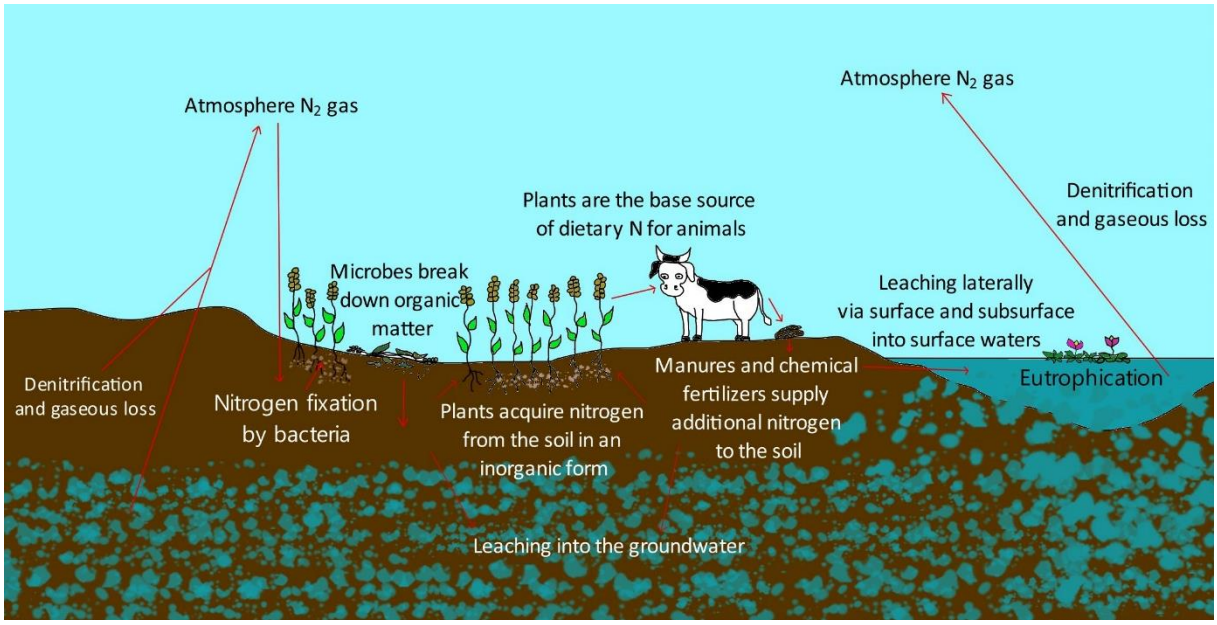

FIGURE 5: VISUAL REPRESENTATION OF THE NITROGEN CYCLE.

2.4.2 Types of nitrate pollution

Nitrate pollution sources can be grouped as either nonpoint/diffuse or point-source pollution. The contamination from nonpoint sources extends over a wide area, for example, the long-term and widespread overuse of manure or chemical fertilizers. When more fertilizer is applied than the crops need, the excess nitrate accumulates in the soil and the potential for it to leach into groundwater and surface water increases (Viers et al., 2012; Zhou et al., 2015). Point sources, on the other hand, have a single identifiable source of contamination affecting mainly a localized area, for example, a leaking septic tank or sewer system (Haller et al., 2013; Zhou et al., 2015).

2.4.3 Nitrate sources

High nitrate concentrations can occur naturally in groundwater under specific climate and topographical conditions. In developed areas such as Europe and the USA, the main source of nitrate pollution in groundwater is from agriculture, whereas in Southern Africa the main source is from on-site sanitation (Tredoux et al., 2009). Graham and Polizzotto (2013) stated that studies of pit latrines and their impacts on groundwater found that nitrate is the most detected pollutant (McGill et al.,

2019). Unlined pit latrines result in the leaching of nitrates and pathogens into the groundwater (Graham and Polizzotto, 2013; McGill et al., 2019).

Dube et al. (2020) modelled groundwater quality across land use and land cover gradient in the Limpopo Province. Ground-based key physicochemical parameters of water quality from different boreholes and remotely sensed Landsat 8-OLI satellite data in different quarters of the year were used to achieve this. Higher concentrations of nitrates were shown during quarter two and quarter four of the year. They also found that the nitrate concentrations were highest in the areas of subsistence farming and lowest in the built-up areas. Phungela et al. (2022) looked at the impact of wastewater treatment effluent on the water quality of the Crocodile River. They noted that effluent from the wastewater treatment plant had a significant impact on ammonium and nitrate concentrations in the Crocodile River. The nitrate in the effluent came from a variety of sources such as home and agricultural waste and N-containing fertilisers. Baloyi & Diamond (2019) looked at the variable water quality of domestic wells in Stinkwater, Hammanskraal, as well as the need for groundwater quality monitoring and protection. Information about the quantity and quality of groundwater is needed for planning and management of the resource to ensure sustainable use. Masindi & Foteinis (2021) Investigated groundwater contamination in sub-Saharan Africa and the implications for groundwater protection in developing countries. Of the 42 samples collected 22 had nitrate levels above the prescribed limit. The lack of other sources of nitrate and the high concentrations of faecal indicator bacteria suggest the contamination is from onsite sanitation systems. NO_3^- concentrations ranged from 0.16 to 104 mg/l.

It can be difficult to distinguish between human and livestock contaminant sources as they have similar nitrate stable isotope signatures and faecal indicator bacteria (Ashbolt, 2001; Fenech et al., 2012; McGill et al., 2019). EOCs (emerging organic contaminants) such as pharmaceuticals and caffeine can be used as tracers for human contamination (Fenech et al., 2012; Lapworth et al., 2012; McGill et al., 2019).

2.4.4 The negative impacts of nitrogen in ground and surface water

In aquatic systems excessive nitrogen results in eutrophication. Eutrophication is the enrichment of surface water with plant nutrients, and while it does sometimes occur naturally, it is normally brought on by anthropogenic activities. Eutrophication boosts the growth of alga and aquatic plants and can result in unwanted consequences such as algae blooms, water column anoxia and increased fish mortality. Alga blooms decrease the penetration of light into the water, decreasing the productivity of plants living in deeper waters. The water also becomes depleted in oxygen, due to the lack of production in the deeper darkened waters and the high oxygen consumption of the algae-decomposing organisms (Wetzel, 2001; Wilson and Carpenter, 1999; Zhou et al., 2015).

2.4.5 Methods to reduce the risk of nitrogen contamination.

Environmental protection policies and regulations can be put into place to limit the nitrogen contamination of ground and surface water as well as to reduce atmospheric pollution. Beneficial Management Practices (BMP) in agriculture are designed to reduce the risk of nitrate pollution by enabling crops to use nitrogen fertilizer efficiently and minimize leaching from the soil (Bundy et al., 1994; Zhou et al., 2015). One of the easiest ways to reduce the amount of nitrogen leaching is to reduce the amount of nitrogen applied to the soil. Applying lower rates more often or by using slow-release nitrogen sources, plants will be able to utilize it and there will be less excess nitrogen available for leaching (Hallberg and Keeney, 1993; Zhou et al., 2015). In many farming areas manure lagoons are a source of contamination. Prevention techniques such as building a concrete manure storage pit or slurry store can be implemented, as they store without leaking. Sewerage networks are designed to transport wastewater to treatment plants. In these plants, organic matter, nutrients, and harmful

substances are removed from the sewage before the effluent is discharged back into the environment (Zhou et al., 2015).

To minimize the risk to public health, the allowable nitrate concentration of drinking water is regulated. According to the World Health Organisation (2017), the value of nitrate in drinking water should not exceed 50 mg/l as NO_3^-. There are a few different methods used to decrease the nitrate concentration in drinking water: A non-treatment technique involves the mixing of contaminated water with clean water from another source, to lower the overall nitrate concentration (Self and Waskom, 2013; Zhou et al., 2015). Ion exchange involves a substance such as chloride being exchanged with the nitrate in the water. This is done by running the nitrate-contaminated water through a tank with special resin beads that are charged with chloride. The chloride then substitutes for the nitrate. Backwashing a sodium chloride solution through the tank then recharges the resin. This method however is not effective with waters that have a high sulphate concentration, as sulphate competes with the nitrate in the exchange process (Self and Waskom, 2013; Zhou et al., 2015). During reverse osmosis water travels through a membrane under high pressure. The pores in the membrane are microscopic and only allow water molecules to pass through and therefore stop nitrate and other inorganic chemicals. Unfortunately, this method is very expensive and removes other useful chemicals not just pollutants (Mahler et al., 1990; Zhou et al., 2015). Photosynthetic algae and chemical materials such as ethanol can also be used to remove nitrates as they convert nitrate ions into nitrogen (Mahler et al., 1990; Zhou et al., 2015).

3 Study Area

3.1 Location

The location of the study area can be seen in Figure 6 bellow. The study area is within the Lowveld region of South Africa in both the Mpumalanga and Limpopo provinces. It initially consisted of a 10 km radius around the Hans Hoheisen Wildlife Research Station, located adjacent to the Orpen Gate of the Kruger National Park, but was then expanded to include the B73E and B73F quaternary catchments of the Lower Olifants catchment and the X40C quaternary catchment of the Sabie-Sand River Catchment.

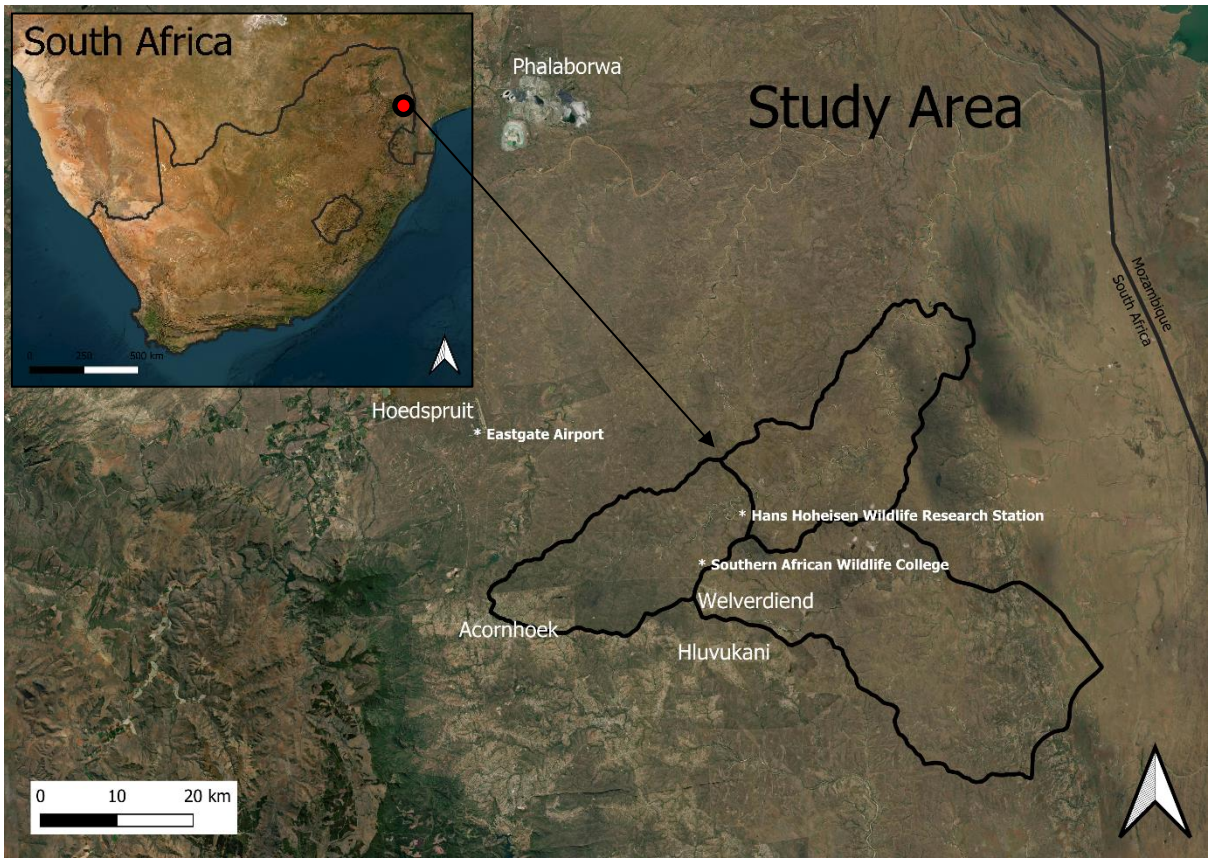

FIGURE 6: LOCATION OF THE STUDY AREA, SOURCE ESIR (2023).

3.1.1 Geology

The geology of the study area can be seen in Figure 7. There are two principal types of gneisses present in the lowveld, south of the Murchison Greenstone Belt. A layered composite variety known as the Makhutswi Gneiss and a homogeneous gneiss referred to as the Klaserie Gneiss (Robb et al., 2006). They are Palaeoarchaean intrusions that formed around 3600-3200Ma. Around 1106-1112 million years ago, large-scale magmatism resulted in the emplacement of huge volumes of mantle-derived magmas, over 2 million km^3, into the Palaeoarchaean to Mesoproterozoic formations and cratonic basement rocks on the Kaapvaal Craton. The group is known as the Umkondo Igneous Province and includes intrusions such as the Timbavati Gabbro (Allsopp et al., 1989; Hanson et al., 2004; Anhaeusser, Johnson and Thomas, 2006).

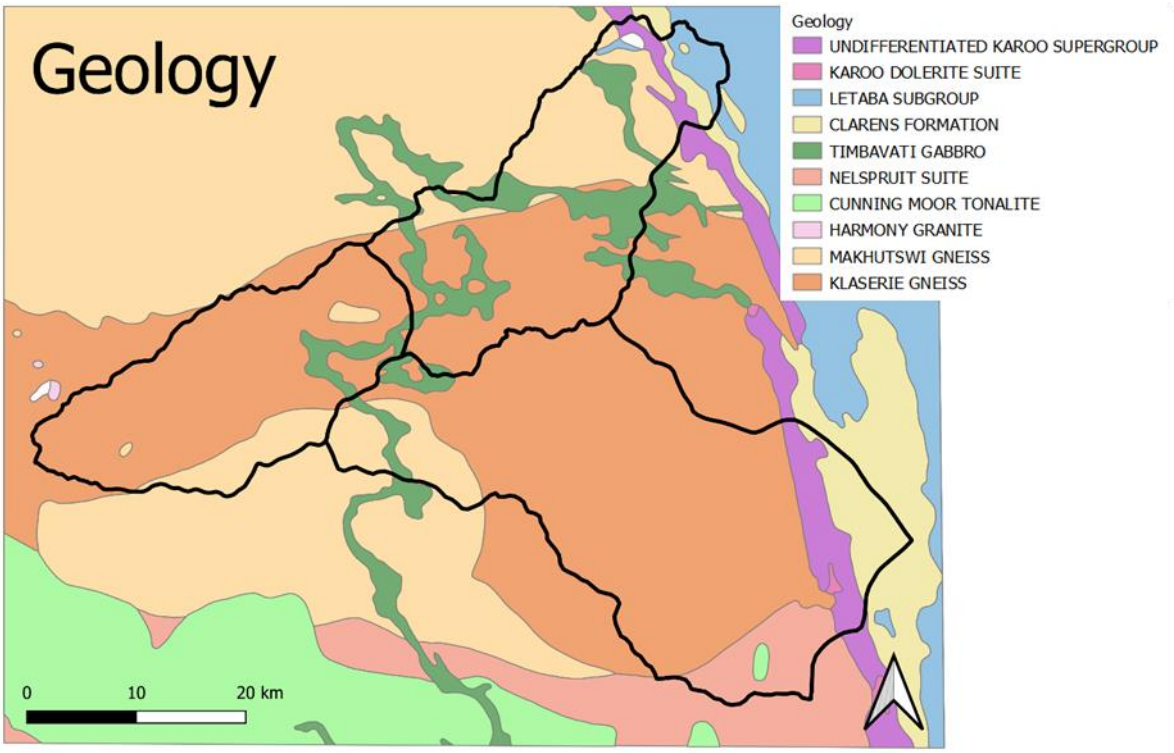

FIGURE 7: GEOLOGY OF THE STUDY AREA, SOURCE COUNCIL FOR GEOSCIENCE (2019).

3.1.1.1 Makhutswi Gneiss

The Makhutswi Gneiss occurs in two sections and is covered by Karoo and Transvaal Supergroup rocks in the east and west respectively. The Makhutswi Gneiss is light grey, fine to medium-grained with alternating leucosome bands of up to 15 cm and complexly folded (Robb et al., 2006; Schutte, 1986; Walraven, 1989). The major minerals found in the rock are plagioclase, microcline, quartz, and biotite, with hornblende and pyroxene seldom present. Limited geochemical data from the area suggest that the Makhutswi Gneiss is tonalitic to granodioritic in composition. Remnants of ultramafic, amphibolite, metaquartzite and calc-silicate rocks are also found within the Makhutswi gneiss (Robb et al., 2006; Schutte, 1986). Poujol et al. (1996) put the age of the Makhutswi gneiss at around 3228±12Ma when sampling close to the contact with the Murchison Greenstone Belt and Barton (1984) found it to be around 3268 ± 113 Ma in the Phalaborwa area. A younger tonalitic, unmigmatised biotite gneiss is locally intruded as dyke or stock-like bodies and is put by Brandl and Kröner (1993) at around 3112±5 to 3078±6 Ma (Robb et al., 2006).

3.1.1.2 Klaserie Gneiss

The Klaserie Gneiss is located between the two sections of Makhutswi Gneiss and contacts the Nelspruit Suite and Cunning Moor Tonalite body. The Klaserie Gneiss has very similar mineralogy to the Makhutswi Gneiss but is coarse-grained, well-foliated, and not migmatised (Robb et al., 2006; Walraven, 1989). It is located roughly at the boundary between the southern section of the Makhutswi Gneiss, the Nelspruit Suite, and the Cunning Moor Tonalite body. The Klasierie Gneiss is believed to post-date the Makhutswi Gneiss but there are no radiometric ages available (Robb et al., 2006).

3.1.1.3 Timbavati Gabbro

The Timbavati Gabbro consists of mafic to ultramafic rocks that have intruded into various older granites, gneisses, and magmatic Archaean basement rocks of the Mpumalanga Lowveld. Discontinuous outcrops occur as a series of small hills and ridges, following a roughly zig-zag pattern, in the western half of the Kruger National Park (Saggerson and Logan, 1970; Walraven, 1986, 1989; Walraven and Hartzer, 1986; Anhaeusser, Johnson and Thomas, 2006). The intrusions appear sill-like

in nature and dip between 20 and 30 degrees towards the east (Schutte, 1986). The emplacement of the Timbavati Gabbro was influenced by the pre-existing structures in the basement granitoid, such as faulting, jointing and regional foliation (Anhaeusser et al., 2006; Bristow et al., 1982). Mapping done by Michaluk (1983) showed that the sill outcrop pattern formed a series of connected arched segments, implying the sill segments must be conical in shape and it was therefore suggested that the Timbavati Gabbro was emplaced along a series of north-south linked conical fractures (Walraven, 1983; Walraven and Hartzer, 1986). In the Orpen area, the sills are believed to be about 200 m wide (Gordon-Welsh, 1980) while in the area of Pretoriuskop, they range between 300 and 480 m (Clubley-Armstrong, 1979). A chill margin is present in the contact between the host rocks and the gabbro, with the host rock showing various degrees of recrystallisation (Schutte, 1986).

A geochemical study conducted by Walraven (1984) concluded that the magma of the Timbavati Gabbro was the result of several separate intrusive pulses, rather than a single differentiated intrusion and that this resulted in at least three different types of gabbro (Anhaeusser et al., 2006; Walraven, 1986).

3.1.2 Hydrology

The study area is located within the B73E and B73F quaternary catchments of the Lower Olifants catchment, within the Olifants Water Management Area, as well as the X40C quaternary catchment of the Sabie-Sand River Catchment, within the Inkomati Water Management Area. The Timbavati River is the main river in the study area. It is perennial and flows towards the northeast.

3.1.2.1 Lower Olifant Catchment

The Lower Olifants catchment represents the catchment of the Olifants River between the Steelpoort confluence and the Mozambique border. According to the 'Olifants Water Management Area Internal Strategic Perspective' compiled by the Department of Water Affairs and Forestry, 2004, the area is characterised by having large agricultural developments, including irrigation and wide traces of game management areas, including the western portion of the Kruger National Park. There is, however, little groundwater development.

The average mean annual precipitation in the catchment is less than 500 mm but can reach 1000 mm along the escarpment. Aquifers are confined to weathered and fractured rock zones and boreholes are between 30 to 80 m deep with water levels between 5 and 15 mbgl. While the groundwater quality is generally good, there are isolated areas with elevated nitrate concentrations. The main use of groundwater is for domestic use and stock watering. Boreholes generally yield between 0,5 l/s and 2 l/s, in areas east of Hoedspruit it can increase to 5 l/s. Groundwater recharge is between 25-37 mm/a in the westernmost section of the B73E quaternary catchment and decreases to 10-15 mm/a in the B73F quaternary catchment. TDS values within the B73E and B73F quaternary catchments are between 500 and 2000 mg/l, with the western half of B73E and the eastern section of B73F generally having the lower values (Department of Water Affairs and Forestry, 2004).

3.1.3 Climate

The lowveld climate is known for having a hot and humid summer with a mild and dry winter. The climate of southern Africa is influenced by anticyclonic systems that are semi-rhythmically moving from east to west (Venter and Gertenbach, 1986). Based on the Köppen climate classification system the study area has a Cwa subtropical climate. The average temperatures and precipitation from the two ends of the study area can be seen in Figures 8 and 9.

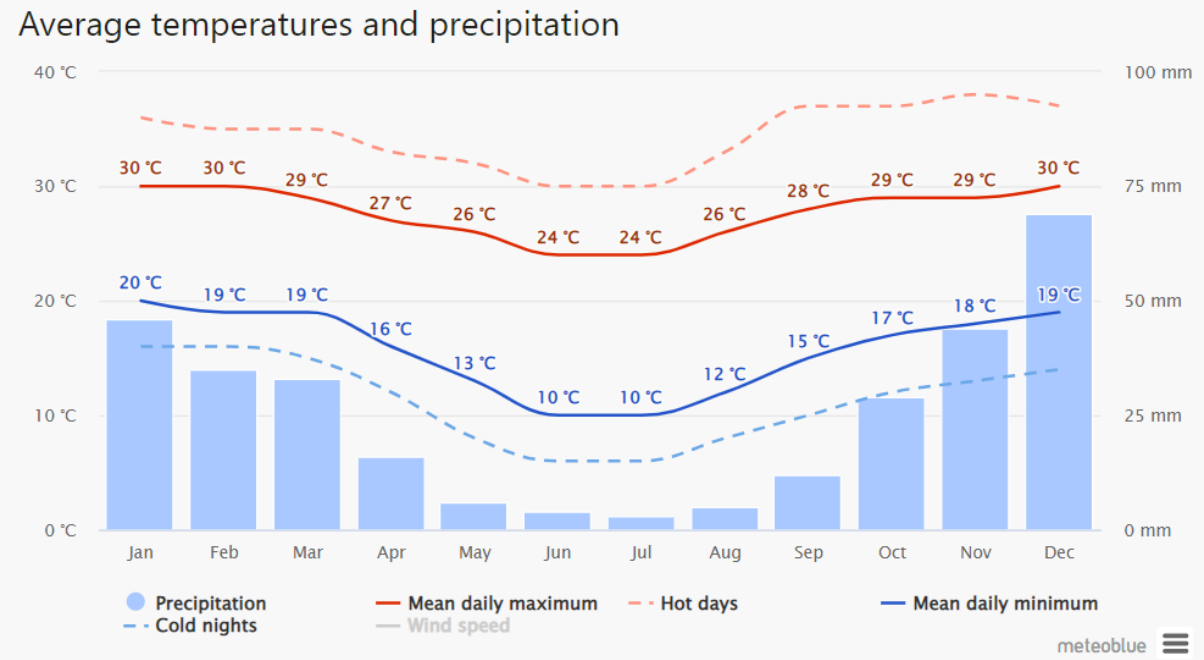

FIGURE 8: MODELLED AVERAGE MONTHLY TEMPERATURES AND PRECIPITATION FOR ORPEN REST CAMP, TAKEN FROM METEOBLUE (2023).

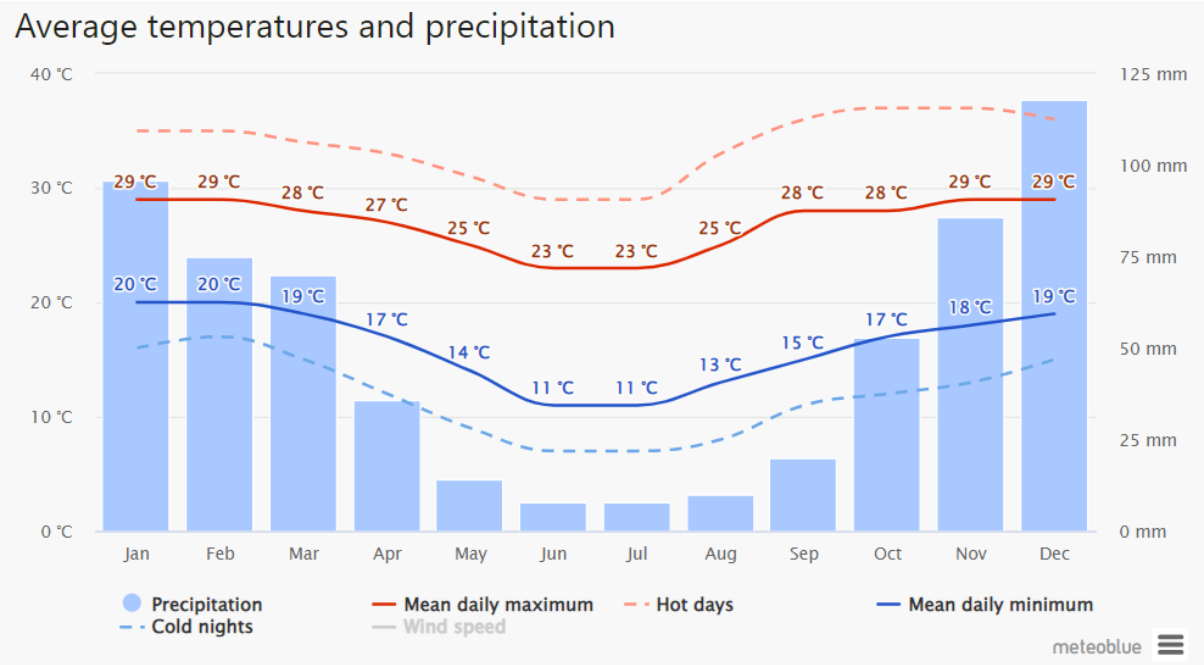

FIGURE 9: MODELLED AVERAGE MONTHLY TEMPERATURES AND PRECIPITATION FOR ACORNHOEK, TAKEN FROM METEOBLUE (2023).

3.1.4 Geography

As can be seen in Figure 10 the study area has a gentle gradient sloping towards the east, from 700 mamsl to 270 mamsl. In Figure 11 it can be seen that the majority of the study area consists of game and wilderness reserves. There are however also the communities of Welverdiend and Acornhoek in the southwestern section of the study area. The land in these communities has been developed to an extent and they also use large areas of land for grazing cattle and other livestock as well as growing the occasional crop.

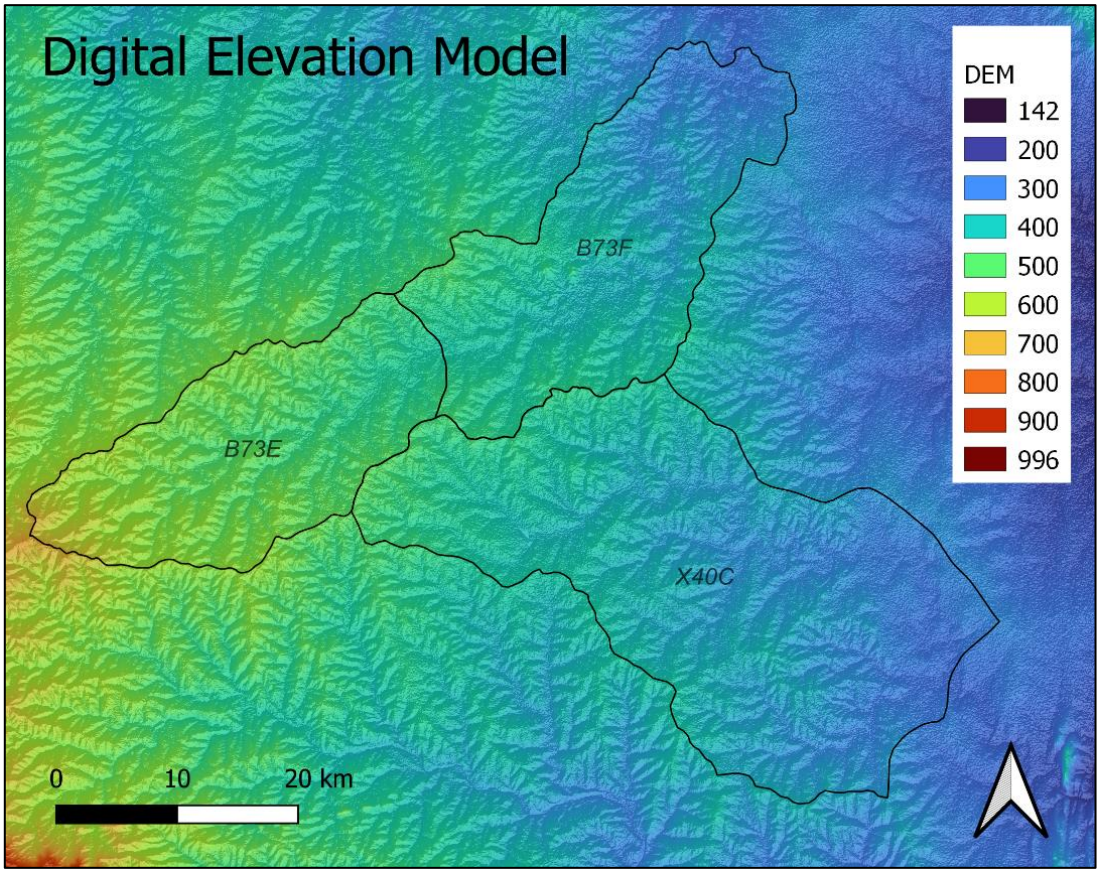

FIGURE 10: DIGITAL ELEVATION MODEL OF THE STUDY AREA FROM USGS EARTH EXPLORER (2022).

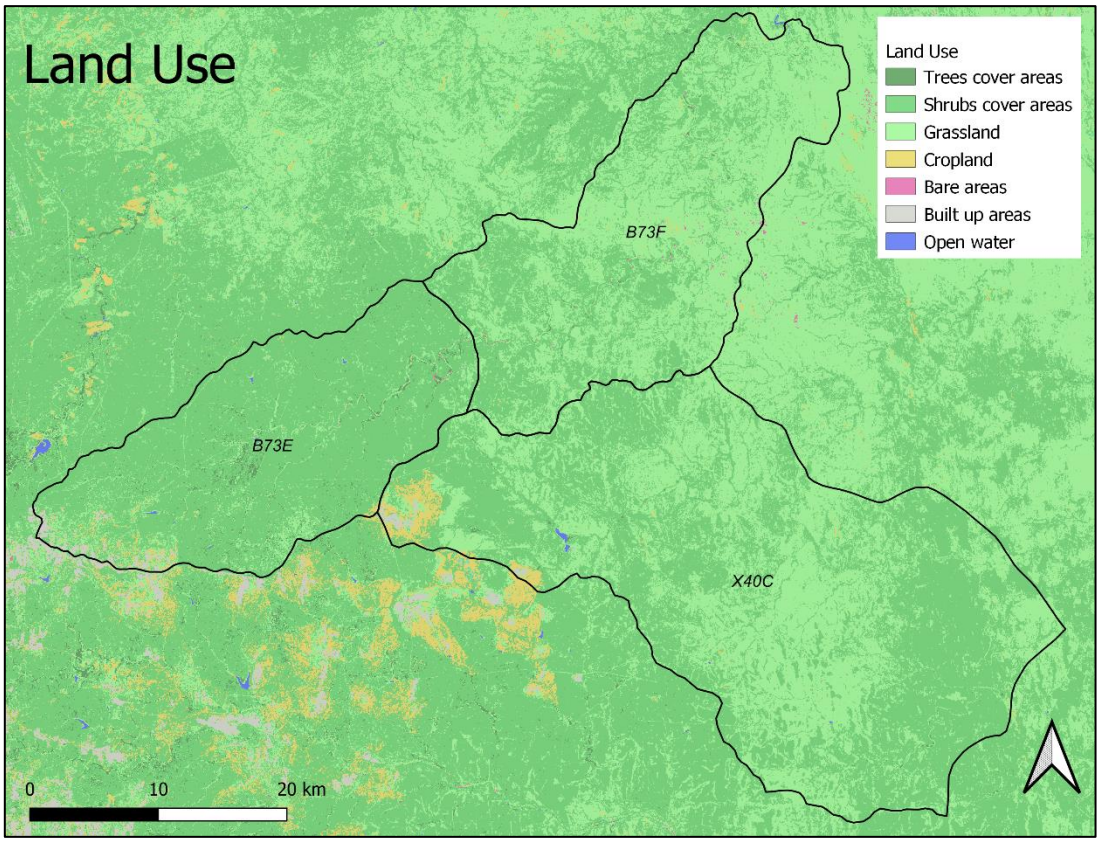

FIGURE 11: LAND USE, FROM THE EUROPEAN SPACE AGENCY CLIMATE CHANGE INITIATIVE LAND COVER PROJECT (2016).

4 Materials and Methods

4.1 Desktop Study

A desktop study was conducted by reviewing existing data and available literature for the study area, such as the climate, geology, hydrology, and hydrogeology. Secondary data was also obtained in the form of GIS data sets. These included land use from the European Space Agency Climate Change Initiative Land Cover project, a digital elevation model from USGS Earth Explorer and geology from the Council for Geoscience.

4.2 Hydrocensus

An initial hydrocensus was conducted in September 2021 before sampling took place and additional data was added to the hydrocensus as more sample sites were identified on later site visits. Landowners and managers as well as community leaders in the Timbavati Catchment area were contacted directly to acquire access to the boreholes and surface water bodies. The following data was recorded for boreholes during the hydrocensus: the owner, the coordinates, date and time of recording, its use, the pump type, the power supply to the pump, borehole construction material, the collar height, the protection, when the borehole was last pumped, and a photograph of the borehole. When possible, the borehole depth, pump depth and water level were also recorded.

4.3 Sampling

From the boreholes and surface water bodies identified in the hydrocensus, 25 sampling points were chosen based on their accessibility. These 25 sites consist of six surface water sample points and 19 groundwater sample points, see Table 2. Where necessary the appropriate documentation and permits were acquired. All participants in the study were also provided with a copy of their water analysis results. While most of the sampling sites were located within game reserves, a few were also located on land belonging to community outreach centres and communal land. For security reasons when sampling in the reserves a game ranger was always present. The locations of the sampling points can be seen in Figure 12, pictures of the sample sites can be seen in Figure 13, Figure 14 and Figure 15. All sampling was done in accordance with SABS ISO 5667 guidelines. Multiple rounds of sampling were conducted over a two-year period to obtain data that reflected seasonal variations in the water chemistry, the sampling schedule can be seen in Table 1. The aim was to collect samples during and just after the wet and dry seasons. A total of 100 samples were collected. The following data was recorded when sampling: sample ID, reason for sampling, location of sampling point, nature of sampling point, date, time, sample method, sample appearance, details of preservation techniques, details of sample storage method employed, possible source of sampling bias, name of sample collector and a photograph of the sample site. Rainwater was collected and rainfall (mm) was recorded at two sites, Hans Hoheisen Wildlife Research Station, and Manyeleti Main Camp for isotope analysis.

TABLE 1: SAMPLING SCHEDULE.

Round of Sampling	Dates of Sampling	Notes
First	14/09/2021 to 15/09/2021 26/10/2021 to 28/10/2021	Minimal sampling was done during this time as sites were still being identified
Second	21/02/2022 to 25/02/2022	
Third	30/05/2022 to 03/06/2022	
Fourth	29/08/2022 to 02/09/2022	Samples were taken for chemical analysis
Fifth	21/11/2022 to 25/11/2022	

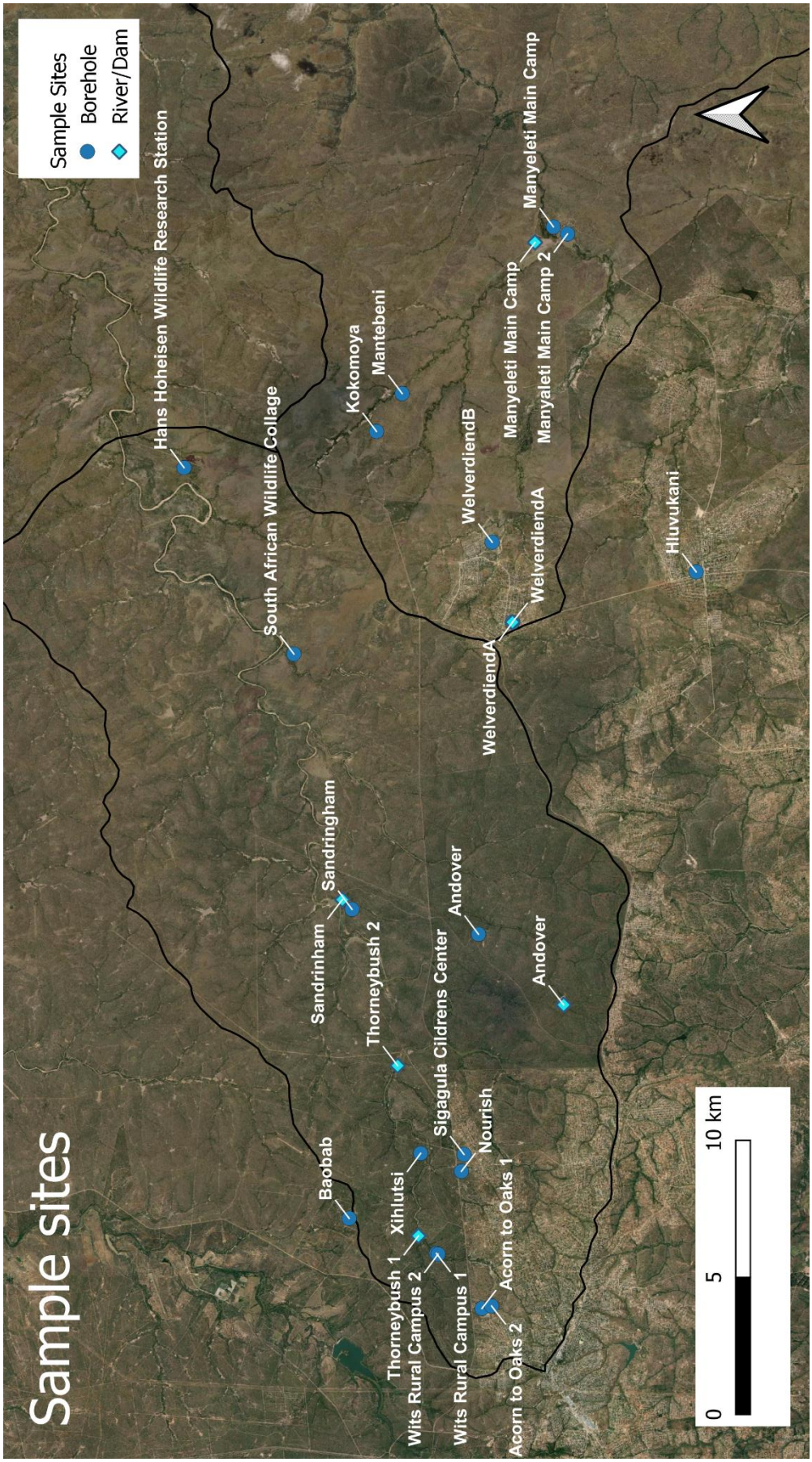

FIGURE 12: LOCATION OF SAMPLING POINTS WITHIN THE TIMBAVATI CATCHMENT.

TABLE 2: LIST OF SAMPLE POINTS WITH SITE IDENTIFIER, COORDINATES, SITE NAME AND SAMPLE TYPE

Site Name	Identifier	Coordinates		Sample Type
Acorn to Oaks 1	A2O1	24°34'17.198" S	31°04'56.878" E	Borehole
Acorn to Oaks 2	A2O2	24°34'28.620" S	31°04'59.934" E	Borehole
Wits Rural Campus 1	Wits1	24°33'24.150" S	31°06'09.510" E	Borehole
Wits Rural Campus 2	Wits2	24°33'26.064" S	31°06'08.772" E	Borehole
Thorneybush	THORSW1	24°33'03.972" S	31°06'32.340" E	Surface Water
Thorneybush	THORSW2	24°32'41.838" S	31°10'13.308" E	Surface Water
Thorneybush - Xihlutsi	Xih	24°33'07.278" S	31°08'19.860" E	Borehole
Baobab	BAO	24°31'41.941" S	31°06'56.004" E	Borehole
Nourish	NOR	24°33'54.990" S	31°07'54.900" E	Borehole
Sigagula Childrens Centre	SCC	24°33'58.409" S	31°08'16.774" E	Borehole
Andover	ANDSW	24°35'59.478" S	31°11'29.598" E	Surface Water
Andover	AND	24°34'19.950" S	31°13'02.910" E	Borehole
Sandringham	SANSW	24°31'38.002" S	31°13'49.033" E	Surface Water
Sandringham	SAN	24°31'49.300" S	31°13'36.400" E	Borehole
WelverdiendA	WelA	24°35'00.694" S	31°19'36.138" E	Borehole
WelverdiendA	WelASW	24°35'04.050" S	31°19'46.026" E	Surface Water
WelverdiendB	WelB	24°34'41.822" S	31°21'30.780" E	Borehole
South African Wildlife Collage	SAWC	24°30'44.088" S	31°19'08.169" E	Borehole
Hluvukani	HLU	24°38'42.714" S	31°20'48.372" E	Borehole
Hans Hoheisen Wildlife Research Station	UPCell	24°28'36.371" S	31°23'11.327" E	Borehole
Kokomoya	KM	24°32'25.320" S	31°23'55.313" E	Borehole
Mantebeni	MANT	24°32'56.325" S	31°24'43.944" E	Borehole
Manyeleti	MANSW	24°35'36.558" S	31°27'58.164" E	Surface Water
Manyeleti Main Camp 1	MANM	24°35'58.013" S	31°28'18.530" E	Borehole
Manyeleti Main Camp 2	MANM2	24°36'14.616" S	31°28'08.566" E	Borehole

4.3.1 Sampling procedure for borehole

Equipment was cleaned and calibrated the night before sampling took place. As all the boreholes being sampled were equipped with pumps, taps or pipes were opened to allow access to the borehole water as close to the pump as possible and before water entered a tank. If the borehole was not currently in use, it was switched on and allowed to run for 10 minutes before the sample was taken. The sample bottles, containers, and Aquaread AP-5000 were all rinsed in the water from the borehole before the samples were taken. Groundwater samples were collected in 2 PET bottles and into the Aquaread AP-5000 calibration cup. Sample bottles were then sealed and labelled with the sample name and date of sampling; no preservation techniques were used. The Aquaread AP-5000 was then lowered into the calibration cup and the analysis run. The reason for the on-site analysis being done in the calibration cup rather than by lowering the Aquaread AP-5000 down the borehole is that all the boreholes had pumps installed. The equipment was cleaned and dried before being packed away.

4.3.2 Sampling procedure for surface water bodies

The sampling procedure for surface water bodies was mostly the same as that for the borehole samples, except that the water was collected from the larger surface water bodies using a bailer before being transferred to the sample bottles and containers. Samples were collected using a bailer

as it was not safe to put the PVC bottles directly in the water due to the presence of crocodiles and hippopotami.

4.3.3 Sampling procedure for rainwater samples

Rainwater was collected in a rain gauge and rainfall volumes were recorded every morning at 08h00 against the previous day's date. Rainwater was then poured into a 5 l bottle, and the lid was tightly sealed to prevent evaporation. At the end of the month, the 5 l bottle was shaken to ensure the water was well mixed, including the water droplets on the side of the bottles. The water was then poured into 2 smaller 50 ml bottles, to the top if possible, and the lid tightly sealed to prevent evaporation. The bottle was then labelled with the respective month and location.

FIGURE 13: PHOTOGRAPHS OF VARIOUS BOREHOLES AND SURFACE WATER BODIES THAT WERE SAMPLED.

FIGURE 14: PHOTOGRAPHS OF VARIOUS BOREHOLES AND SURFACE WATER BODIES THAT WERE SAMPLED.

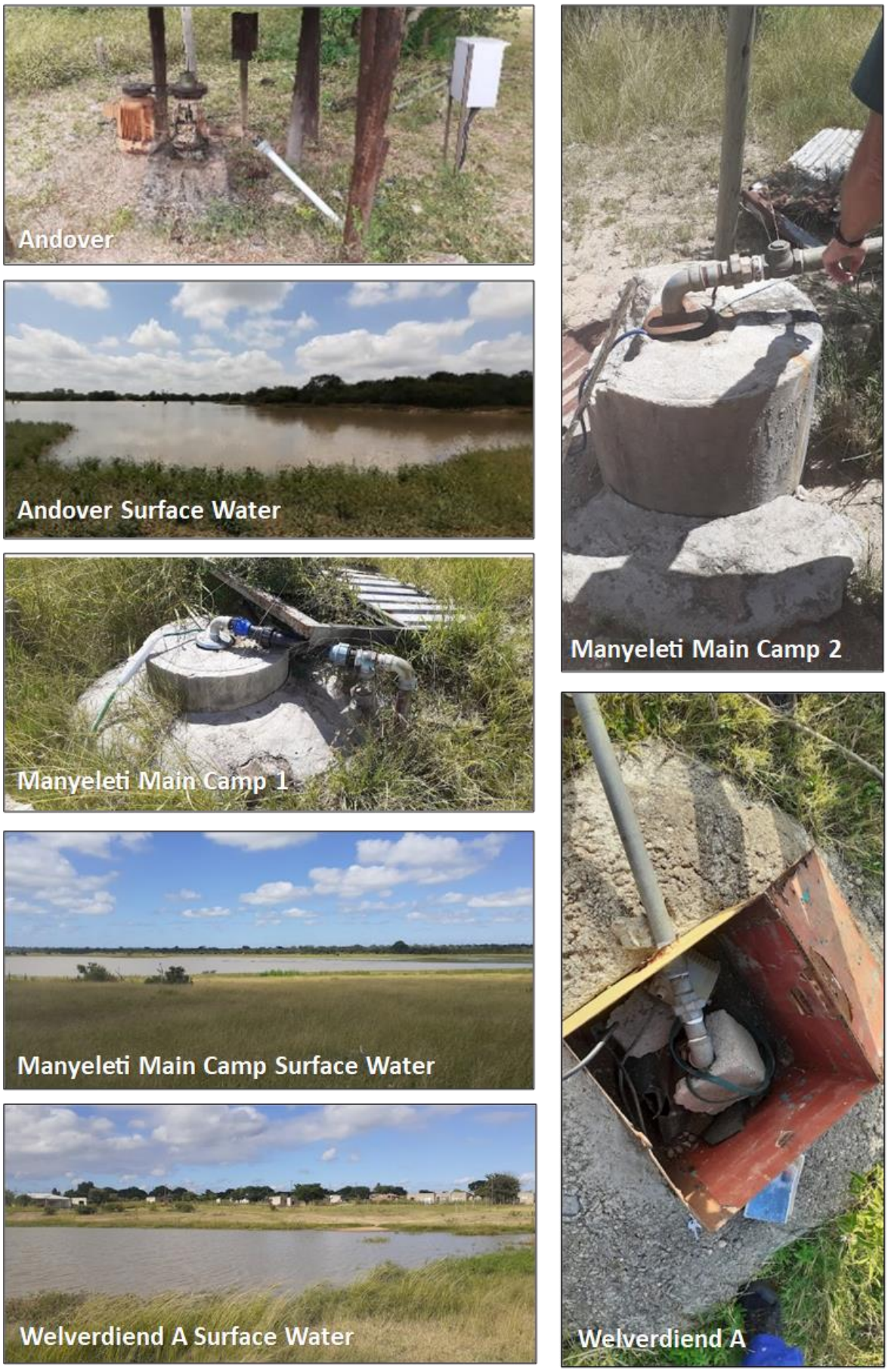

FIGURE 15: PHOTOGRAPHS OF VARIOUS BOREHOLES AND SURFACE WATER BODIES THAT WERE SAMPLED.

4.4 Water Analysis

4.4.1 Hydrogen and oxygen isotope analysis

Rainwater, groundwater, and surface water samples were taken to iThemba LABS in Johannesburg where hydrogen and oxygen isotope ratios were analysed in the Environmental Isotope Laboratory (EIL). The analysis was done using a Los Gatos Research (LGR) Liquid Water Isotope Analyser and laboratory standards, calibrated against standard mean ocean water (SMOW), were analysed with each batch of samples.

4.4.2 Water chemistry analysis

During the fourth round of sampling both groundwater and surface water samples were collected for more detailed chemical analysis at Aquatico Laboratories in Pretoria. The analysis conducted can be seen in Table 3 below. Water samples were collected in 500 ml PET bottles, sealed, and labelled. The bottles were then placed in a cooler box and stored in the fridge until they could be delivered to the laboratory.

TABLE 3: AQUATICO LABORATORIES, SANAS ACCREDITED ANALYSIS.

Method	Variable/Description
ALM 01	Total Alkalinity
ALM 02	Chloride (Cl)
ALM 03	Sulphate (SO_4)
ALM 04	Orthophosphate (PO_4) as P
ALM 05	Ammonium (NH_4) as N
ALM 06	Nitrate (NO_3) as N
ALM 07	Nitrite (NO_2) as N
ALM 08	Fluoride (F)
ALM 20	pH @ 25 °C
ALM 26	Bicarbonate alkalinity
ALM 30	Calcium (Ca), Magnesium (Mg), Potassium (K), Sodium (Na)
ALM 31	Iron (Fe), Manganese (Mn)
ALM 37	Dissolved Uranium (U)
ALM 30	Calcium (Ca), Magnesium (Mg), Potassium (K), Sodium (Na)
ALM 91	ICP-MS: Aluminium (Al), Antimony (Sb), Arsenic (As), Barium (Ba), Beryllium (Be), Bismuth (Bi), Boron (B), Cadmium (Cd), Cerium (Ce), Cesium (Cs), Chromium (Cr), Cobalt (Co), Copper (Cu), Dysprosium (Dy), Erbium (Er), Europium (Eu), Gadolinium (Gd), Gallium (Ga), Germanium (Ge), Gold (Au), Hafnium (Hf), Holmium (Ho), Indium (In), Iridium (Ir), Iron (Fe), Lanthanum (La), Lead (Pb), Lithium (Li), Lutetium (Lu), Manganese (Mn), Mercury (Hg), Molybdenum (Mo), Neodymium (Nd), Nickel (Ni), Niobium (Nb), Osmium (Os), Palladium (Pd), Platinum (Pt), Praseodymium (Pr), Rhenium (Re), Rhodium (Rh), Rubidium (Rb), Ruthenium (Ru), Samarium (Sm), Scandium (Sc), Selenium (Se), Silicon (Si), Silver (Ag), Strontium (Sr), Tantalum (Ta), Tellurium (Te), Terbium (Tb), Thallium (Tl), Thorium (Th), Thulium (Tm), Tin (Sn), Titanium (Ti), Tungsten (W), Uranium (U), Vanadium (V), Ytterbium (Yb), Yttrium (Y), Zinc (Zn), Zirconium (Zr)

4.4.3 Aquaread AP-5000 analysis

As the boreholes being sampled were all production boreholes and had pumps installed it was not possible to lower the probe down into the boreholes. Instead, the water sample was collected in the

Aquaread Calibration cup and the probe was placed into the calibration cup. The probe was then turned on, the analysis was run, and the results were recorded in a fieldwork notebook.

TABLE 4: ION SELECTIVE ELECTRODES DETAILED SPECIFICATION TAKEN FROM THE AQUAREAD MANUAL (2021)

Ammonium	**Range**	0 – 9,000 mg/L (ppm)
	Resolution	2 Auto-range scales: 0.00 - 99.99 mg/L, 100.0 – 8999.9 mg/L
	Accuracy	± 10% of reading or 2ppm (whichever is greater)
	MLD*	1.0 ppm
	Interfering Ions**	Potassium, Sodium and Magnesium
	pH Range	5 – 8
Nitrate	**Range**	0 – 30,000 mg/L (ppm)
	Resolution	2 Auto-range scales: 0.00 - 99.99 mg/L, 100.0 – 29999.9 mg/L
	Accuracy	± 10% of reading or 2 ppm (whichever is greater)
	MLD*	0.5 ppm
	Interfering Ions**	Chloride, Bromide, Fluoride, Sulphate, Chlorate and Perchlorate
	pH Range	3 - 10

*Minimum Level of Detection

** Each ion selective electrode is prone to interference from ions that are similar in nature to the target ion. The main interfering ions for each electrode type are listed here. If the water under test contains interfering ions, the electrode will produce erroneous readings. Ion Selective Electrodes are not recommended for use in brackish or salt water due to the high level of interfering ions.

The Aquaread AP-5000 was used in the field to measure the following parameters: temperature, pH, dissolved oxygen (DO), electric conductivity (EC), total dissolved solids (TDS), salinity (SAL), oxidation-reduction potential (ORP), nitrate (NO_3^-), and ammonium (NH_4^+). The Aquaread optical electrodes are described as being standalone, fixed-frequency fluorometers specifically tuned to excite and detect the fluorescence of selected substances in water. They do this by emitting short pulses of high-energy light at the excitation wavelength and responding to fluorescence in the detection range. Inaccuracies in measurements can be due to microbiological species, compounds which fluoresce at similar wavelengths and differences in fluorescence caused by temperature, ambient light, and turbidity.

4.4.4 Durridge RAD7 analysis

The Durridge RAD7 was used for the radon analysis. Samples were taken back to camp and analysed there as it was not possible to take the Durridge machine into the field. Samples were analysed as soon after sampling as possible, usually within 12 h and often within 6 to 8 h, correction factors used can be seen in Table 5. Before samples were analysed the machine was purged for 10 minutes with the system being open but still being connected to the drying unit. This was done to remove any excess radon from the system left behind by previous analysis. After 10 minutes the system was closed, and the purging would continue until the relative humidity reading had dropped below 6%. The analysis of the sample would then be done. Results were printed out as the analysis was taking place. The same purging and drying process was completed between every sample analysis to prevent cross-contamination. Another precaution taken to prevent cross-contamination was to analyse the samples in order of least presumed radon to most presumed radon i.e., surface water samples were analysed before groundwater. According to the RAD7 Instruction Manual, the device works by using an electrostatic collection of alpha emitters with a spectral analysis. The passivated ion-implanted planar silicon detector SNIFF mode counts polonium-218 decays while the NORMAL mode counts both polonium 218 and polonium 214 decays (Durridge Company Inc, 2022).

TABLE 5: TIME AFTER SAMPLING AND THE DECAY CORRECTION FACTORS TO BE APPLIED (DURRIDGE COMPANY INC. 2022).

Hours	Decay Correction Factors
0	1.000
1	1.008
2	1.015
3	1.023
4	1.031
5	1.038
6	1.046
7	1.054
8	1.062
9	1.070
10	1.078
11	1.087
12	1.095

TABLE 6: RAD7 SPECIFICATIONS TAKEN FROM THE RAD7 RADON DETECTOR PRODUCT BRIEF (2019).

Technology	A Passivated Implanted Planar Silicon Detector enables high-resolution alpha spectroscopy of decay energies
Sensitivity	0.0067 cpm/(Bq/m3) (SNIFF mode) 0.013 cpm/(Bq/m3) (NORMAL mode) Virtually background-free raw-data readings
Spectral Resolution	50 keV: high enough for independent radon and thoron measurements and near-perfect ^{210}Pb background rejection
100% immune to ^{210}Po background build-up over the life of the instrument	Yes
Operating Range	4 - 750,000 Bq/m^3 4 - 7,500,000 Bq/m^3 (with optional Range Extender accessory) RAD7 + Range Extender provides a 3.75x AlphaGuard range and maintains accuracy over a lifetime, at a significantly lower price
Response Time	15 minutes (SNIFF mode) 3 hours (NORMAL mode)
Instrument calibration error	± 5%
Intrinsic Background	0.2 Bq/m^3 for lifetime of the instrument

4.5 Data interpretation

The field data as well as the lab results were all recorded and organised using Microsoft Excel 365. The Aquaread AP5000 chemistry, radon and isotope data was then imported into CoPlot Version 6.45 and scatter plots were created to visually represent the data. QGIS 3.26.1 was used to represent the radon and nitrate concentrations as graduated symbols overlaying the geology and land use respectively. The ionic concentrations from the lab data were converted from mg/l to meq/l. This was done by dividing the concentrations by the molar mass and then multiplying it by the charge of the ion. Piper plots, Stiff plots and Schoeller diagrams were then created using OriginPro 2022b (Learning Edition) to represent the ionic concentrations of the water samples.

4.6 Restraints

Not all sample sites were sampled at the beginning of the study. This is because in order to access the sampling sites permission from the landowners or government agencies such as South African National Parks and the Mpumalanga Tourism and Parks Agency was required, and the permits took time to be issued. Some of the boreholes identified in the hydrocensus could not be sampled either because they were no longer functional or because there was no way to access the water before it went into tanks. Surface water samples often had to be taken close to the shore of the river or dam due to the presence of hippopotami and crocodiles.

5 Results

5.1 TDS, ORP, DO and pH

The graphs below in Figure 16, Figure 17and Figure 18 show the relationship between TDS, ORP, DO and pH concentrations respectively for the five rounds of sampling, an additional graph is also given showing the combined data for all five rounds of sampling.

The pH values in the groundwater samples range from 6.97 to 8.40 with a mean value of 7.48 and the surface water samples range from 7.47 to 9.3 with a mean value of 8.30. Most of the groundwater samples and all the surface water samples are alkaline.

Groundwater TDS values ranged from 540 to 3580 mg/l with a mean value of 1220 mg/l. Surface water samples ranged from 140 to 620 mg/l with a mean value of 330 mg/l. While visually there appears to be a trend of decreasing TDS with increasing pH the r (Pearson correlation coefficients) values show no correlation with a value of -0.15 for the groundwater samples and minimal correlation with a value of -0.5 for the surface water samples (Figure 16)

It can be seen the ORP values of the groundwater samples range from 19 to 200 mV with a mean of 99 mV and 35 to 196 mV with an average of 91 mV for the surface water samples. Pearson's r values of 0.45 for the surface water samples show a minimal correlation between ORP and pH, while the groundwater samples show no correlation with r = 0.20 (Figure 17).

DO concentrations in the groundwater samples range from 2.65 to 8.60 mg/l with a mean of 5.33 mg/l and surface water samples ranged from 6.26 to 12.66 mg/l with a mean of 8.22 mg/l. DO and pH have no correlation with Pearson's r values of 0.06 and 0.13 for the groundwater and surface water samples respectively, (Figure 18).

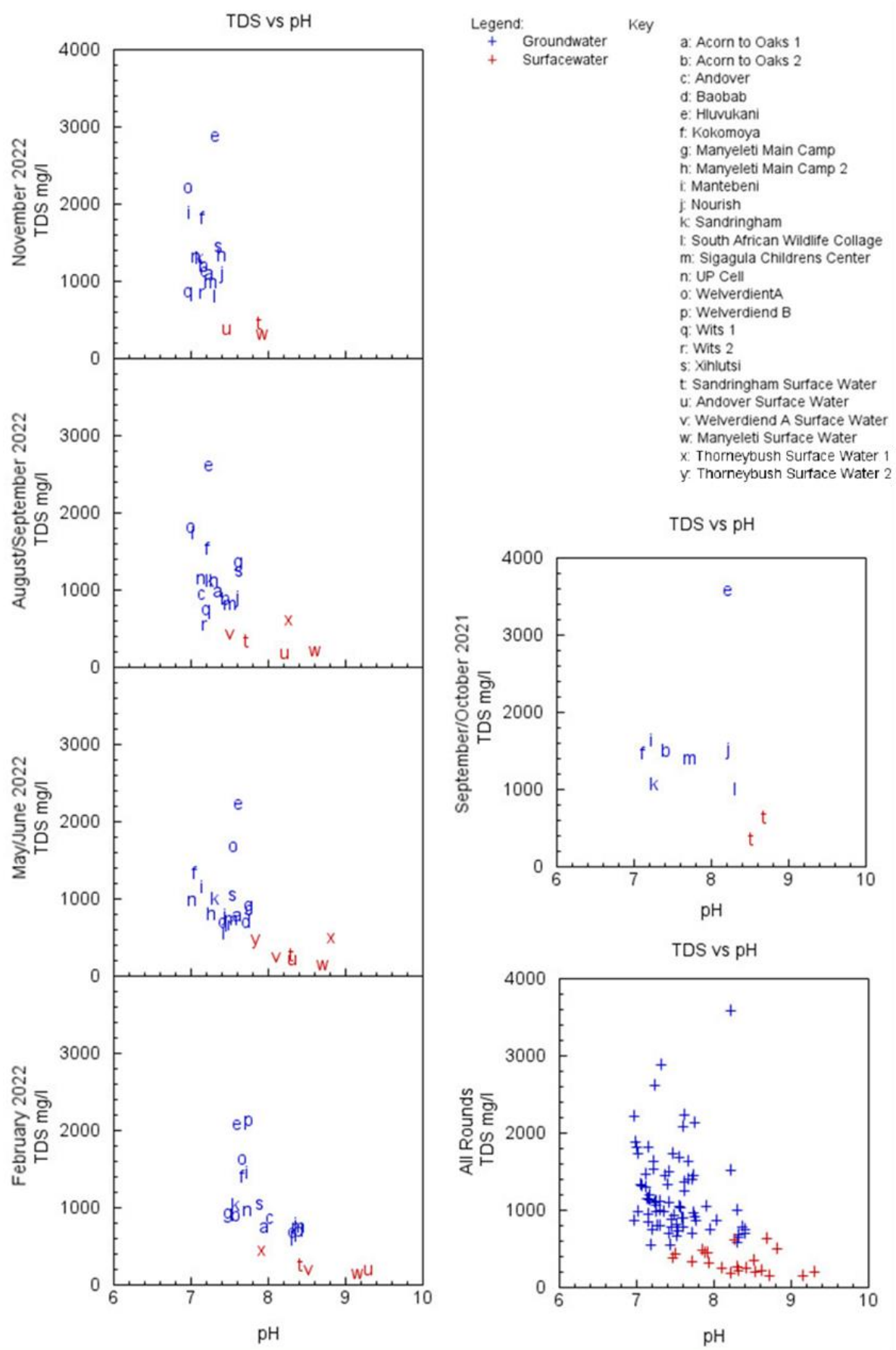

FIGURE 16: GRAPHS SHOWING THE RELATIONSHIP BETWEEN TOTAL DISSOLVED SOLIDS AND PH FOR THE GROUNDWATER AND SURFACE WATER SAMPLES TAKEN DURING THE 5 ROUNDS OF SAMPLING.

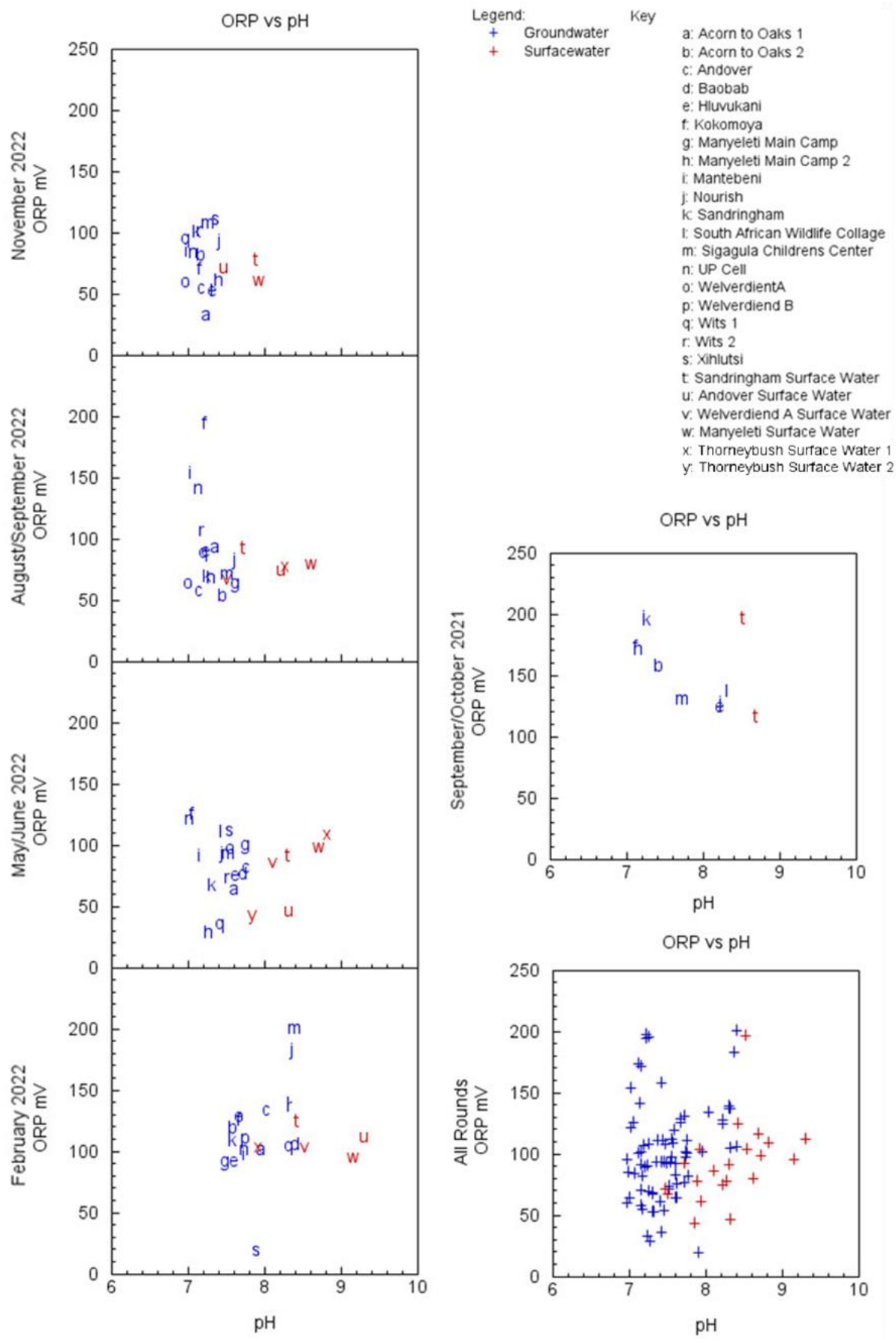

FIGURE 17: GRAPHS SHOWING THE RELATIONSHIP BETWEEN THE OXIDATION REDUCTION POTENTIAL AND PH FOR THE GROUNDWATER AND SURFACE WATER SAMPLES TAKEN DURING THE 5 ROUNDS OF SAMPLING.

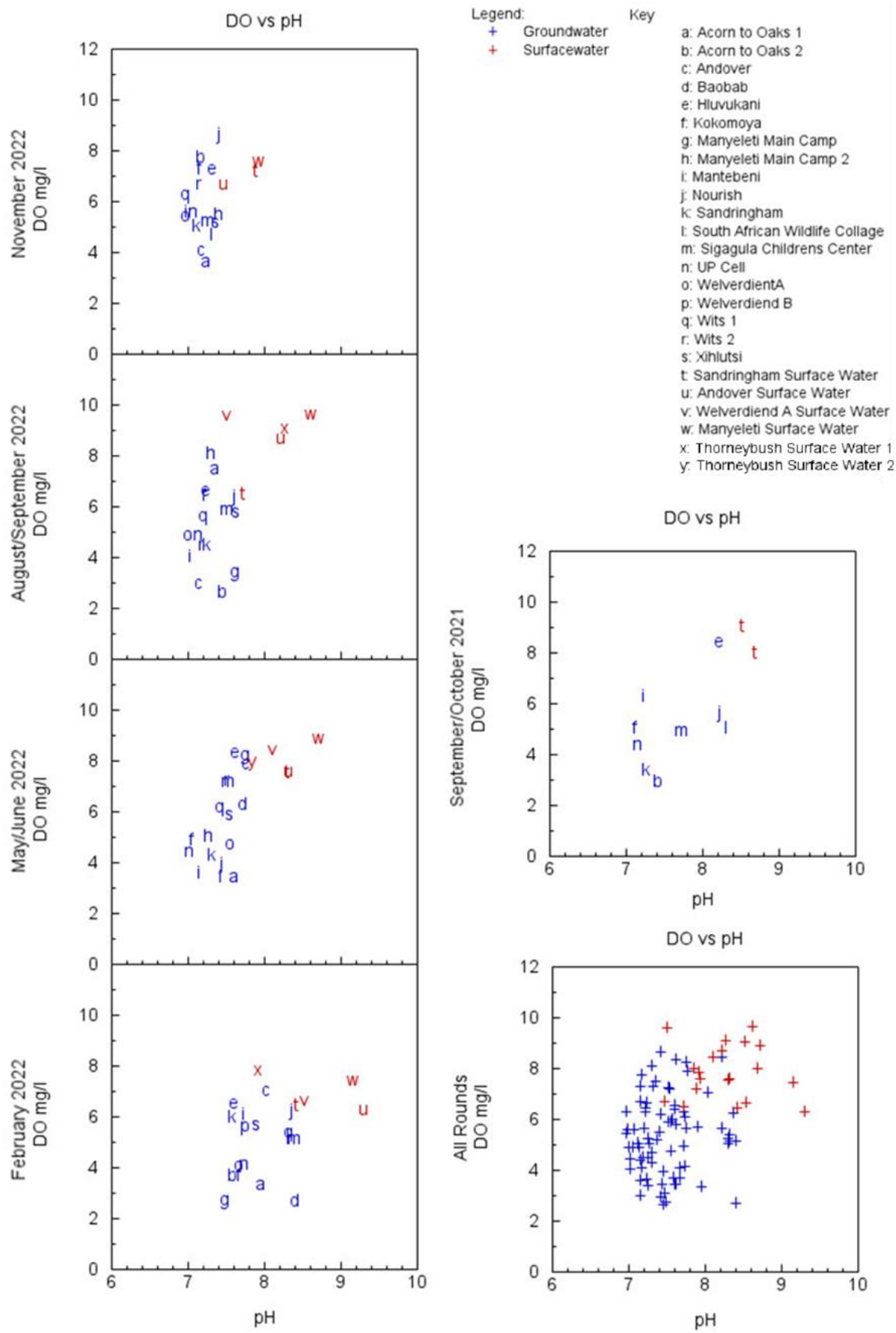

FIGURE 18: GRAPHS SHOWING THE RELATIONSHIP BETWEEN DISSOLVED OXYGEN AND PH FOR THE GROUNDWATER AND SURFACE WATER SAMPLES TAKEN DURING THE 5 ROUNDS OF SAMPLING.

5.1 NH_4, NO_3 and TDS

The graphs below in Figure 19 and Figure 20 show the relationship between NH_4, NO_3^- and TDS concentrations respectively for the five rounds of sampling, an additional graph is also given showing the combined data for all five rounds of sampling. Figure 21 to Figure 25 show the nitrate concentrations overlaying the areas land use for the five rounds of sampling. It can be noted that nitrate concentrations are always higher in the more built-up areas.

NH_4 concentrations ranged from 0.01 to 0.75 mg/l with a mean value of 0.20 mg/l for the groundwater samples and 0.02 to 1.7 mg/l with a mean value of 0.34 mg/l for the surface water samples. There is minimal correlation between NH_4 and TDS with a Pearson's r value of 0.47, however, there is no correlation in the surface water samples with an r-value of 0.19 (Figure 19).

NO_3 groundwater concentrations range from 0.28 to 1350 mg/l with a mean value of 83.1 mg/l and surface water concentrations ranged from 1.59 to 10.4 mg/l with a mean value of 5.56 mg/l. The surface water samples show no correlation between nitrate and TDS with a Pearson's r correlation of -0.19 but the groundwater samples show a fairer correlation of 0.59 (Figure 20).

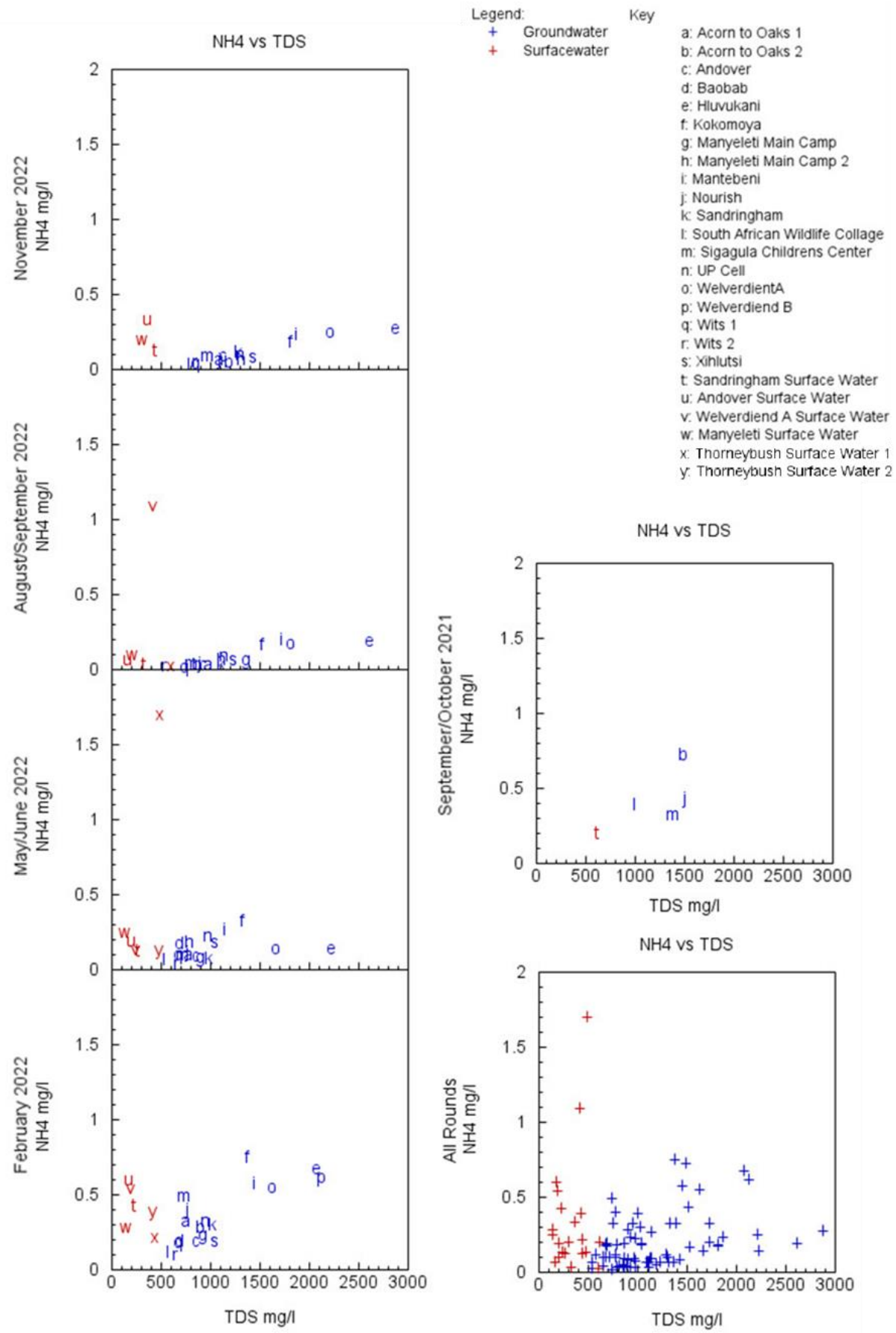

FIGURE 19: GRAPHS SHOWING THE RELATIONSHIP BETWEEN AMMONIUM AND TOTAL DISSOLVED SOLIDS FOR THE GROUNDWATER AND SURFACE WATER SAMPLES TAKEN DURING THE 5 ROUNDS OF SAMPLING.

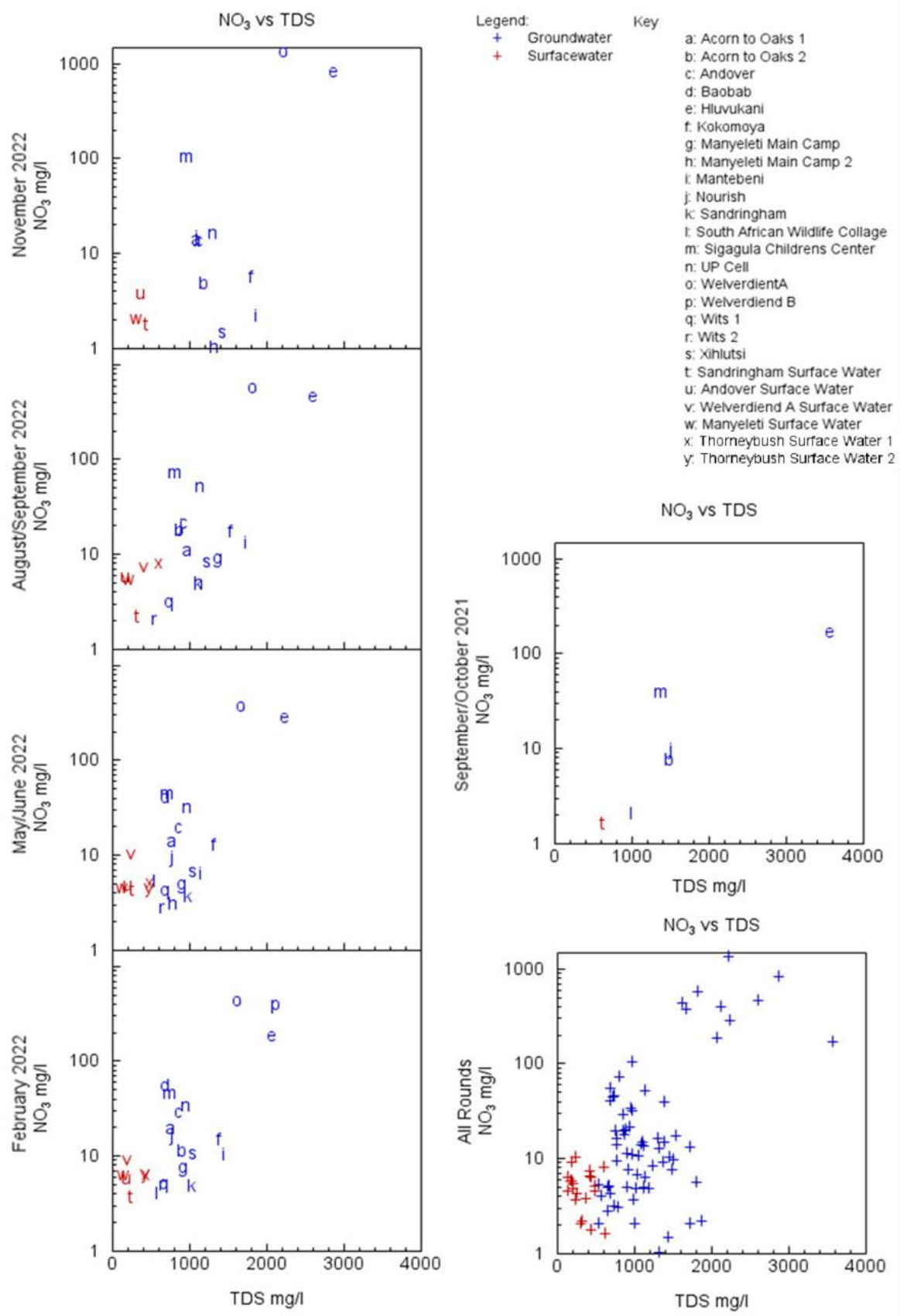

FIGURE 20: GRAPHS SHOWING THE RELATIONSHIP BETWEEN NITRATE AND TOTAL DISSOLVED SOLIDS FOR THE GROUNDWATER AND SURFACE WATER SAMPLES TAKEN DURING THE 5 ROUNDS OF SAMPLING.

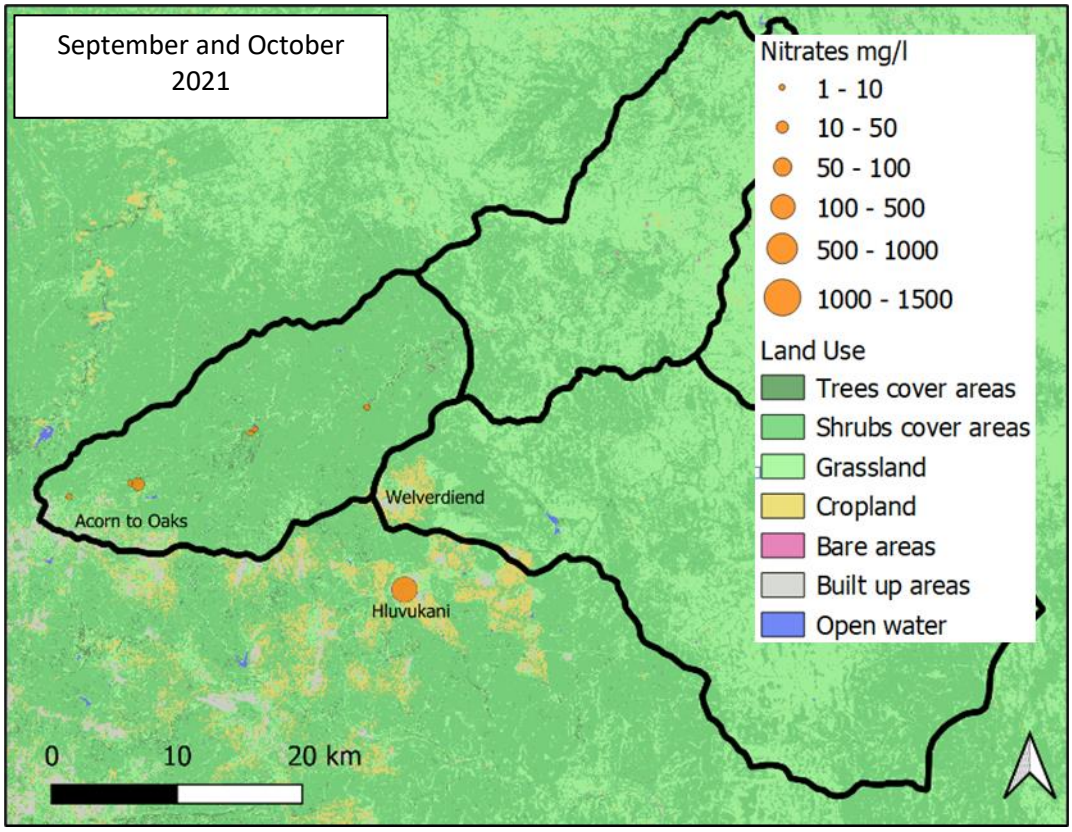

FIGURE 21: NITRATE CONCENTRATIONS AND LAND USE FOR WATER SAMPLES TAKEN IN SEPTEMBER AND OCTOBER 2021.

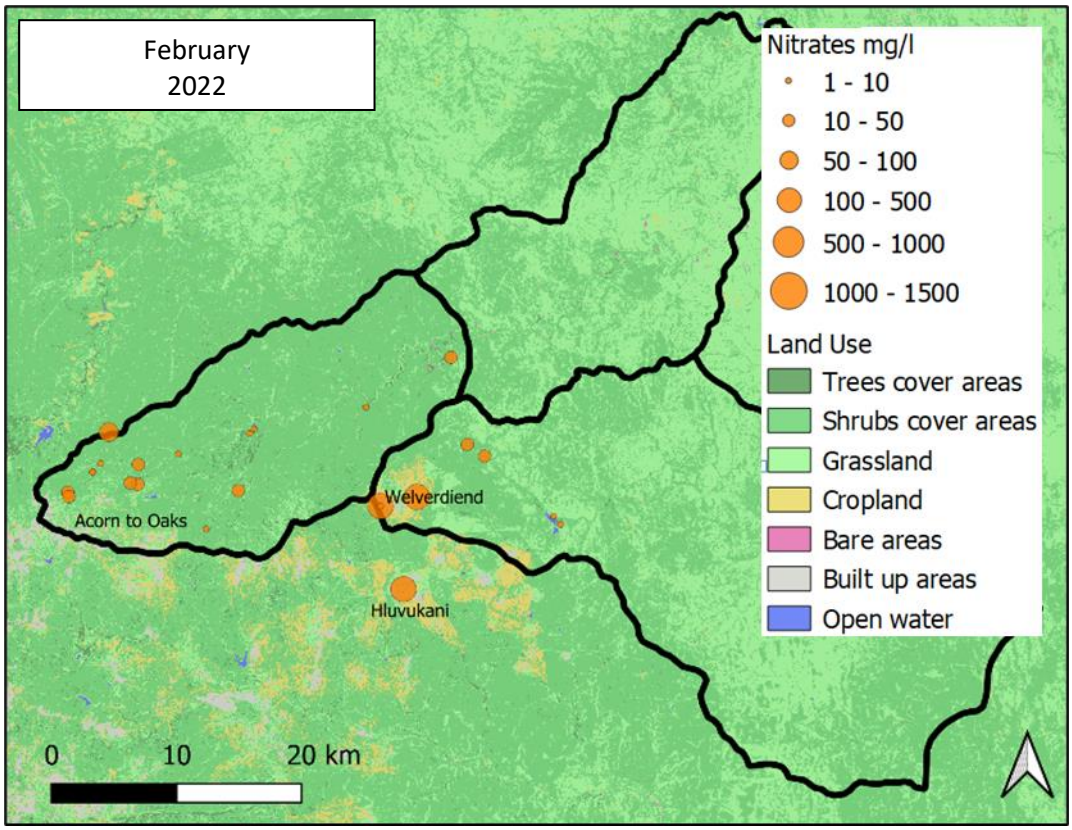

FIGURE 22: NITRATE CONCENTRATIONS AND LAND USE FOR WATER SAMPLES TAKEN IN FEBRUARY 2022.

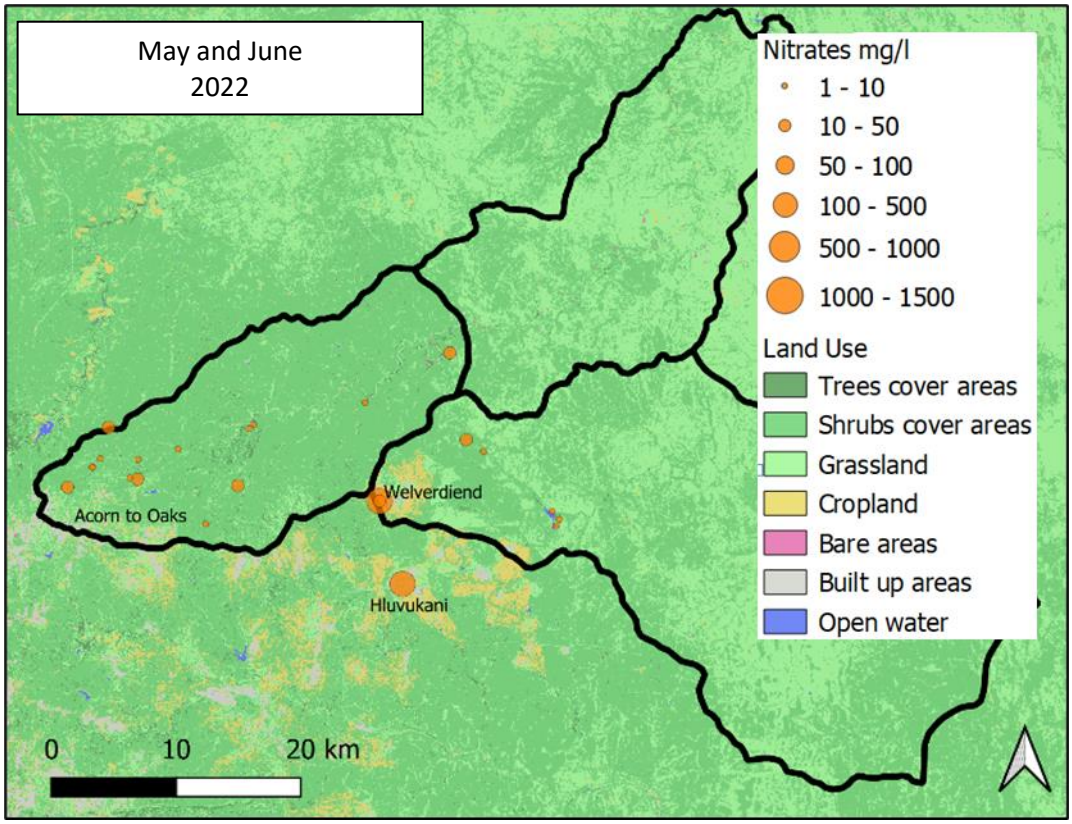

FIGURE 23: NITRATE CONCENTRATIONS AND LAND USE FOR WATER SAMPLES TAKEN IN MAY AND JUNE 2022.

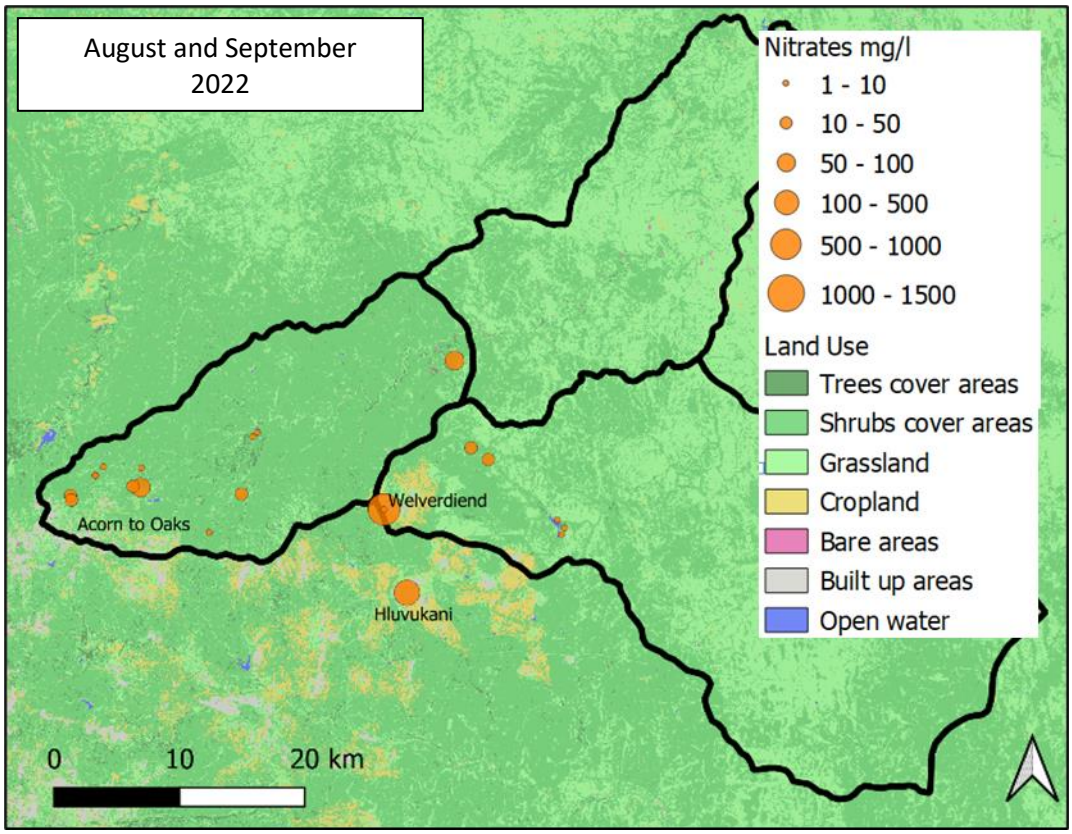

FIGURE 24: NITRATE CONCENTRATIONS AND LAND USE FOR WATER SAMPLES TAKEN IN AUGUST AND SEPTEMBER.

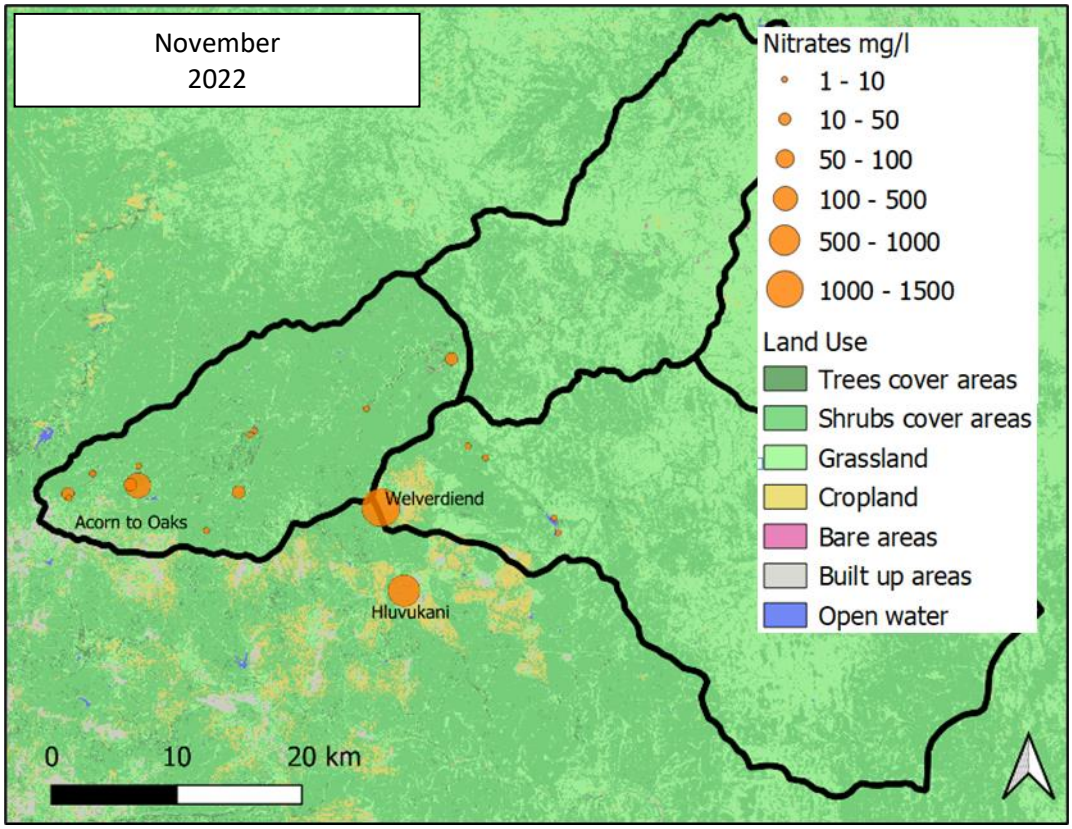

FIGURE 25: NITRATE CONCENTRATIONS AND LAND USE FOR WATER SAMPLES TAKEN IN NOVEMBER 2022.

5.2 Cations and Anions

Overall, the cation-anion balance shows good chemical data with only two samples having an error greater than 5%, namely ANDSW with -5.18% and WelASW -8.51%, see Table 7. The reasons for ion imbalances could be due to lab errors, some dissolved species not being analysed or the samples containing suspended particulate matter. Suspended matter such as carbonates could dissolve during the titration process used to determine alkalinity or cations could be adsorbed onto suspended solids in an exchange with the H^+ titrate and increasing the anion concentration of the sample (Hill Laboratories, 2023). Considering both these samples were taken from dams that were turbid in appearance the presence of suspended particles is the most likely reason for the larger cation concentration in comparison to the anion concentration.

TABLE 7: CATION ANION BALANCE FOR THE WATER SAMPLES. SAMPLES THAT EXCEEDED 5% ARE HIGHLIGHTED IN ORANGE.

Sample ID	Cation Anion Balance (%)
SCC	0,68
NOR	-1,35
A2O1	-4,19
A2O2	-4,60
SAN	-3,94
SANSW	-3,32
AND	-0,41
ANDSW	-5,18
Wits1	-3,95
Wits2	-4,76
WelA	-4,36
WelASW	-8,51
HLU	-4,06
THORSW1	-3,31
Xih	-2,14
MANM1	-4,85
MANM2	-4,33
MANSW	-4,00
MANT	-4,81
KM	-3,01
UPCell	-3,16
BAO	1,14

5.2.1 Piper Plot

From the Piper plot, Figure 26, it was observed that all but three of the water samples, WelA, HLU and UPCell, have similar cation and anion compositions. It can be seen that the majority of samples are located within the mixed cation and anion facies. The cation facies have compositions of Na^++K^+ ranging from 49% to 76%, Mg^{2+} from 12% to 29% and Ca^{2+} from 7% to 30%, therefore a predominantly Na^++K^+ composition and it can be seen from the Schoeller diagrams (Figure 27 and Figure 28) that Na^+ concentrations are significantly higher than the K^+ concentrations. While the anion facies have compositions ranging from 48% to 80% for HCO_3^-, from 17% to 49% for Cl^- and 1% to 9% for SO_4^{2-}. Apart from potassium, the cation and anion concentrations of the groundwater sample were higher than the surface water samples. UPCell differed from the rest in that it falls into the magnesium bicarbonate type category and has a cation composition of 66% Mg^{2+}, 19% Na^++K^+ and 15% Ca^{2+} and an anion composition of 71% HCO_3^-, 24% Cl^- and 4% SO_4^2. WelA and HLU are chloride types and have respective cation composition of 42%; 40% Na^++K^+, 32%; 32% Mg^{2+} and 26%; 28% Ca^{2+} and respective anion composition of 60%; 63% Cl^-, 36%; 31% HCO_3^- and 4%; 6% SO_4^2.

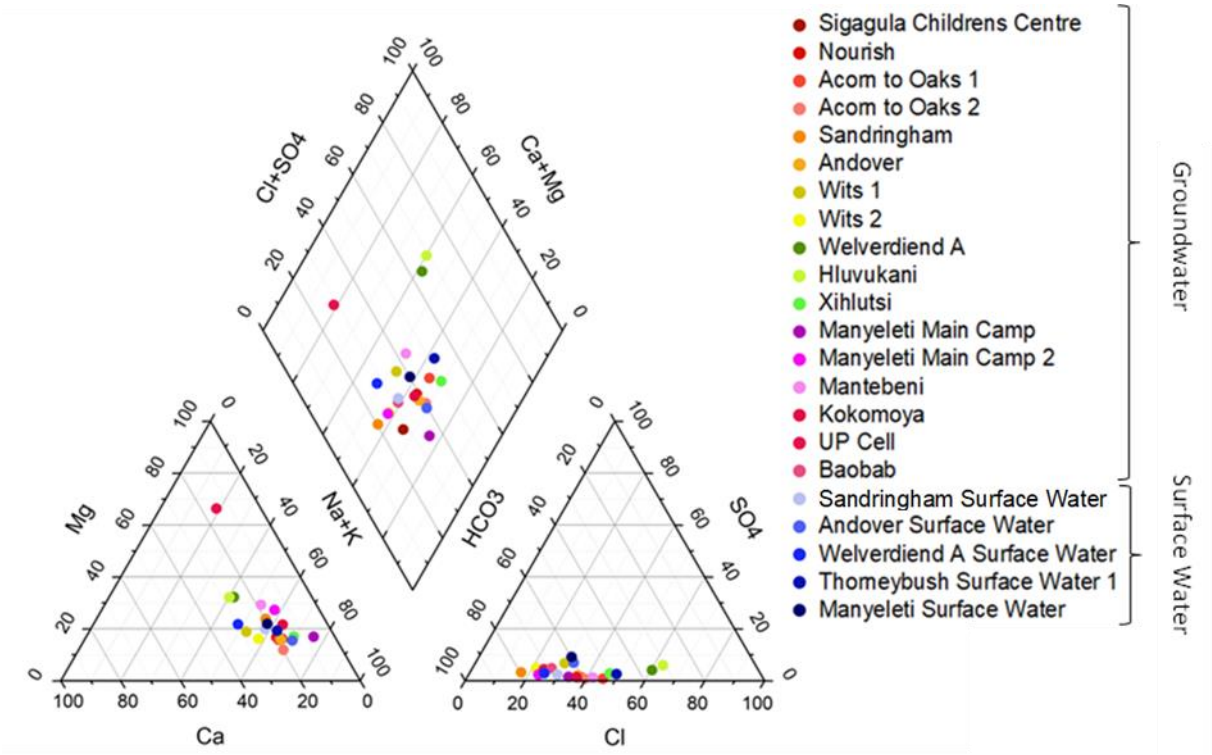

FIGURE 26: PIPER PLOT SHOWING THE CHEMISTRY OF THE GROUND AND SURFACE WATER SAMPLES COLLECTED DURING AUGUST AND SEPTEMBER 2022.

5.2.2 Schoeller Diagram

When looking at the Schoeller diagrams, Figure 27 and Figure 28, it can be seen that once again all the groundwater samples but WelA, HLU and UPCell followed the same trend. UPCell had a lower Na^+ concentration in comparison to the other samples. HLU and WelA had higher Cl^- concentrations when compared to the other groundwater samples. The surface water samples on average have lower ion concentrations, except for K^+, which is on average higher when compared to the groundwater samples. It appears that the surface water samples follow a similar trend to the groundwater samples but with less variation in the ion concentrations, except for THORSW1 which has a lower K^+ concentration more akin to those of the groundwater samples.

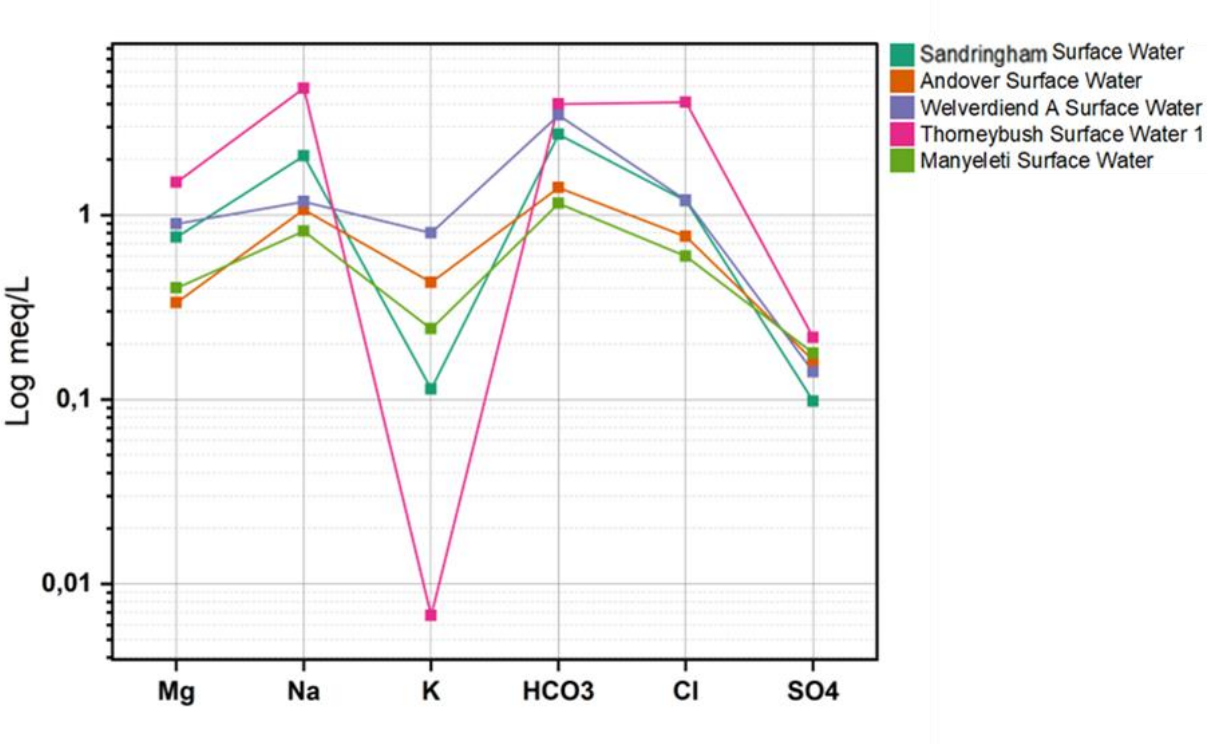

FIGURE 27: SCHOELLER DIAGRAM SHOWING THE CHEMISTRY OF SURFACE WATER SAMPLES TAKEN DURING AUGUST AND SEPTEMBER 2022.

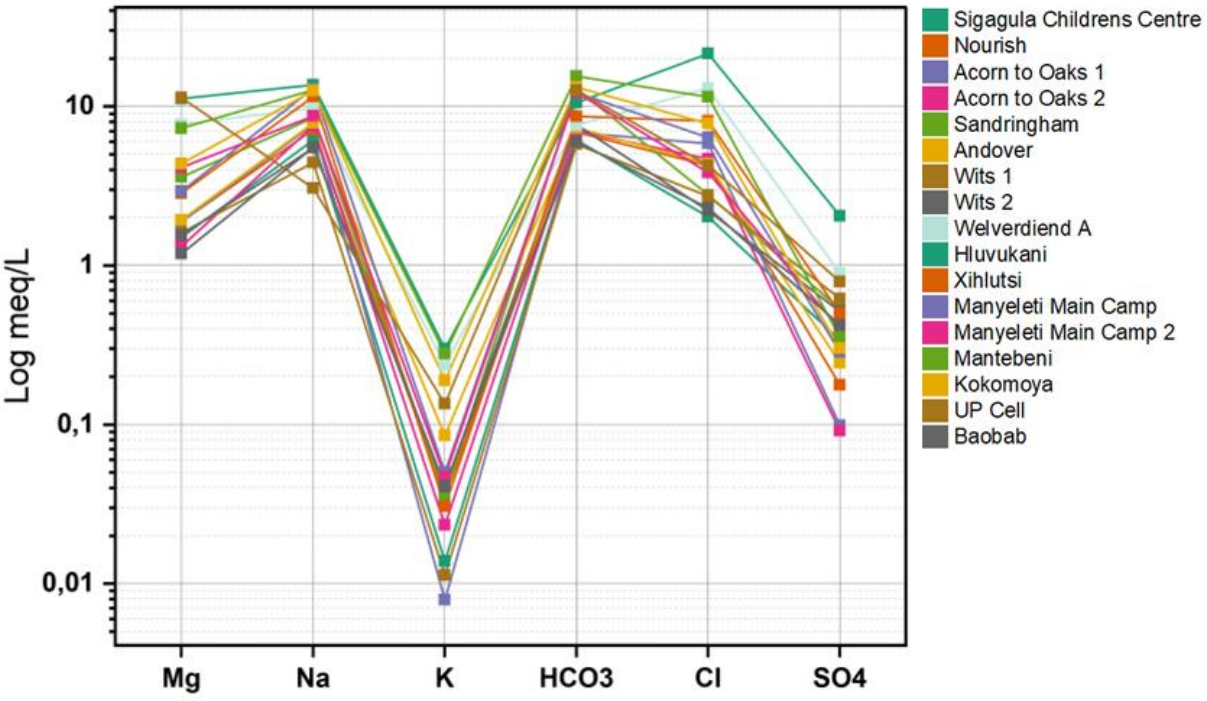

FIGURE 28: SCHOELLER DIAGRAM SHOWING THE CHEMISTRY OF GROUNDWATER SAMPLES TAKEN DURING AUGUST AND SEPTEMBER 2022.

5.2.3 Stiff Plots

Based on the shapes of the stiff plots, Figure 29 to Figure 31, the following water samples can be grouped together; SCC, NOR, A2O2, AND, Wits1, Wits2 and BAO of the groundwater samples and SANSW, ANDSW, WelASW and MANSW of the surface water samples, in these samples Na^++K^+ has the

highest concentration followed by HCO_3^- > Cl^- > Ca^{2+} > Mg^{2+} > SO_4^{2}. MANM, MANT and KM have a similar but slightly different composition to the previous samples consisting of Na^++K^+ > HCO_3^- > Mg^{2+} > Ca^{2+} > Cl^- > SO_4^{2-}. In the A2O1 sample Na^++K^+ has the highest concentration followed by Cl^- > HCO_3^- > Ca^{2+} > Mg^{2+} > SO_4^{2-}. Xih and THORSW1 are similar to A2O1 and have a composition of Na^++K^+ > Cl^- > HCO_3^-> Mg^{2+} > Ca^{2+} > SO_4^{2}. SAN has a composition of HCO_3^- > Na^++K^+ > Mg^{2+} > Ca^{2+} >= Cl^- > SO_4^{2-} and MANM2 has a similar composition consisting of HCO_3^- > Na^++K^+ > Mg^{2+} >= Cl^- > Ca^{2+} > SO_4^{2-}. In WelA and HLU, Cl^- has the highest concentration followed by Na^++K^+ > Mg^{2+} > Ca^{2+} > HCO_3^- > SO_4^{2-}. UPCell has the most unique shape with Mg^{2+} having the highest concentration with lower HCO_3^{2-} > Cl^- > Na^+ > K^+ > Ca^{2-} > SO_4^{2-} concentrations. When looking at the cation and anion concentrations of the samples THORSW1 had a composition that more closely resembled the groundwater samples and WelASW, SANSW and THORSW1 had higher ion concentrations than the other surface water samples.

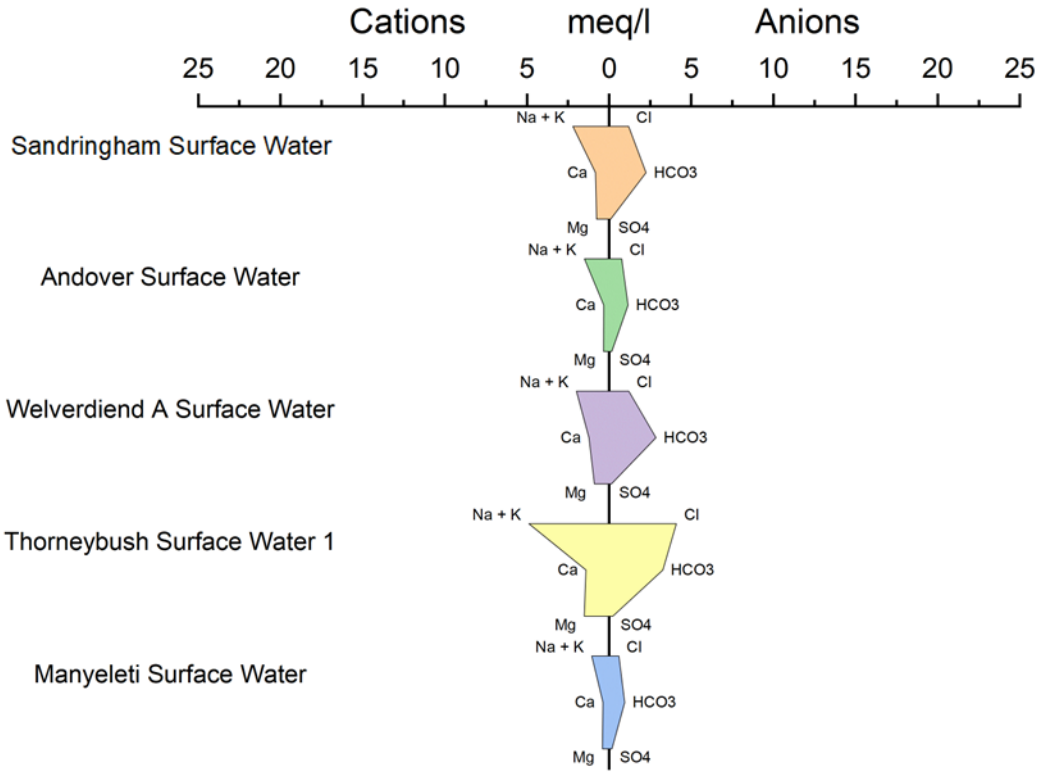

FIGURE 29: STIFF PLOT SHOWING THE CHEMISTRY OF THE SURFACE WATER SAMPLES COLLECTED DURING AUGUST AND SEPTEMBER 2022.

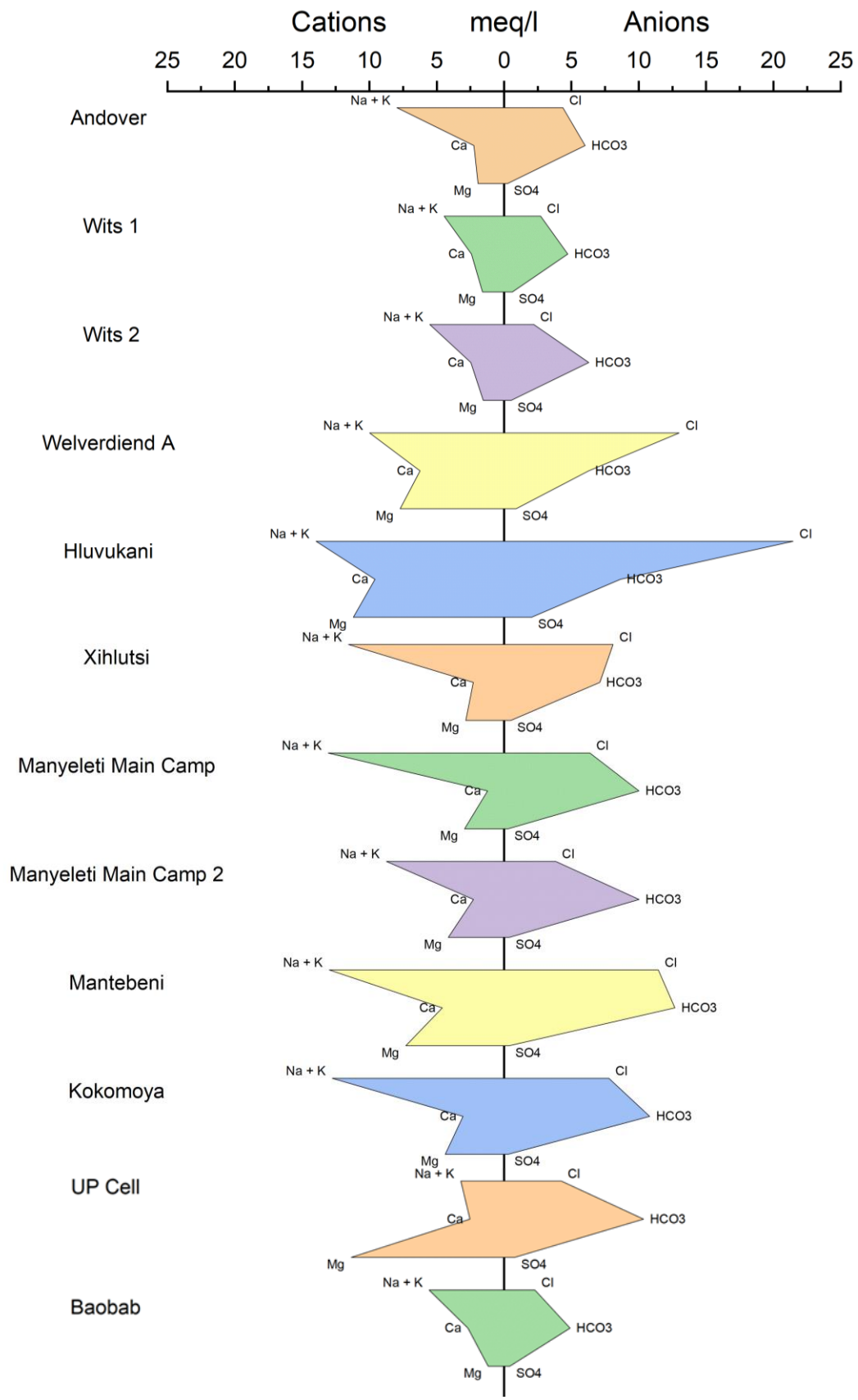

FIGURE 30: STIFF PLOT SHOWING THE CHEMISTRY OF THE GROUNDWATER SAMPLES COLLECTED DURING AUGUST AND SEPTEMBER 2022.

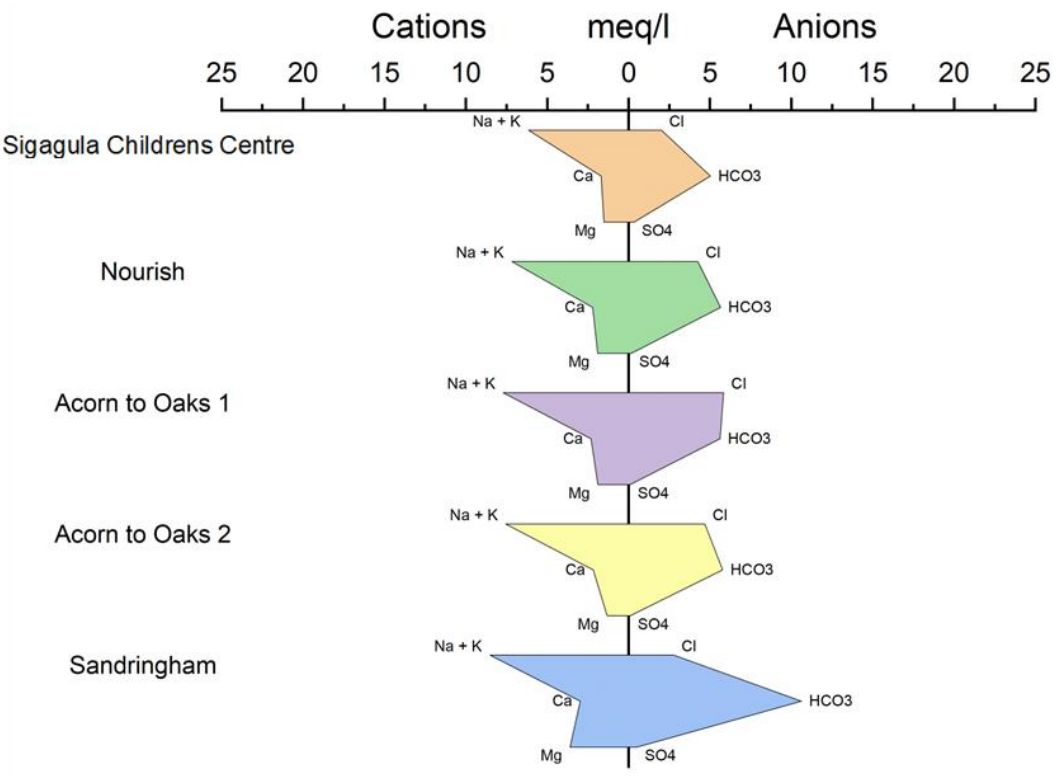

FIGURE 31: STIFF PLOT SHOWING THE CHEMISTRY OF THE GROUNDWATER SAMPLES COLLECTED DURING AUGUST AND SEPTEMBER 2022.

5.3 ICP Metal Scan

Figure 32 to Figure 35 show a summary of the results from the ICP-Metal scan in the form of logarithmic graphs. Of all the elements analysed during the metal scan only lithium, boron, aluminium, silicon, scandium, titanium, vanadium, manganese, iron, cobalt, nickel, copper, zinc, arsenic, rubidium, strontium, rhodium, caesium, barium, and europium were present in one or more of the samples with a concentration of 0.001 mg/l or above.

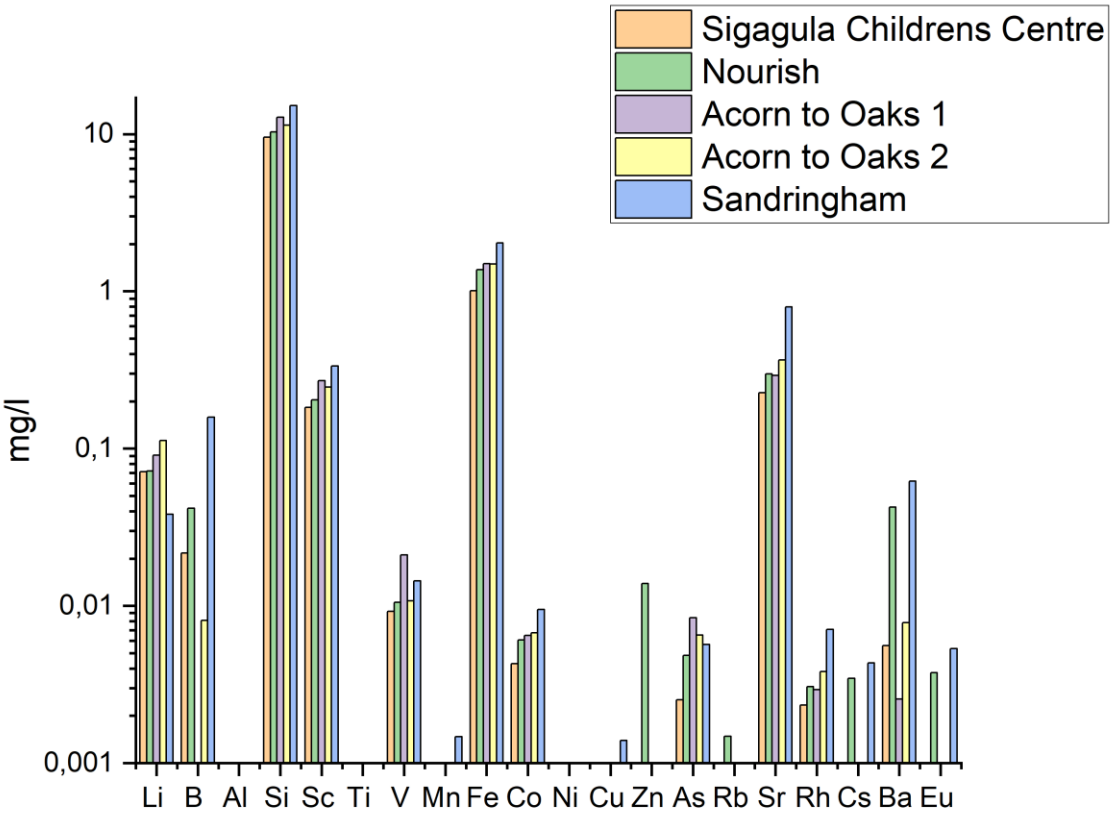

FIGURE 32: SUMMARISED RESULTS OF THE ICP- METAL SCAN FOR SAMPLES.

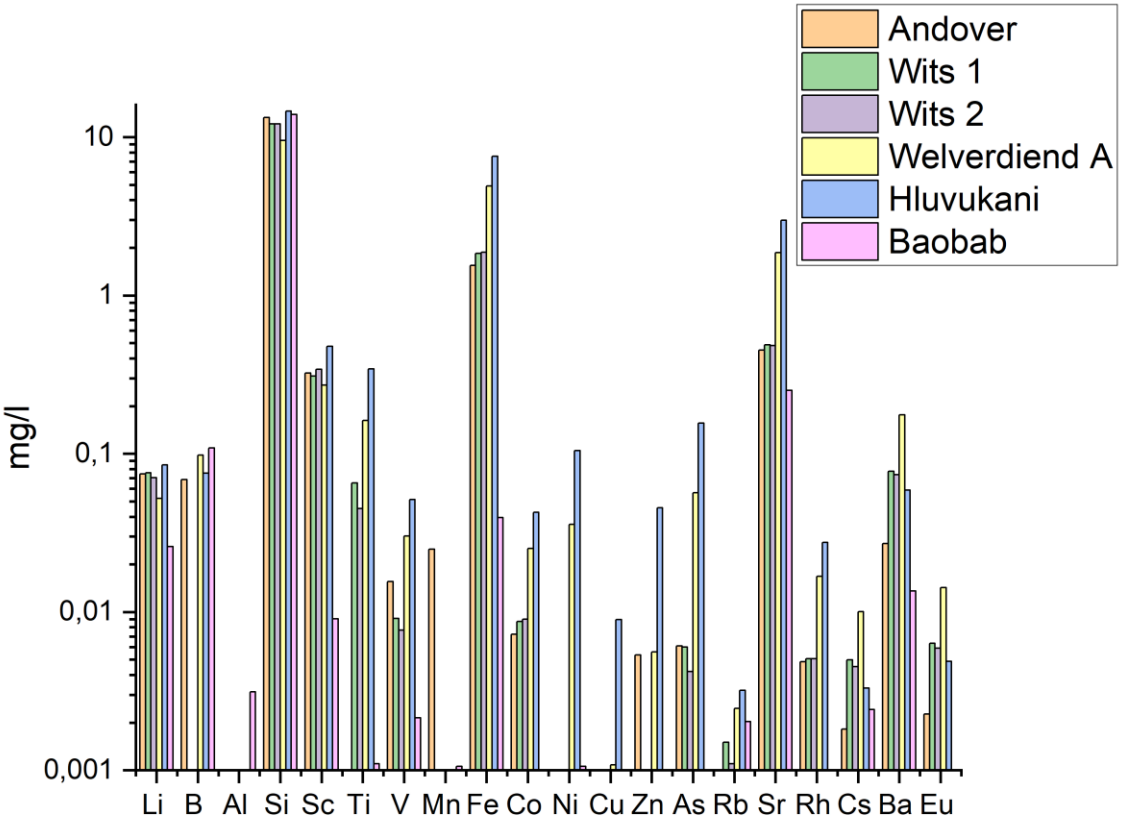

FIGURE 33: SUMMARISED RESULTS OF THE ICP- METAL SCAN FOR SAMPLES.

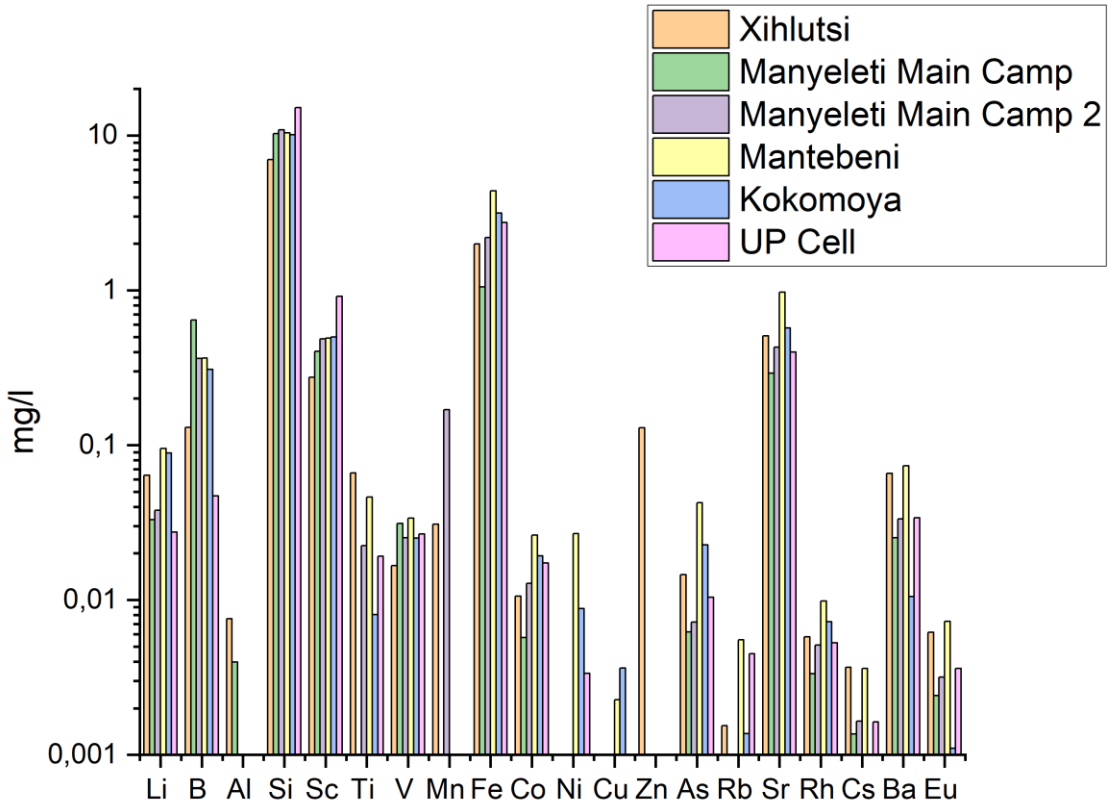

FIGURE 34: SUMMARISED RESULTS OF THE ICP- METAL SCAN FOR SAMPLES.

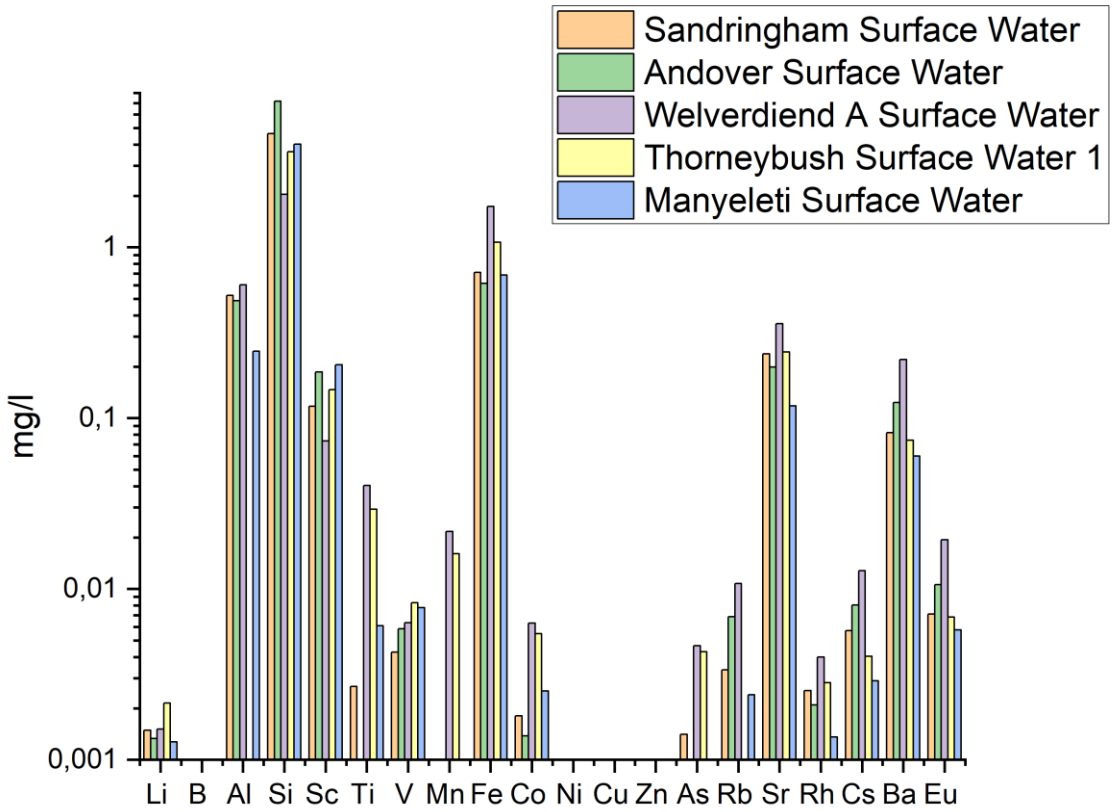

FIGURE 35: SUMMARISED RESULTS OF THE ICP- METAL SCAN FOR SAMPLES.

5.4 Radon

The RAD7 printout gives the arithmetic mean of the radon concentrations, the highest and lowest radon concentrations and the standard deviation of the readings taken during the run. The graphs below in Figure 36 show the relationship between mean radon and pH concentrations for the five rounds of sampling, an additional graph is also given showing the combined data for all five rounds of sampling. Figure 37 and Figure 38 shows the change in the average mean radon concentrations for the combined surface water and groundwater samples for each round of sampling. Figure 39 to Figure 43 show the mean radon concentrations for each round of sampling overlaying the geology of the study area in order to observe any links between underlying geology and radon concentrations.

The mean surface water radon concentrations ranged from 0 to 522 Bq/m^3 and had an average concentration of 119 Bq/m^3 while the mean groundwater sample concentrations ranged from 188 to 51400 Bq/m^3 with an average of 16900 Bq/m^3 (Figure 36).

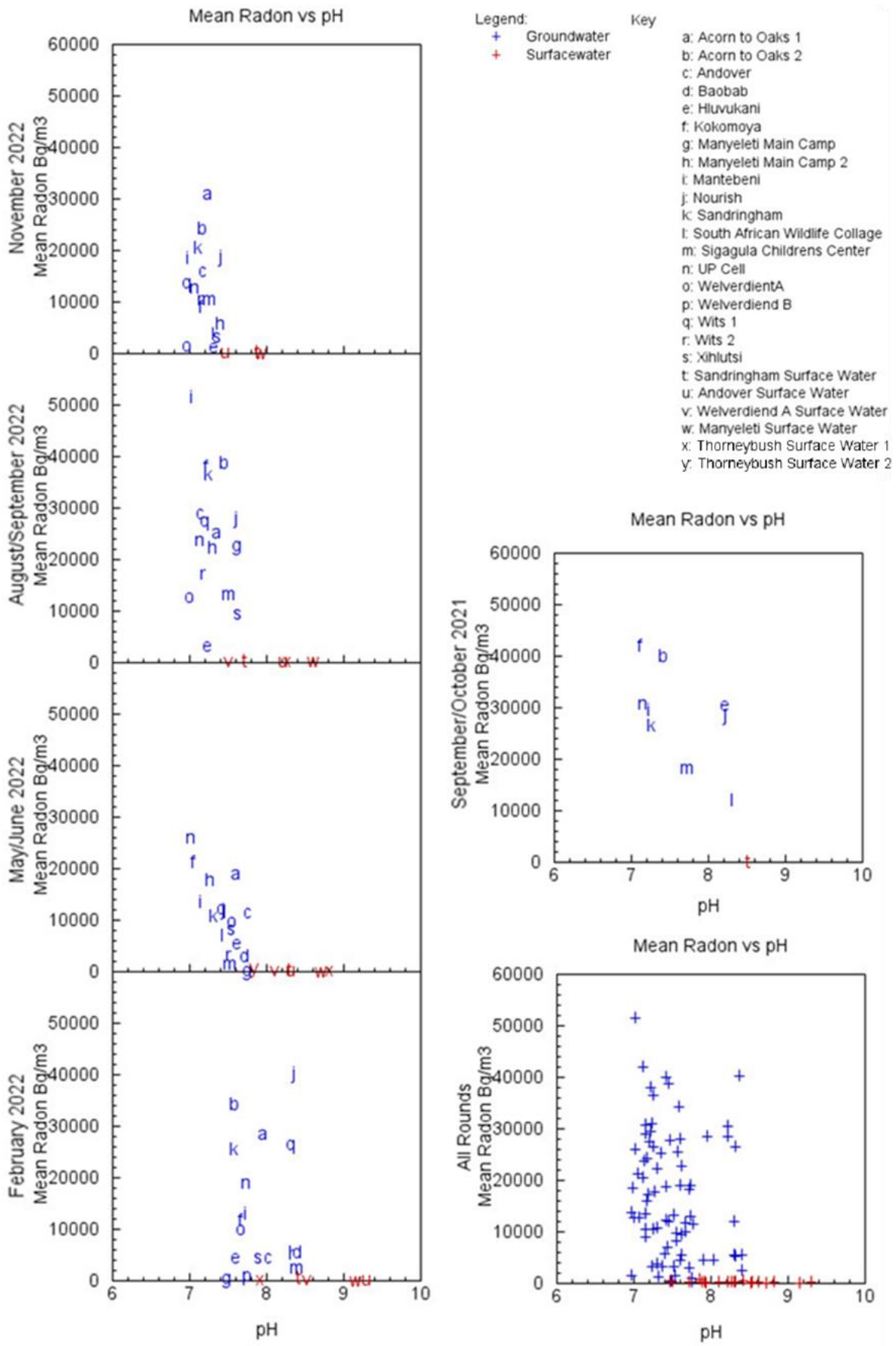

FIGURE 36: GRAPHS SHOWING THE RELATIONSHIP BETWEEN MEAN RADON CONCENTRATION AND PH FOR THE GROUNDWATER AND SURFACE WATER SAMPLES TAKEN DURING THE 5 ROUNDS OF SAMPLING.

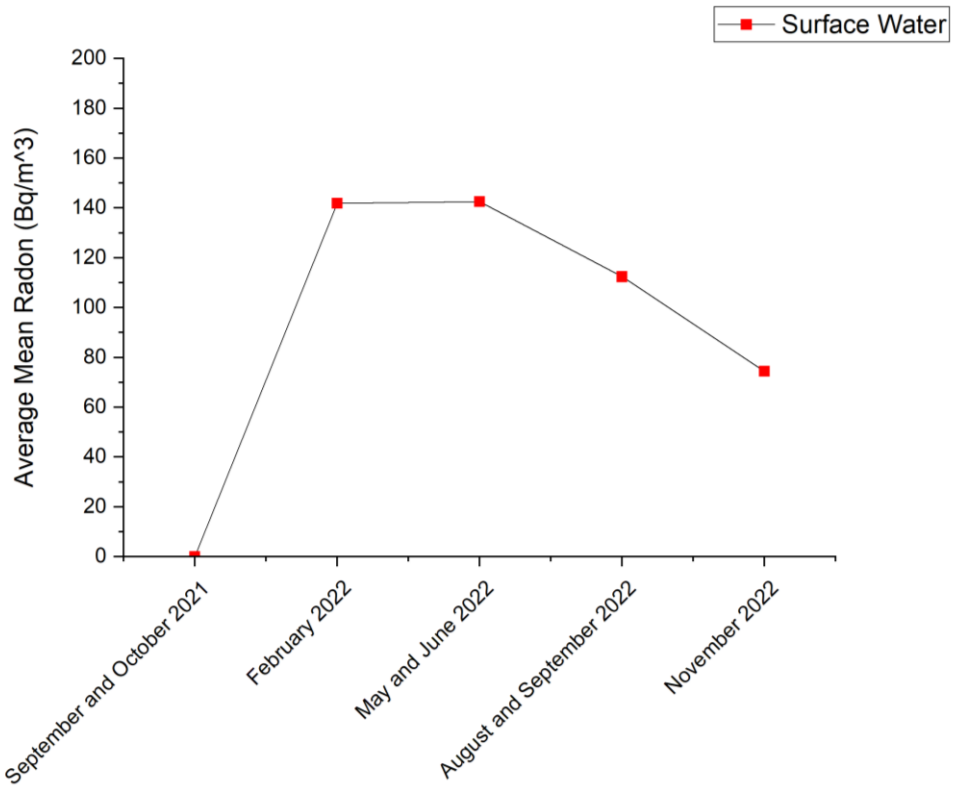

FIGURE 37: GRAPH SHOWING THE AVERAGE MEAN RADON CONCENTRATIONS FOR THE SURFACE WATER SAMPLES FOR EACH ROUND OF SAMPLING.

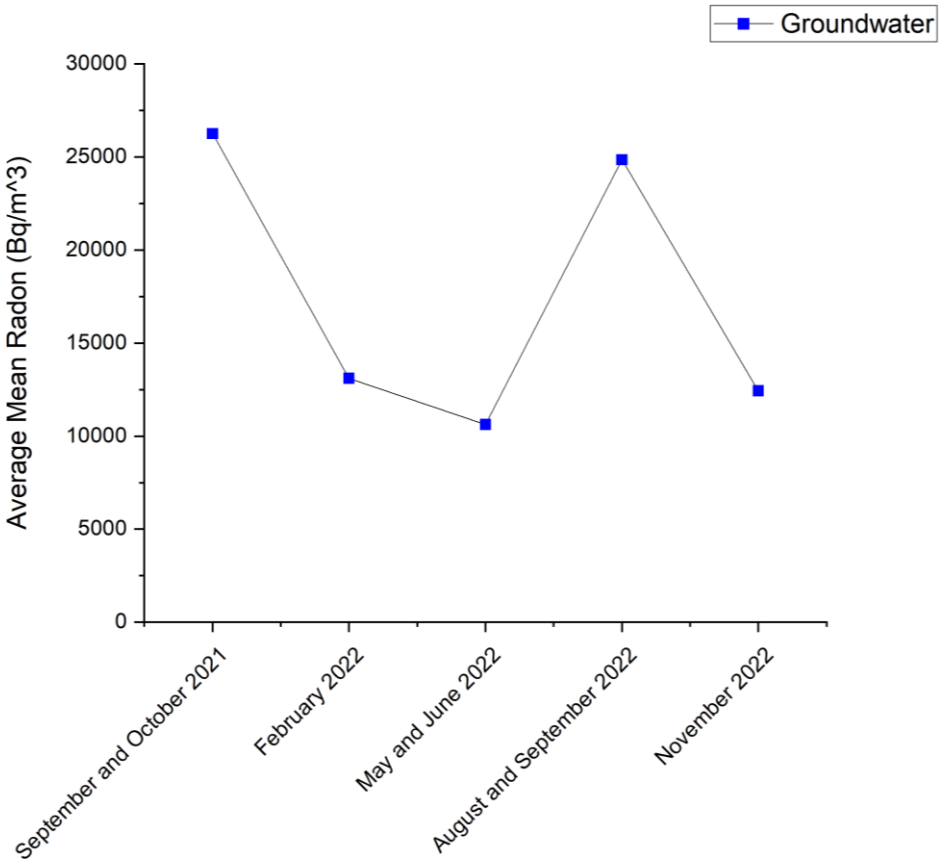

FIGURE 38: GRAPH SHOWING THE AVERAGE MEAN RADON CONCENTRATIONS FOR THE GROUNDWATER SAMPLES FOR EACH ROUND OF SAMPLING.

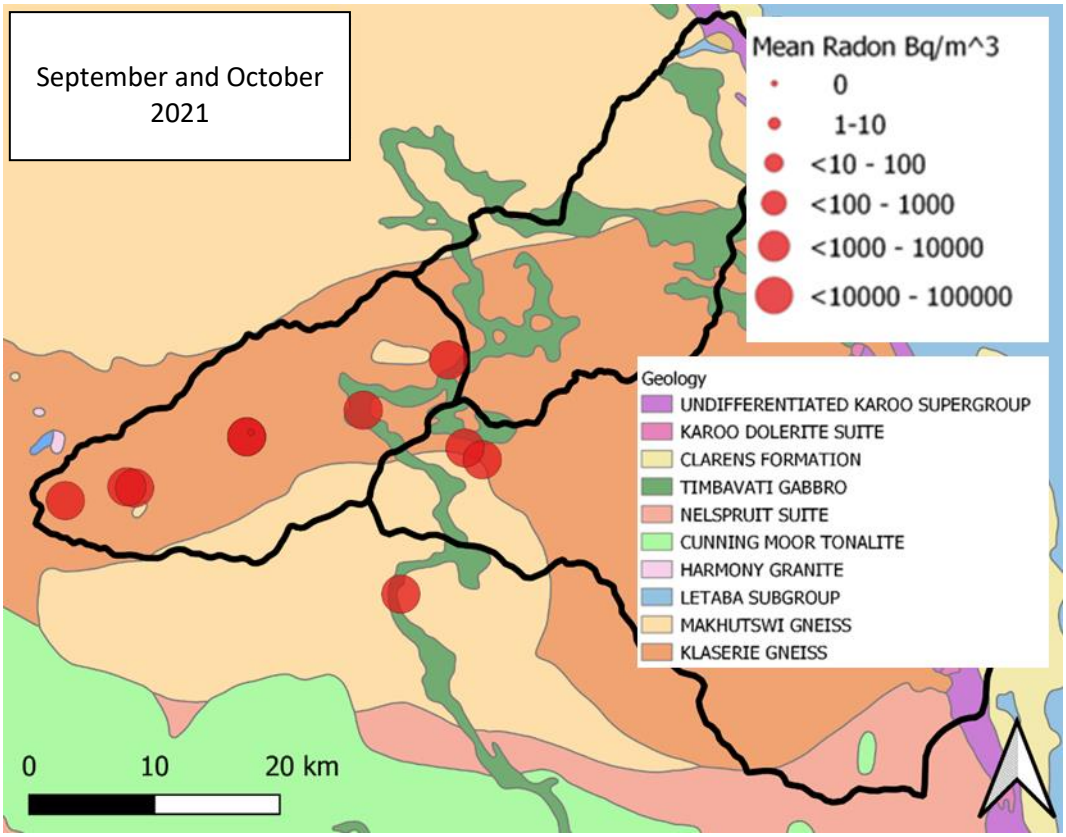

FIGURE 39: MEAN RADON CONCENTRATIONS FOR SAMPLES TAKEN DURING SEPTEMBER AND OCTOBER 2021.

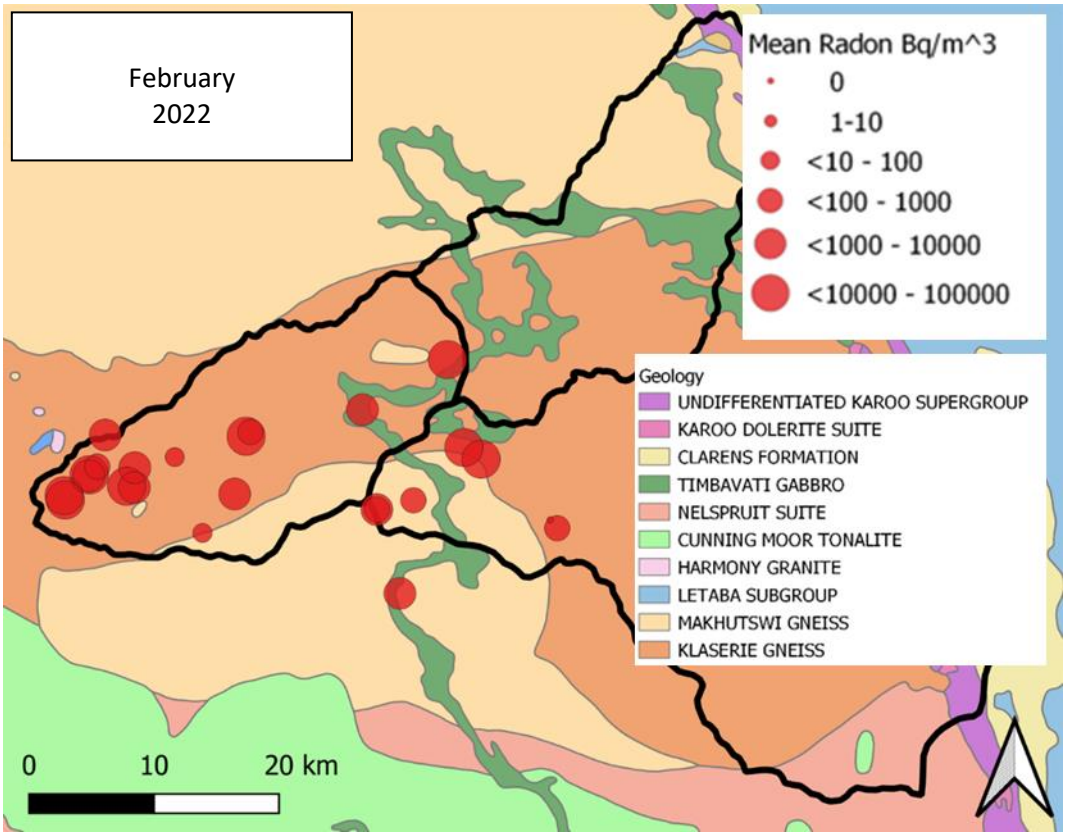

FIGURE 40: MEAN RADON CONCENTRATIONS FOR SAMPLES TAKEN DURING FEBRUARY 2022.

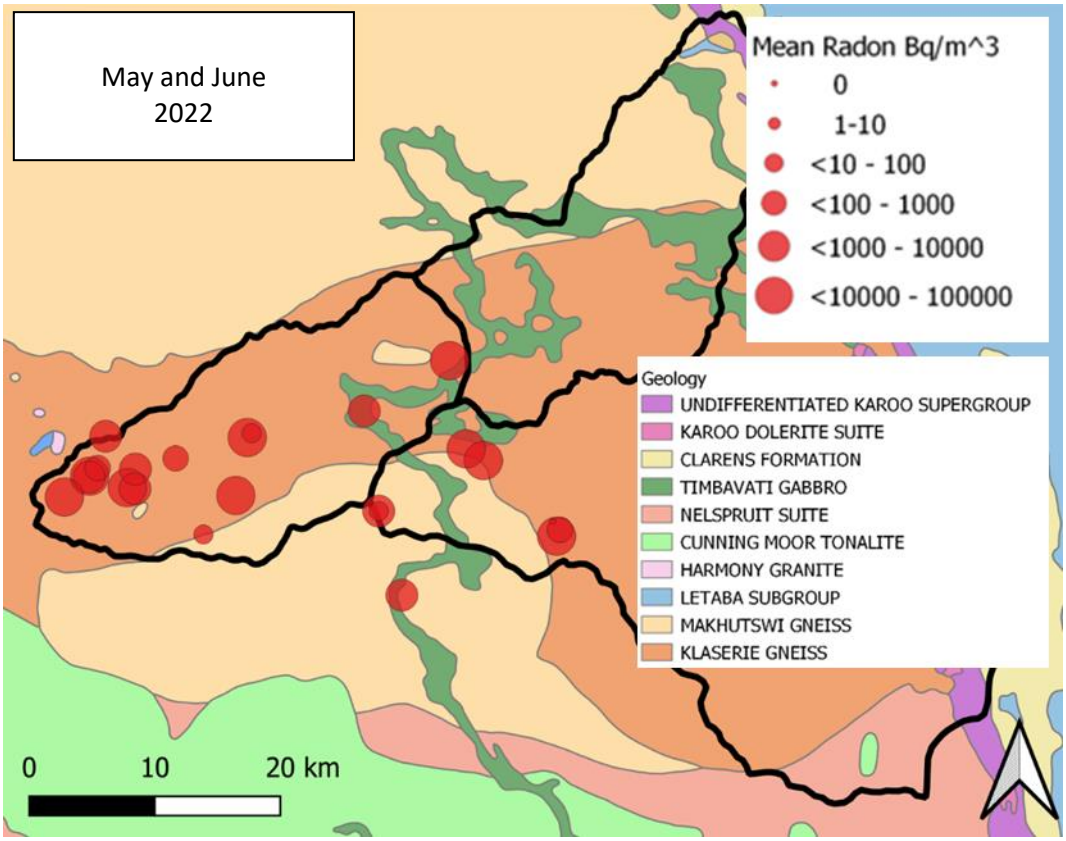

FIGURE 41: MEAN RADON CONCENTRATIONS FOR SAMPLES TAKEN DURING MAY AND JUNE 2022.

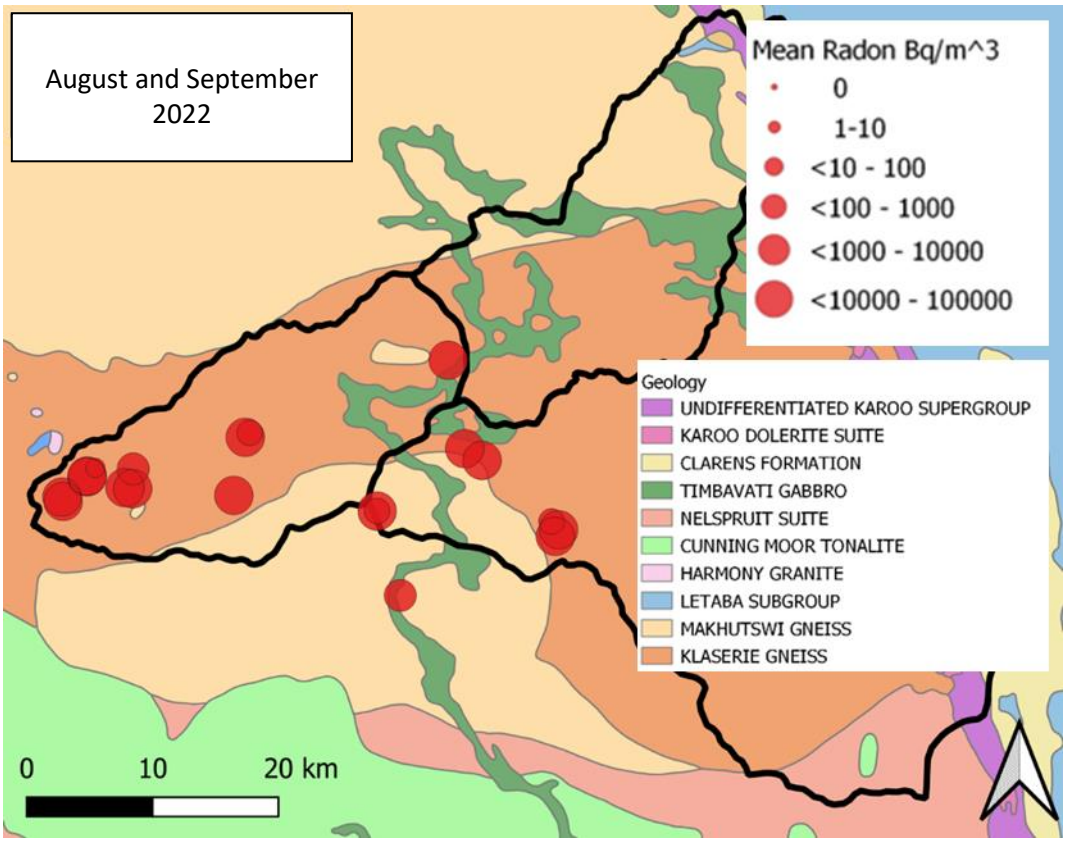

FIGURE 42: MEAN RADON CONCENTRATIONS FOR SAMPLES TAKEN DURING AUGUST AND SEPTEMBER 2022.

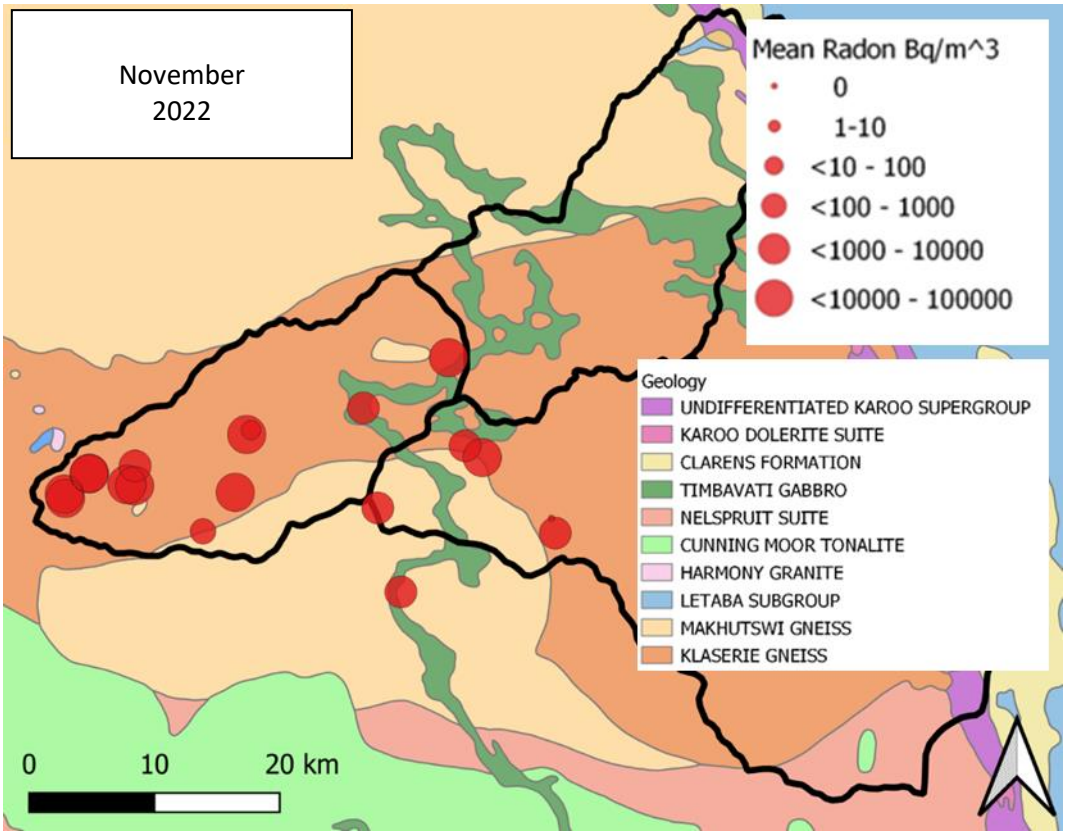

FIGURE 43: MEAN RADON CONCENTRATIONS FOR SAMPLES TAKEN DURING NOVEMBER 2022.

5.5 Hydrogen and Oxygen Isotopes

The variation between the mean ground and surface water samples isotope compositions is -32.7‰ for δD and -6.1‰ for $\delta^{18}O$. The graphs below in Figure 44 showing the relationship between δD (‰) and $\delta^{18}O$ (‰) for the five rounds of sampling, an additional graph is also given showing the combined data for all five rounds of sampling. Surface water samples were used to calculate the equation for the local evaporation line, $\delta D = 5.1\ \delta^{18}O + 0.3$. The weighted regression equation for the local meteoric water line is $\delta D = 6.2\delta^{18}O + 8.3$, while the regression line calculated for the groundwater had the equation of $\delta D = 4.9\ \delta^{18}O - 1.7$. Table 8 show the min, max and mean groundwater and surface water isotopic compositions.

TABLE 8: MIN, MAX AND MEAN GROUNDWATER AND SURFACE WATER ISOTOPE COMPOSITIONS.

	Min		Max		Mean	
	δD (‰)	**$\delta^{18}O$ (‰)**	**δD (‰)**	**$\delta^{18}O$ (‰)**	**δD (‰)**	**$\delta^{18}O$ (‰)**
Groundwater	-27.7	-0.8	-5.0	1.3	-20.5	-3.8
Surface water	-14.2	-2.2	41.9	7.5	12.2	2.3
Rain	-24.9	-4.8	33.1	5.4	-2.76	-1.9

Figure 45 gives the average δD (‰) and δ18O (‰) for the groundwater and surface water samples over the five rounds of sampling. It can be seen that the groundwater samples have a lighter isotopic composition when compared to the surface water samples. The monthly precipitation at Hans Hoheisen and the corresponding isotopic compositions of the monthly rainfall can be seen in Figure 46. It can be noted that the months with the lowest rainfall had the heaviest isotopic compositions.

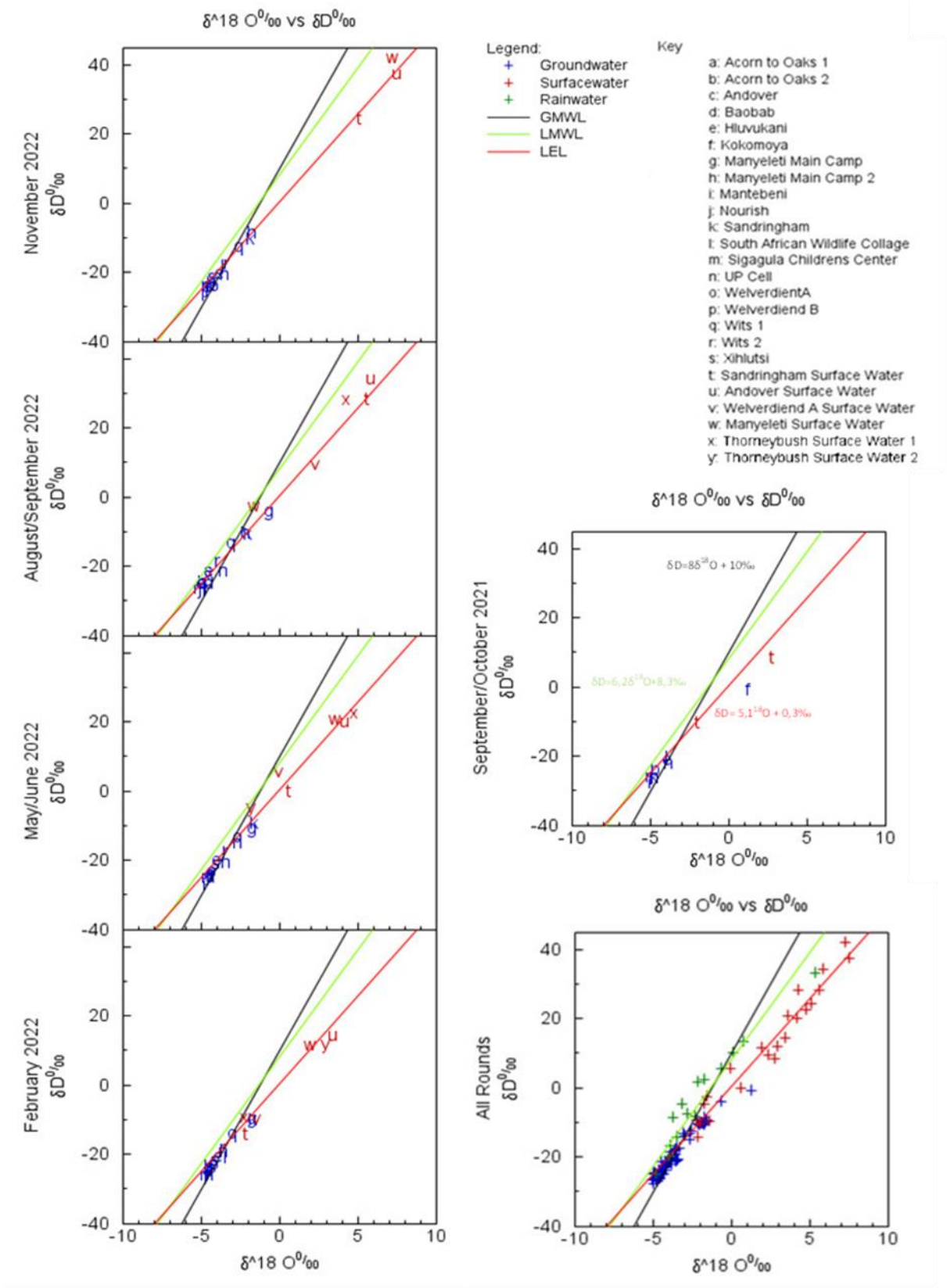

FIGURE 44: GRAPHS SHOWING THE RELATIONSHIP BETWEEN $\delta^{18}O$ AND δD FOR PRECIPITATION, GROUNDWATER AND SURFACE WATER SAMPLES TAKEN DURING THE 5 ROUNDS OF SAMPLING

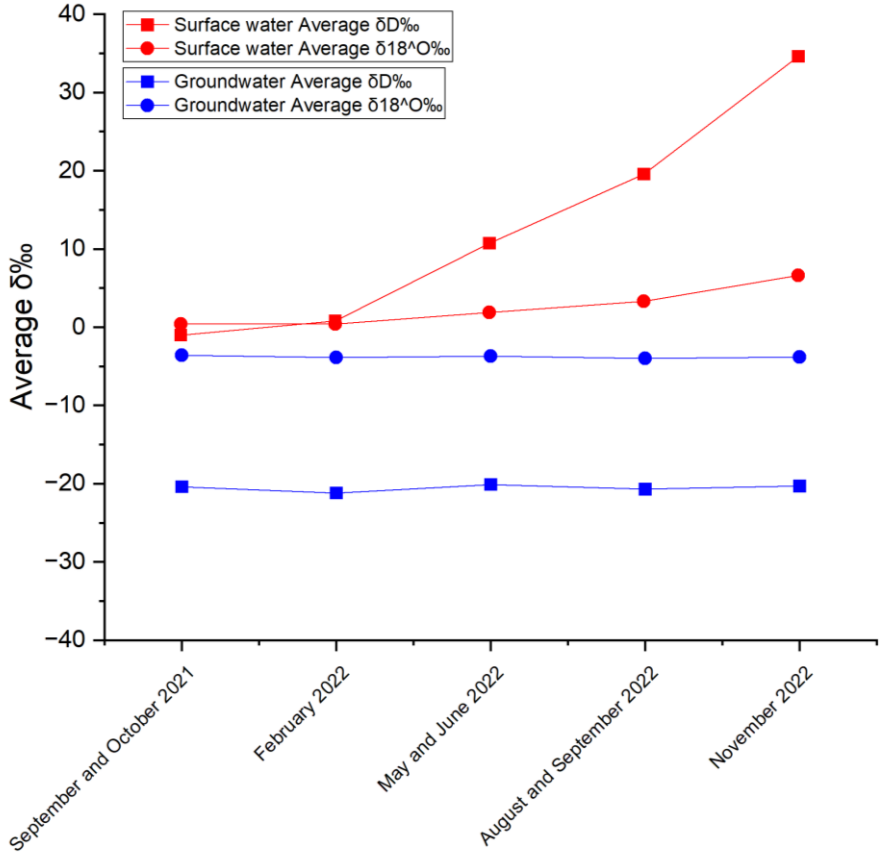

FIGURE 45: AVERAGE δD (‰) AND $\delta^{18}O$ (‰) FOR THE GROUNDWATER AND SURFACE WATER SAMPLES OVER THE FIVE ROUNDS OF SAMPLING.

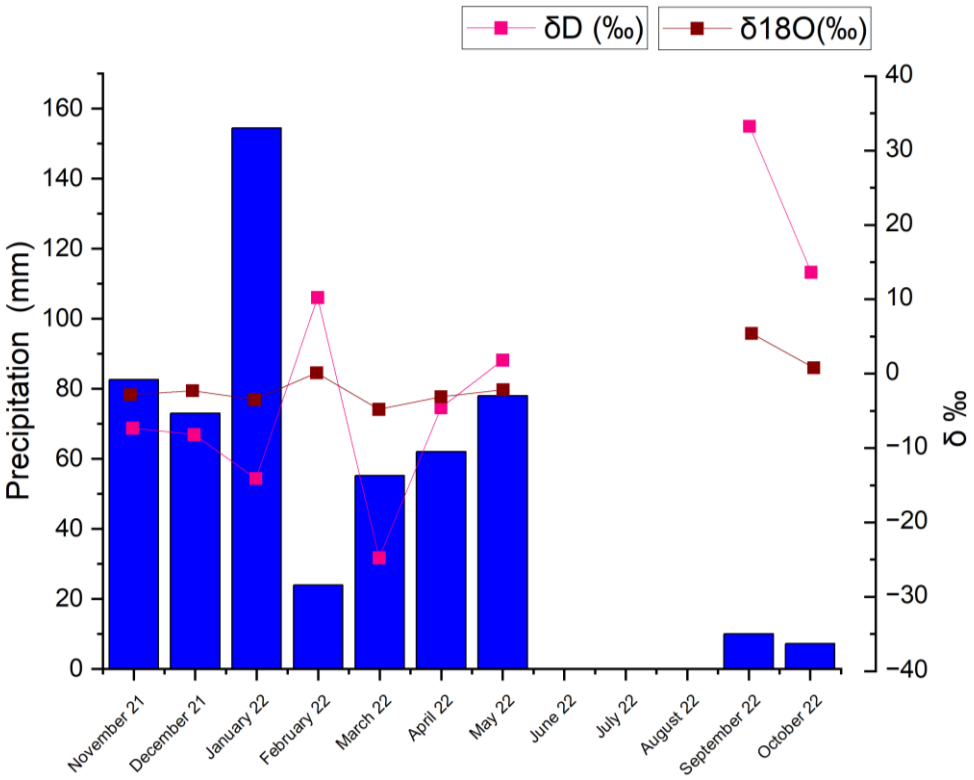

FIGURE 46: MONTHLY PRECIPITATION AT HANS HOHEISEN AND CORRESPONDING HYDROGEN AND OXYGEN ISOTOPE COMPOSITIONS.

6 Discussion

6.1 Groundwater Quality

Below in Table 9, the comparison of sample water quality with the WHO (2017) and SABS (2022) guidelines for drinking water can be seen. Some of the guidelines are purely for aesthetic purposes while others are for health purposes. Groundwater values are shown in blue and surface water in red. Values exceeding the recommended guidelines are highlighted in orange.

TABLE 9: WORLD HEALTH ORGANIZATION (2017) AND SOUTH AFRICAN BUREAU OF STANDARDS (2022) DRINKING WATER GUIDELINES COMPARED TO THE MIN, MAX AND MEAN VALUES OBTAINED DURING SAMPLING.

Constituent	Unit	Min	Max	Mean	WHO Guideline	SABS Guideline
pH		6.97	8.4	7.5		5 to 9.7
		7.47	9.3	8.34		
Total Dissolved Solids	mg/l	541	3580	1216	≤1000 (Aesthetic)	≤1200 (Aesthetic)
		139	622	326		
Ammonium (NH_4^+)	mg/l	0.03	0.75	0.20	≤35 (Aesthetic)	
		0.02	1.7	0.36		
Chloride (Cl^-)	mg/l	4.4	98	28	≤250 (Aesthetic)	
		4.7	10	7.7		
Sulphate (SO_4^{2-})	mg/l	4.4	98.3	24.3	≤250 (Aesthetic)	≤250 (Aesthetic) 500 (Health)
		4.7	10.4	7.7		
Fluoride (F^-)	mg/l	0	2.0	0.94	≤1.5	≤1.5
		0.29	0.37	0.13		
Calcium (Ca^{2+})	mg/l	25	190	62	≤200	
		6.5	28	17		
Magnesium (Mg^{2+})	mg/l	14	140	49	≤150	
		4.1	18	9.5		
Potassium (K^+)	mg/l	0.31	12	3.6	≤10	
		0.26	31	12		
Sodium (Na^+)	mg/l	100	314	196		≤200 (Aesthetic)
		19	48	46		
Iron (Fe^{2+})	mg/l	0.04	7.6	2.4	≤0.3 (Aesthetic)	≤0.3(Aesthetic) ≤2(Health)
		0.61	1.7	0.96		
Manganese (Mn^{2+})	mg/l	0.003	0.026	0.002	≤0.4	≤0.1 (Aesthetic) ≤0.4 (Health)
		0	0	0		
Boron (B^{3+})	mg/l	0	0.64	0.14	≤2.4	≤2.4
		0	0	0		
Aluminium (Al^{3+})	mg/l	0	0.0076	0.0008	≤0.2	≤0.3
		0	0.60	0.37		
Nickel (Ni^{2+})	mg/l	0	0.10	0.01	≤0.07	≤0.07
		0	0	0		
Copper (Cu)	mg/l	0	0.009	0.001	≤2	≤2
		0	0	0		
Arsenic (As^{3+})	mg/l	0.0007	0.16	0.02	≤0.01	≤0.01
		0.0006	0.005	0.002		
Barium (Ba^{2+})	mg/l	0.003	0.18	0.05	≤1.3	≤0.7
		0.06	0.22	0.1		

Figure 47 to Figure 54 are graphs showing where one or more of the samples exceeded the recommended WHO (2017) and SABS (2022) aesthetic or health guidelines.

Figure 47 shows the average TDS values for the groundwater samples compared with the WHO (2017) and SABS (2022) recommended aesthetic guidelines. Samples that exceeded both SABS and WHO guidelines were HLU, KM, MANT, WelA and WelB. Samples that exceeded only the WHO guidelines were MANM1, MANM2, NOR, SAN, SCC and Xih. According to the USGS (2018) classification samples that have TDS values above 1000 mg/l fall under brackish water. The rest of the samples with TDS values below 1000 mg/l can be considered fresh water. Samples with the highest TDS values, above 2000 mg/l, were found in the X40C quaternary catchment. This corresponds with values given in the Olifants Water Management Area Internal Strategic Perspective (DWAF, 2004).

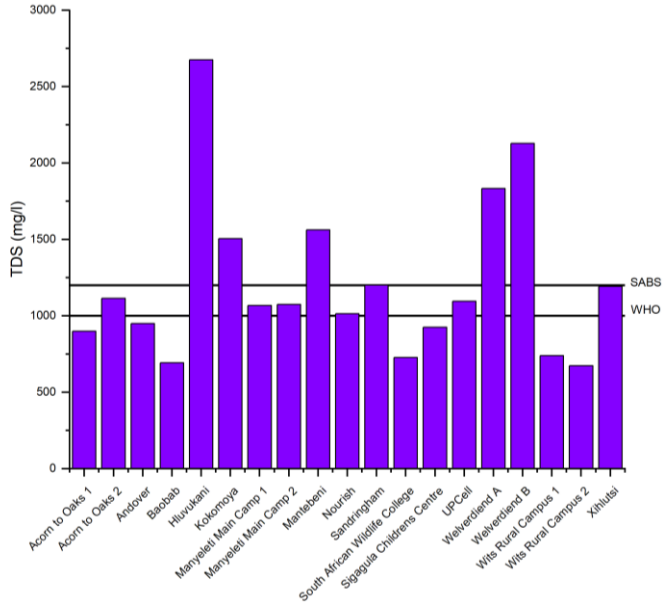

FIGURE 47: AVERAGE TDS VALUES FOR GROUNDWATER SAMPLES.

Samples that exceeded the recommended SABS aesthetic guidelines for sodium can be seen in Figure 48, these were WelA, HLU, Xih, MANM2, MANT and KM.

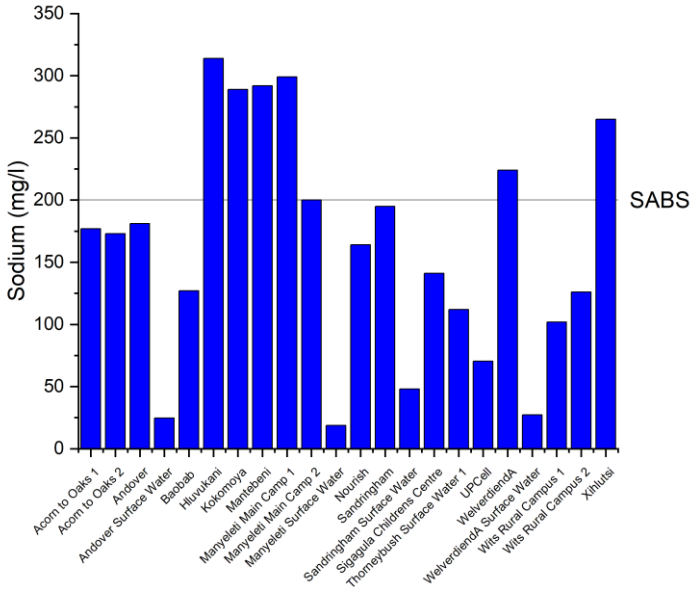

FIGURE 48: SODIUM CONCENTRATIONS COMPARED WITH SABS (2022) GUIDELINES.

Only four samples had potassium concentrations that exceeded the WHO recommended guidelines, MANT, HLU, ANDSW and WelASW, as seen in Figure 49.

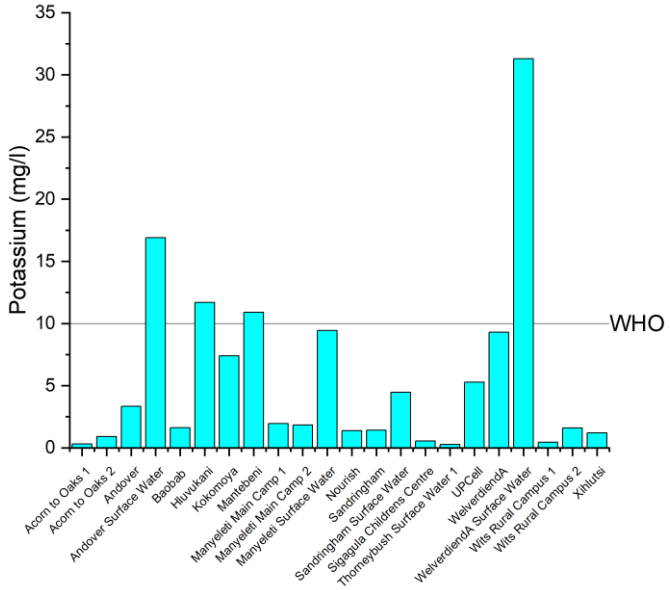

FIGURE 49: POTASSIUM CONCENTRATIONS COMPARED WITH WHO (2017) GUIDELINES.

The recommended WHO guideline for fluoride is 1.5 mg/l. The two samples that exceeded the guidelines were BAO and Xih as can be seen in Figure 50. High concentrations of fluoride can lead to painful skeletal deformations known as fluorosis (Jacks et al., 1993).

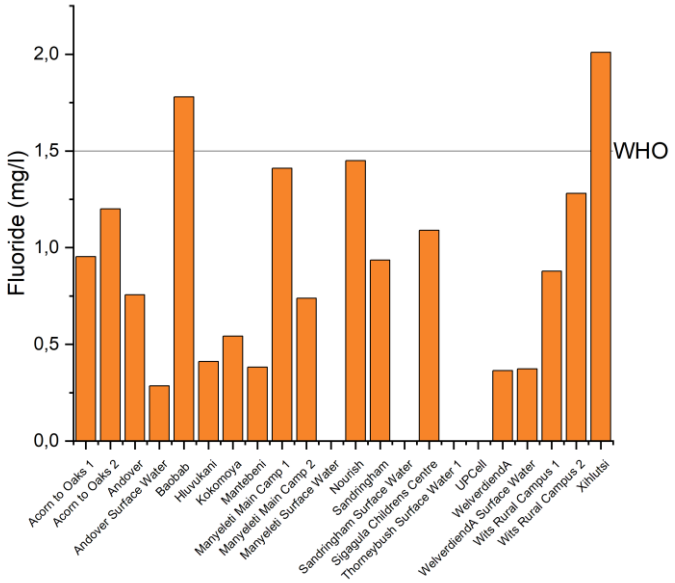

FIGURE 50: FLUORIDE CONCENTRATIONS COMPARED WITH WHO (2017) GUIDELINES.

According to Shmeis (2022), heavy metals are some of the most harmful water pollutants, because of their ability to bind to proteins and enzymes and disturb their functions. Heavy metals such as arsenic and nickel are very poisonous and therefore the WHO (2017) and SABS (2022) recommended guidelines are low. For example, arsenic poisoning can result in skin lesions, hyperkeratosis, skin cancer and liver disease (Karim, 2000). At around neutral pH heavy metals remain fixed by sorption or

solid equilibrium, however, under more acidic conditions they become mobilized (Appelo and Postma, 2005).

Arsenic is naturally released into the environment by the weathering of arsenic-bearing rocks, oxidation of arsenic-bearing sulphide minerals, arsenic desorption from the surface of mineral iron or manganese's oxides, reductive dissolution of iron oxides and due to evaporative concentration in arid and semi-arid regions (Irunde et al., 2022). The anthropogenic sources of arsenic are processes such as mining, agricultural pesticide application, industrial discharge and landfilling of sewage sludge are also potential sources of arsenic. While climate factors such as droughts and flooding as well as land use patterns and the depth of aquifers can also contribute to arsenic release into groundwater. Irunde et al. (2022) conducted a review of the general arsenic occurrence concepts and spatial variability on the limited arsenic studies conducted in Africa and found that while both anthropogenic and geogenic activities are indicated as sources of high arsenic levels in aquatic environments most studies focus primarily on the anthropogenic sources.

The six samples that had arsenic levels above the WHO guidelines are HLU, WelA, MANT, KM Xih and UPCell, Figure 51. HLU had by far the highest arsenic concentration with 0.16 mg/l. The concentrations of arsenic, iron and nickel are much higher in HLU compared with WelA which is on the same geology, however, it is not in the same catchment. The groundwater sample was taken from the borehole at Hluvukani Animal Clinic. The clinic is located in the middle of the town of Hluvukani. The source of the heavy meals is likely both anthropogenic and geogenic activities, with anthropogenic sources being the major contributing factor. This would however need to be confirmed with further research and sampling.

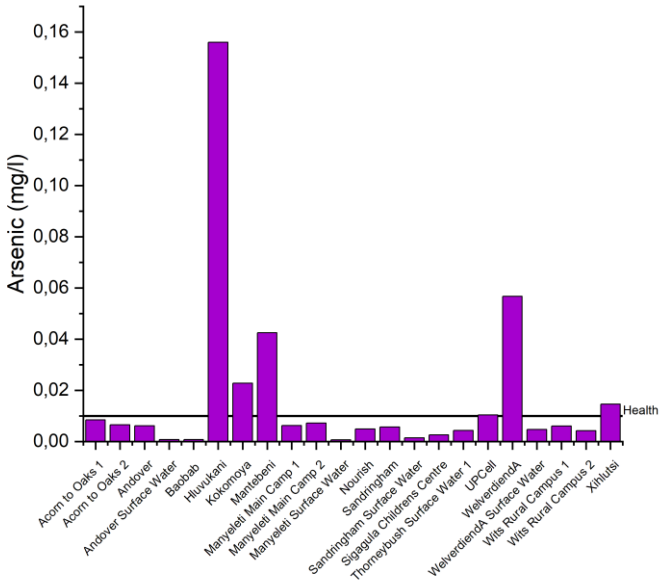

FIGURE 51: ARSENIC CONCENTRATIONS COMPARED WITH THE WHO (2017) AND SABS (2022) GUIDELINES FOR HEALTH PURPOSES.

Four of the samples had aluminium concentrations above the WHO (2017) recommended guideline, WELASW, SANDSW, ANDSW and MANMSW as seen in Figure 52. MANMSW is the only one of these three samples falling below the SABS (2022) guideline. All of these were surface water samples taken from dams. In 1984 Miller et al. looked at the occurrence of aluminium in drinking water across the USA. Based on their data they found that aluminium is more likely to exist in surface waters than in groundwater, with only 9% of their groundwater samples containing detectable amounts of aluminium compared with 78% of the surface water samples. While the weathering of amphiboles,

biotite and clay minerals could be the source of aluminium, the fact that it is only present in the surface water samples suggests that atmospheric input is a far more likely source (Appelo and Postma, 2005).

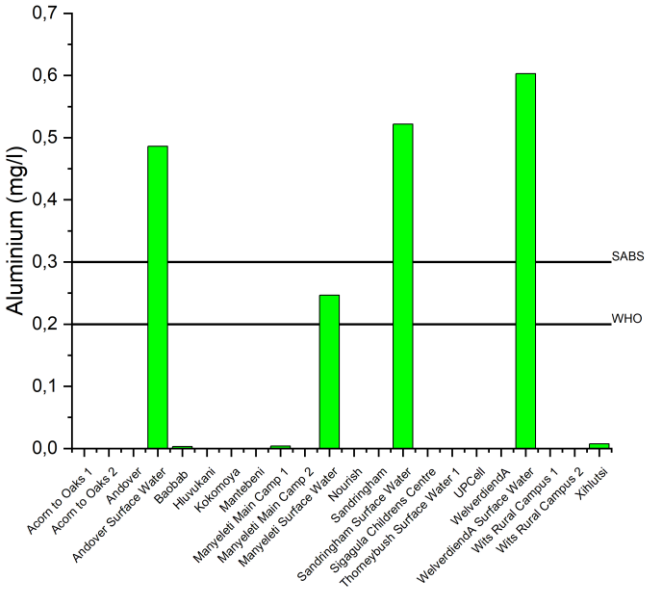

FIGURE 52: ALUMINIUM CONCENTRATIONS COMPARED WITH WHO (2017) AND SABS (2022) GUIDELINES.

All the samples have iron concentrations above the SABS (2022) recommended guidelines for taste and can be seen in Figure 53. This could be one of the contributing factors towards the poor taste of the water. Six of the samples had concentrations above the recommended SABS (2022) health guidelines: WelA, HLU, MANM2, MANT, KM and UPCell. HLU,

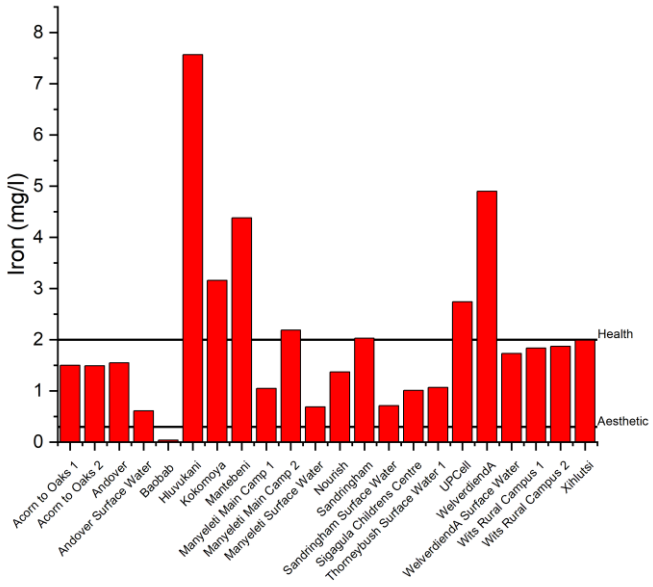

FIGURE 53: IRON CONCENTRATIONS COMPARED WITH THE SABS (2022) GUIDELINES FOR AESTHETIC AND HEALTH PURPOSES.

Figure 54, was the only sample that exceeded the WHO standard for nickel with 0.1 mg/l. According to Welch et al. (2000), high arsenic concentrations in groundwater can be found in inland basins in arid and semi-arid climates as well as in alluvial plain sediments with strongly reduced groundwater.

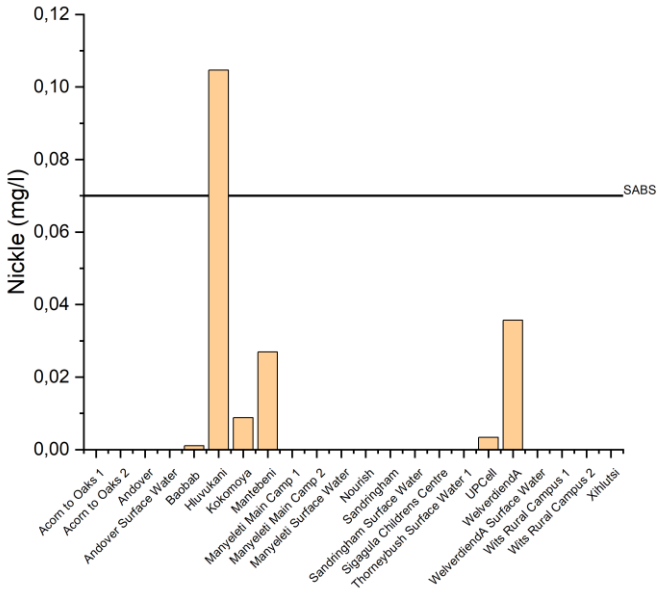

FIGURE 54: NICKEL CONCENTRATIONS COMPARED WITH THE SABS (2022) GUIDELINES FOR AESTHETIC AND HEALTH PURPOSES.

6.2 Water Chemistry

The Olifants Water Management Area Internal Strategic Perspective (DWA, 2004) stated that the TDS values in the B73E and F quaternary catchments are between 500 and 2000 mg/l which corresponds with the data collected during the sampling. Groundwater and surface water TDS values are shown in comparison to the $\delta^{18}O$ compositions of the samples in Figure 55 below.

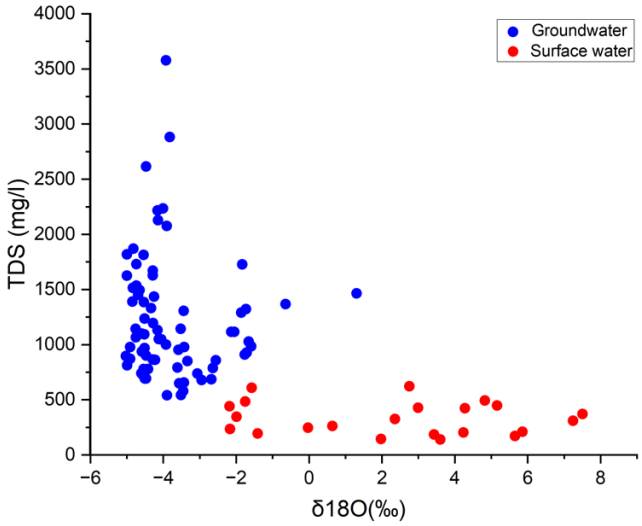

FIGURE 55: A COMPARISON OF $\delta^{18}O$ AND TDS CONCENTRATIONS IN GROUNDWATER AND SURFACE WATER SAMPLES.

The higher TDS values are found in the groundwater samples; however, these samples also have the lowest $\delta^{18}O$ values. The lower $\delta^{18}O$ values indicate a lighter isotopic composition. During evaporation the lighter isotopes (e.g. $^{1}H_2{}^{16}O$) evaporate first, leaving behind liquid water that is enriched in heavier isotopes. Therefore, the lighter isotopic composition is evidence that little to no evaporation has taken place. The lower TDS values are found in the surface water samples where there is evidence of evaporation in the form of the heavier isotopic composition. This is evidence that the source of the solutes is from weathering and water-rock interactions and not from evaporation.

The Makhutswi and Klaserie Gneiss consist primarily of plagioclase ($NaAlSi_3O_8 – CaAl_2Si_2O_8$), microcline ($KAlSi_3O_8$), quartz ($SiO_2$) and biotite ($K(Mg,Fe)_3AlSi_3O_{10}(F,OH)_2$) (Schutte , 1986; Robb, et al., 2006).
The Timbavati Gabbro consists primarily of olivine ($(Mg,Fe)_2SiO_4$), clinopyroxene ($Ca(Mg,Fe)Si_2O_6$), orthopyroxene ($(Mg,Fe,Ca)(Mg,Fe,Al)(Si,Al)_2O_6$) and plagioclase ($NaAlSi_3O_8 – CaAl_2Si_2O_8$,) (Walraven, 1986).

The weathering of silicate minerals results in the addition of cations and silica to the water chemistry. The following equations are taken from Appelo & Postma (2005) and show the weathering reactions of albite, anorthite, microcline and biotite to kaolinite:

$$2Na(AlSi_3)O_8 + 2H^+ + 9H_2O \rightarrow Al_2Si_2O_5(OH)_4 + 2Na^{2+} + 4H_4SiO_4$$

EQUATION 2

$$Ca(Al_2Si_2)O_8 + 2H^+ + H_2O \rightarrow Al_2Si_2O_5(OH)_4 + Ca^{2+}$$

EQUATION 3

$$2K(AlSi_3)O_8 + 2H^+ + 9H_2O \rightarrow Al_2Si_2O_5(OH)_4 + 2K^+ + 4H_4SiO_4$$

EQUATION 4

$$2K(Mg_2Fe)(AlSi_3)O_{10}(OH)_2 + 10H^+ + 0.5O_2 + 7H_2O \rightarrow Al_2Si_2O_5(OH)_4 + 2K^{2+} + 4Mg^{2+} + 2Fe(OH)_3 + 4H_4SiO_4$$

EQUATION 5

The sample sites overlying the corresponding geology can be seen in Figure 56. Based on the cation and anion concentrations of the groundwater samples, as observed in the Piper plot, Schoeller diagrams and Stiff plots, the samples could be divided into three groups. Most of the samples fall into group 1. They have a composition where Na^++K^+ is the highest cation concentration and HCO_3^- is the highest anion concentration, the samples that belong to this group are SCC, NOR, A201, A202, SAN, AND, Xih, MANT, KM, WITS1, WITS2, BAO, MANM1 and MANM2. The sample sites are situated on the Klaserie Gneiss. Group 2 is situated primarily on the Makhutswi Gneiss. They have a composition where Na^++K^+ is the highest cation concentration and Cl^- is the highest anion concentration, the samples that belong to this group are, WELA and HLU. UPCell is the only sample in group 3. It has a composition where Mg^{2+} is the highest cation concentration and HCO_3^- is the highest anion concentration. While the geological map shows group UPCell to be situated on the Klaserie Gneiss, the presence of outcroppings of the Timbavati gabbro near and around the sampling site suggests that the map is incorrect in this area. Surface water samples have a much lower ion concentration than the groundwater samples, this corresponds with their lower TDS values. Of the surface water samples, all except THORSW1 have the same ion composition as group 1. THORSW1 has the same composition as the samples in group 2.

The high sodium concentrations in the groundwater samples of groups 1 and 2 are most likely derived from the weathering of albite, potassium from the weathering of microcline and biotite and calcium ions in the water samples are likely from the weathering of anorthite in the gneisses. The high magnesium concentrations in the UPCell sample are likely from the weathering of olivine and pyroxenes, while calcium and sodium ions are from the weathering of plagioclase in the Timbavati gabbro. The high bicarbonate (HCO_3^-) concentrations in the groundwater samples are a byproduct of the silicate weathering process. Carbonic acid (H_2CO_3), formed by CO_2 dissolving in water, has its protons consumed during the formation of clay minerals such as kaolinite to form bicarbonate (Appelo and Postma, 2005). While WELA and HLU have a similar cation composition to the samples in group 1, their dominant anion is chlorine. The average bicarbonate concentration in WELA and HLU is very close to the average of group 1, 455 mg/l and 459 mg/l respectively, however, the chlorine concentrations are significantly higher, 611 mg/l compared to 174 mg/l. According to Hunt et al. (2012), high chloride levels can be regarded as an indicator of pollution. Potassium and aluminium are likely from the weathering of microcline and biotite while magnesium and iron are also from biotite.

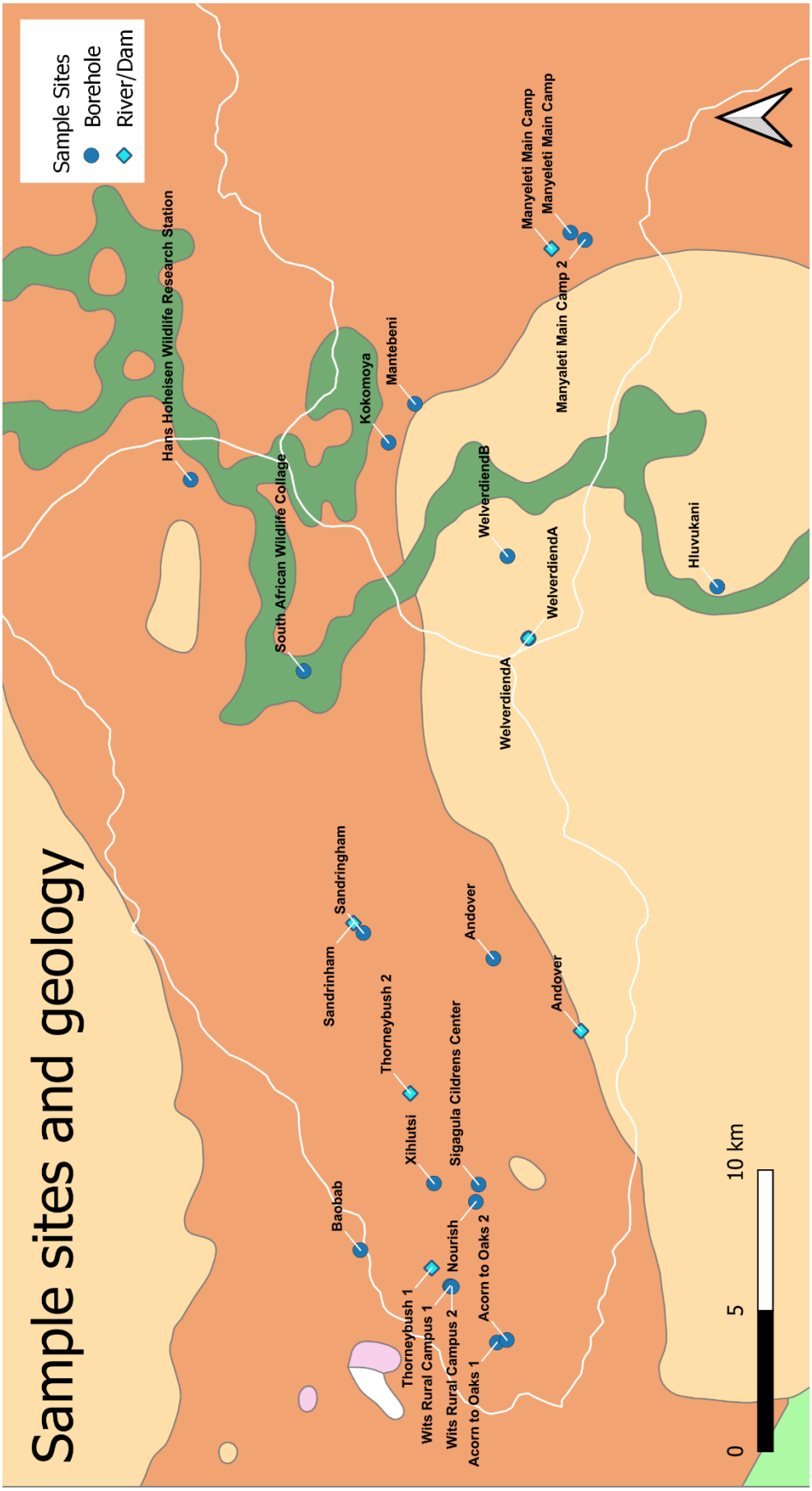

FIGURE 56: SAMPLE SITES OVERLAYING THE GEOLOGY OF THE STUDY AREA.

6.3 Nitrates

The nitrate concentrations were higher in the groundwater samples than in the surface water samples. It was evident that the groundwater nitrate (NO_3^- mg/l) concentrations from Welverdiend A, Welverdiend B and Hluvukani were much higher than those from other sample locations (Figure 20), likely due to them being more populated and urbanized environments when compared to the other sample locations that are in nature preserves and areas with significantly less development. The three sample locations could therefore be considered as a separate group. Table 10 shows the average nitrate concentrations for groundwater and surface water samples for each of the five rounds of sampling as well as the overall averages. There are three averages given for the groundwater samples, one for all the samples, one without Welverdiend A, Welverdiend B and Hluvukani and one for just Welverdiend A, Welverdiend B and Hluvukani.

TABLE 10: AVERAGE NO_3^- CONCENTRATIONS FOR SURFACE WATER AND GROUNDWATER SAMPLES, AS WELL AS THE AVERAGE GROUNDWATER CONCENTRATION WITH THE OUTLIERS REMOVED.

Round of Sampling	Average NO_3^- (mg/l)			
	Surface water	Groundwater: All	Groundwater: Without Welverdiend A, Welverdiend B and Hluvukani	Groundwater: Just Welverdiend A, Welverdiend B and Hluvukani
September and October 2021	1.49	38.5	12.3	169.4
February 2022	6.30	71.8	18.2	339.6
May and June 2022	5.63	51.3	14.0	331.3
August and September 2022	5.76	81.8	18.3	526.1
November 2022	5.76	148	12.9	1092
All Rounds	5.56	83.1	15.6	508.7

The average surface water nitrate concentration remained relatively constant throughout the five rounds of sampling, excluding round 1 where there was only one dam sampled. The groundwater nitrate concentrations (without Welverdiend A, Welverdiend B and Hluvukani) seem to show a pattern of increasing then decreasing alternating with each round of sampling. This trend does however not appear to be seasonal or related to rainfall events. The samples from Welverdiend A, Welverdiend B and Hluvukani show an overall drastic increase in nitrate concentrations as sampling continued. According to Tredoux et al., (2009), on-site sanitation is the main source of nitrate pollution in southern Africa. When sampling in the communities of Welverdiend A and B it was noted that the boreholes were located downslope from the settlements, pit latrines, cattle kraals and dipping stations, suggesting this is the likely source of the nitrate pollutants.

FIGURE 57: CATTLE IN WELVERDIEND A.

The Aquaread AP-5000 Nitrate ISE electrode records nitrate as NO_3^-. To be able to compare the nitrate concentrations measured with the Aquaread probe during sampling with the WHO (2017) and SABS (2022) guidelines the data first needed to be converted into NO_3^- as N. This was done by multiplying the NO_3^- concentration by 0.2259. Figure 58 shows the 16 samples with nitrate (as NO_3^--N) concentrations, measured using the Aquaread probe during the five rounds of sampling, that have concentrations above the World Health Organization and South African Bureau of Standards recommended guidelines. These samples were taken at HLU, SCC, BAO, WelA and WelB.

When looking at Figure 21 to Figure 25 it can be seen that these sampling sites are all located in built-up areas and croplands. This indicates that the source of the nitrate contamination is most likely from human, animal, and agricultural waste. According to Tredoux et al., (2009), on-site sanitation is the main source of nitrate pollution in southern Africa. When sampling in the communities of Welverdiend A and B it was noted that the boreholes were located downslope from the settlements, pit latrines, cattle kraals and dipping stations, suggesting this is the likely source of the nitrate pollutants.

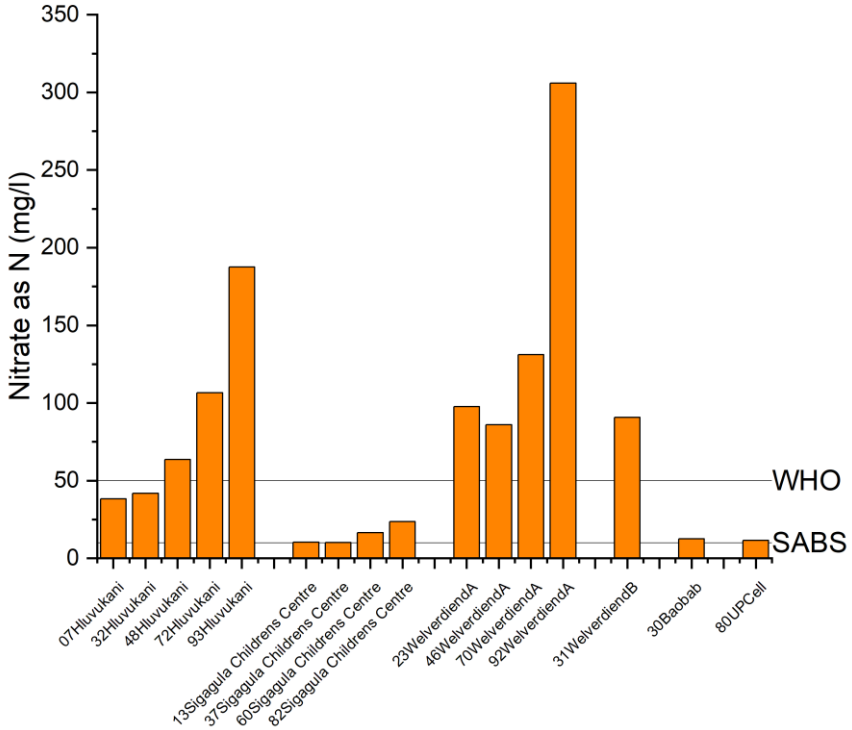

FIGURE 58: NITRATE CONCENTRATIONS ABOVE THE WHO (2017) AND SABS (2022) RECOMMENDED GUIDELINES FOR DRINKING WATER.

Figure 59 shows the comparison between the nitrate (NO_3^--N mg/l) concentrations measured with the Aquaread probe and those determined by the lab. The Aquaread readings were 0.5 times higher than the laboratory measurements. When plotting the Lab concentrations against the Aquaread concentrations it can be seen that they have a near-perfect linear relationship with a Pearson's r correlation of 0.9983. As the probe was checked and calibrated daily the cause of this difference was not sensor drift. According to the Aquaread AP-5000 instruction manual, the probe has an accuracy of ~10% or 2ppm of the reading (whichever is greater) but chloride, bromide, fluoride, sulphate, chlorate, and perchlorate ions could have interfered with the ISE electrode readings. When looking at the chemical data from the lab it could be noted that WelA, HLU and BAO had the highest chloride concentrations of 42.8 mg/l, 98.3 mg/l and 81.4 mg/l respectively while WelA and HLU also had the highest sulphate concentration of 42.8 mg/l and 98.3 mg/l respectively.

However, the difference between the lab results and the Aquaread readings is consistent for all the samples, suggesting this is not the cause of the discrepancy. It is likely that the discrepancy in the concentrations is due to the difference in how long it took for the samples to be analysed. The Aquaread analysis was done on-site while the lab was only able to analyse the samples a month after sampling took place, due to complications with the lab. Degassing of the samples likely took place during this time.

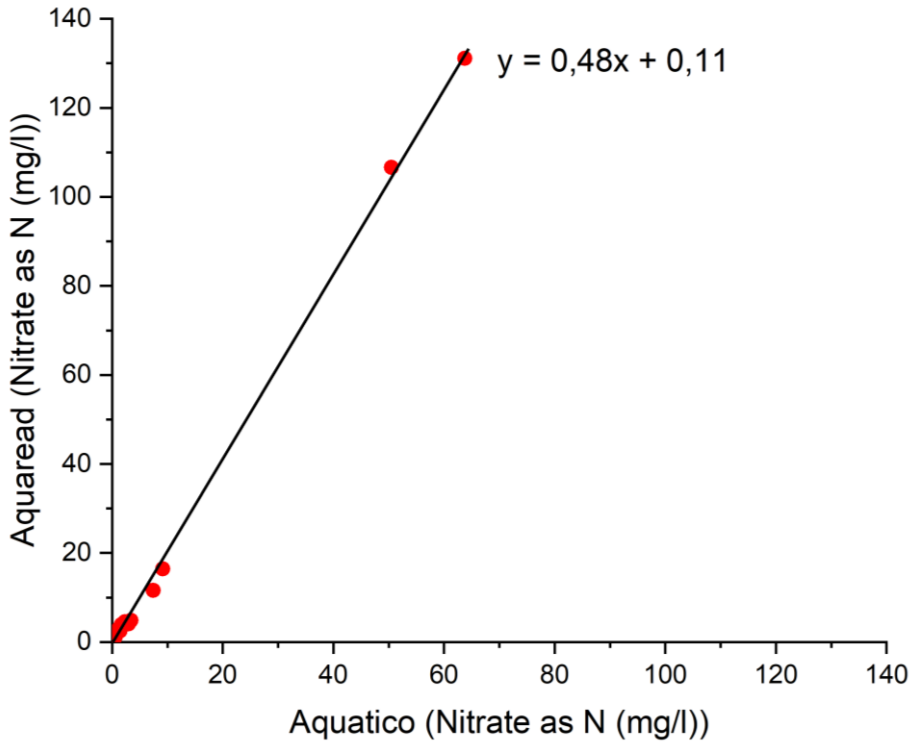

FIGURE 59: RELATIONSHIP BETWEEN THE LAB AND AQUAREAD NO_3 CONCENTRATIONS.

The NO_2^- found in trace levels in Wits1, WelA, WelASW and HLU, see Figure 60, could be evidence of ongoing denitrification (Appelo & Postma, 2005).

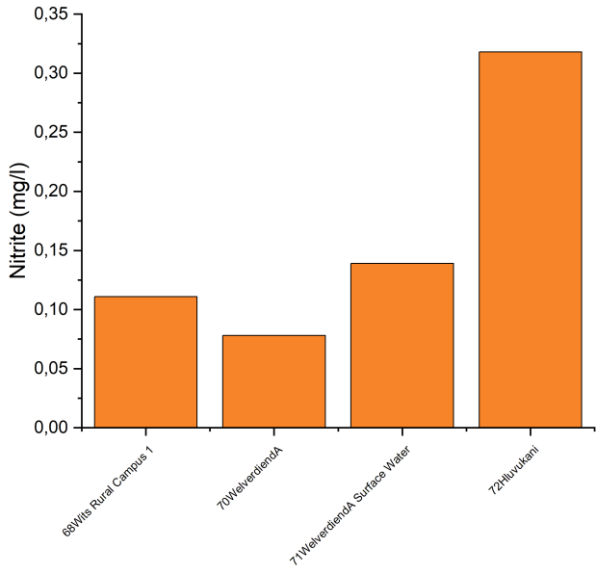

FIGURE 60: TRACE LEVELS OF NITRITE WERE FOUND IN FOUR OF THE SAMPLES.

6.4 Hydrogen and Oxygen Isotopes

The study area has a Lowveld climate with rainfall occurring during the summer months. However, when comparing Figure 8 of the average monthly precipitation in Orpen Rest Camp with Figure 46 it can be seen that the rainfall does not follow the usual trend. Unusually heavy rainfall occurred during April and May 2022 and very little rainfall during September and October 2022.

A weighted meteoric water regression line was used as it better characterises the average rainfall for the area. This is because it considers the heavier rainfall events and minimises the effect of evaporation from the smaller rainfall events sampled (Hughes and Crawford, 2012). The weighted regression equation for the local meteoric water line is $\delta D = 6.2\delta^{18}O + 8.3$, having a shallower gradient than the GMWL. The shallower gradient of the LMWL compared with the GMWL is common in warmer regions (Clark, 2015).

Looking at Figure 46 it can be seen that the months with the lowest rainfall (February, September, and October) had the heaviest isotopic compositions. This is part of the amount effect, where there is a shift to lighter isotope compositions with heavier rainfall events and vice versa where light rainfall events have heavier isotopic compositions (Diamond, 2022). Diamond and Harris (2019) also attributed the more negative delta values of the groundwater in the Table Mountain group to recharge taking place during heavier rainfall events. A possible reason for the high δD values for September is that it was the first rain after the dry winter season ended and humidity was therefore very low. Raindrops are subject to evaporation during precipitation and, as evaporation is relatively high in dry air, the lighter isotopes would have evaporated first. The amount effect is also likely a contributing factor as all 10 mm of precipitation for September occurred during a single event.

D-excess values can be seen in Figure 61, higher d-excess values during April and May 2022 suggesting the water evaporated under less humid conditions at the moisture source region in comparison to the previous months that were sampled. September 2022 had a negative d-excess value of -10‰. According to Dansgaard (1964), a negative d-excess value means that evaporation took place under non-equilibrium conditions, such as fast evaporation, and evaporation was likely from a water source that had a negative d-excess.

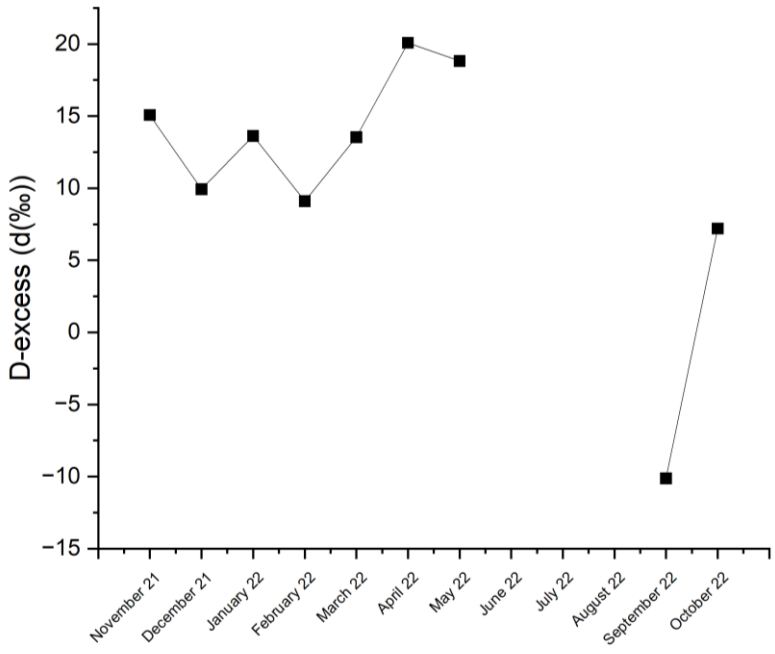

FIGURE 61: DEUTERIUM EXCESS OF THE RAINWATER SAMPLES

As seen in Figure 45, the groundwater samples have a lighter isotopic composition. They fall near the lower half of the GMWL. Petersen et al. (2023), who used stable isotopes to identify surface water-groundwater interactions in the Kruger National Park, also found that their groundwater samples had the most negative isotopic ratios compared to the rain and surface water samples. The light isotope composition is likely due to recharge occurring as a result of heavy rainfall events when the lighter isotopes have a chance to condense and precipitate. The groundwater samples plot along the lower end of the LEL and to the right of the lower end of the LMWL. The regression equation for the groundwater samples has a gradient very close to the LEL but with a more negative intercept. This suggests that some evaporation is taking place before the rainwater enters the aquifer. When looking at the averages for each round of sampling in Figure 46 the groundwater isotope compositions remained relatively constant over the sampling period. During September/October 2021 the groundwater sample from Kokomoya had an isotopic composition that was plotted closer to the surface water samples rather than the groundwater samples. This could be from not allowing the borehole to purge for long enough and accidentally sampling water from the pipe rather than fresh groundwater.

Surface water samples are enriched in heavier isotopes compared to the groundwater samples. Surface water samples fall further to the right of the GMWL as $\delta^{18}O$ concentrations increase. There appears to be seasonal variation in the surface water sample, values vary by 33,5‰ δD and 6,2‰ $\delta^{18}O$. δD and $\delta^{18}O$ values continued to increase as the dry season progressed, with the heaviest compositions occurring towards the end of the dry season. The heavy isotope compositions of the surface water samples are likely a sign of enrichment due to evaporation. However, the lack of an increase in TDS with an increase in $\delta^{18}O$, observed in Figure 55, in the surface water samples could suggest that evaporation is not solely responsible for the heavier isotopic composition. A possible explanation could be that the heavier isotopes are from the light rainfall events occurring at the end of the dry season where the heavier isotopes condense and rained down. This would however be easier to determine with a larger data set. In February 2022 SANSW, THORSW1 and THORSW2 and in May/June 2022 THORSW2 had isotope compositions that overlapped with the groundwater samples, perhaps indicating some surface water groundwater interaction.

During the final round of sampling, only the large dams at Manyeleti, Andover and Sandringham had water in them, the rest of the sample sites had dried up (see Figures 62 and 63). Manyeleti and Andover were the most enriched in heavier isotopes during the final round of sampling in November 2022, likely due to the dams having the largest surface areas and therefore undergoing more evaporation. The dam at Sandringham also had more vegetation, water lilies specifically, that covered a large portion of the surface area of the dam, somewhat reducing the amount of evaporation.

FIGURES 62 AND 63: THE DRY DAM IN WELVERDIENDA AND THE DRY RIVER AT THORNEYBUSH, PHOTOS TAKEN IN NOVEMBER 2022.

6.5 Radon

ANDSW, WelASW, SANSW and THORSW1 were the only surface water samples that contained radon during all the rounds that they were sampled. However, during August/September 2022 all the surface water samples contained radon. The radon in the surface water, along with the pH, TDS, ORP and DO values that overlapped with the groundwater samples could be a sign of groundwater discharge into the rivers and dams. THORSW2 was the only surface water sample to have a radon concentration as high as some of the groundwater samples during the May/June 2022 round of sampling. Table 10 shows the average mean, high and low radon concentrations, as well as the average standard deviations for the different groundwater sample sites, and as well as the underlying geology. BAO had the lowest average radon concentration with a mean value of 4190 Bq/m^3 while Acorn to Oaks 2 had the highest mean radon concentrations of 34200 Bq/m^3.

TABLE 11: THE AVERAGE MEAN, HIGH, LOW AND STANDARD DEVIATIONS OF RADON CONCENTRATIONS AS WELL AS CORRESPONDING GEOLOGY FOR THE DIFFERENT SAMPLING LOCATIONS.

Site name	Radon (Bq/m^3)				Geology
	Mean	High	Low	SD	
Baobab	4000	5000	3000	800	Klaserie Gneiss
Thorneybush - Xihlutsi	6000	7000	6000	600	Klaserie Gneiss
South African Wildlife College	7000	8000	6000	1000	Klaserie Gneiss
Manyeleti Main Camp 1	8000	9000	7000	700	Klaserie Gneiss
WelverdiendA	8000	9000	8000	600	Makhutswi Gneiss
Hluvukani	9000	10000	8000	1000	Makhutswi Gneiss
Wits Rural Campus 2	9000	10000	8000	800	Klaserie Gneiss
Sigagula Childrens Centre	9000	10000	8000	1000	Klaserie Gneiss
Manyeleti Main Camp 2	15000	17000	13000	1000	Klaserie Gneiss
Andover	15000	17000	13000	2000	Klaserie Gneiss
Wits Rural Campus 1	20000	22000	18000	2000	Timbavati Gabbro
UPCell	22000	25000	20000	2000	Klaserie Gneiss/Timbavati Gabbro
Kokomoya	24000	26000	22000	5000	Klaserie Gneiss
Sandringham	24000	26000	22000	2000	Klaserie Gneiss
Mantebeni	25000	28000	23000	2000	Klaserie Gneiss
Nourish	25000	27000	23000	2000	Klaserie Gneiss
Acorn to Oaks 1	26000	27000	24000	2000	Klaserie Gneiss
Acorn to Oaks 2	34000	38000	31000	3000	Klaserie Gneiss

Uranium concentrations in the groundwater samples were below the detection limit of 0.015 mg/l of the analysis performed by the lab. It was therefore not possible to see if there was a trend with radon and uranium concentrations. There were also no clear relationships between pH, DO, EC, TDS, SAL, ORP and radon concentrations. This corresponds with Cho & Choo (2029) who also noted that radon tended to behave independently concerning most geochemical parameters.

7 Conclusion and Recommendations

The aim of the study was to assess hydrostratigraphic systems in a fairly undisturbed area underlain by intrusive igneous and metamorphic rocks where no such data has yet been recorded, providing a foundation, and highlighting areas of importance, for further hydrogeological investigations in the area. The objectives of the study were, therefore, to conduct a baseline study of the hydrochemistry of the greater Timbavati area, to gain a better understanding of the relationship between the groundwater, surface water and local geology in the area and to investigate the impact of the surrounding geography on the groundwater geochemistry and quality. Groundwater and surface water geochemistry, hydrogen and oxygen isotopes, and radon were used to achieve these objectives.

The Aquaread AP-5000 probe was used to monitor pH, TDS, DO, ORP, NH_4 and NO_3^- levels of groundwater and surface water in the field over 5 rounds of sampling from September 2021 to November 2022. The Durridge RAD7 was used for radon analysis of groundwater and surface water samples usually within 6 to 8 h of sampling. Groundwater, surface water and rainwater samples were analysed for hydrogen and oxygen isotope ratios using a Los Gatos Research Liquid Water Isotope Analyser. Additionally, groundwater and surface water samples were collected during August and September 2022 and sent to the lab for a more detailed chemical analysis.

While there was some overlap between the groundwater and surface water samples with regard to pH, TDS, ORP and DO, the two groups tended to plot separately. Surface water samples have a higher mean pH of 8.3 compared with the mean groundwater pH of 7.5. The mean surface water DO was 8.22 mg/l, and the mean groundwater value was 5.33 mg/l. Groundwater samples had a significantly higher mean TDS of 1220 mg/l compared with 330 mg/l in the surface water samples. There was no major difference in the surface water and groundwater ORP values, having an average of 91 mV and 99 mV respectively.

The ion compositions of the surface water samples were similar to the groundwater samples but with the groundwater samples having much higher ion concentrations. Based on the relationship between TDS and $\delta^{18}O$, the source of the high TDS values in the groundwater is from weathering and water-rock interactions rather than from evaporation. The differences in the groundwater and surface water chemistry are therefore due to the addition of ions and other chemical constituents from the weathering of rocks and minerals. Based on the chemistry of the groundwater samples, they could be divided into three groups:

- Group 1 has a Na^++K^+ and HCO_3^- dominant composition and contains most of the samples. These sites are all situated on the Klaserie Gneiss.
- Group 2 has a Na^++K^+ and Cl^- dominant composition and consists of HLU and WELA. These sites are situated on the Makhutswi Gneiss.
- Group 3 has a Mg^{2+} and HCO_3^- dominant composition and consists only of UPCELL. This site is situated on the Timbavati gabbro.

SAWC could not be sampled when the other samples were taken for the detailed chemical analysis, during August and September 2022, as the site was inaccessible. It would be interesting to see if SAWC has the same ion composition as UPCell since they are both situated on the Timbavati gabbro. It would also be beneficial to future research if a way could be found to access more groundwater and surface water samples situated on different geological formations in the area.

Groundwater samples have a lighter mean isotopic composition of -20.5‰ δD and -3.8‰ $\delta^{18}O$ in comparison to the mean surface water samples values of 12.2‰ δD and 2.3‰ $\delta^{18}O$, and the mean composition of the rainwater samples, -2.76‰ δD and -1.9‰ $\delta^{18}O$. This lighter isotopic composition in the groundwater samples is due to recharge occurring as a result of heavy rainfall events and the

amount effect. However, as the regression equation for the groundwater samples and the LEL have very similar gradients it suggests that some evaporation is taking place before recharge can occur. There is also a possibility of evaporations not being solely responsible for the heavier isotopic composition of the surface water samples. This is suggested by the lack of an increase in TDS with an increase in $\delta^{18}O$. Continuing the collection of monthly rainwater samples from multiple sites across the entire study area, as well as quarterly groundwater and surface water samples, would allow for a more detailed understanding of the relationship between rainfall events and groundwater recharge as well as surface water - groundwater interactions.

In the DWAF (2004) report it was noted that there are isolated areas with elevated nitrate concentrations in the Timbavati catchment. HLU, SCC, BAO, WelA and WelB all had nitrate concentrations above the recommended WHO and SABS guidelines. The nitrate concentrations were on average higher in the groundwater samples, with a mean value of 83.1 mg/l and ranging as high as 1350 mg/l in WelA during the final found of sampling. The surface water samples on the other hand had a mean value of 5.56 mg/l and only ranged as high as 10.4 mg/l in WelASW. Samples with the highest nitrate concentrations were located in the communities of Welverdiend, Hluvukani and Acornhoek as well as the more built-up and populated areas. This indicates that the source of the nitrate contamination is most likely from human, animal, and agricultural waste. It was also noted that in some of these areas' boreholes were located downslope from pit latrines and cattle kraals. Analysis of nitrogen isotopes in the future would be able to give a clearer picture of the exact source of the nitrate contamination. When comparing nitrate readings from the Aquaread AP-5000 with the values from the lab it was noted that the readings were 0.5 times higher than the nitrate concentrations obtained in the laboratory. It is however unclear if this is due to interfering ions in the groundwater or degassing of the samples before they were analysed. In order to determine the reason for this difference in nitrate values, new samples should be taken and analysed with the Aquaread and at the laboratory as close to one another as possible, time-wise.

While groundwater quality from hard rock aquifers is usually better than the surface water (Wright, 1992) during the detailed water chemistry analysis conducted in August and September 2022 a few drinking water quality issues were identified in some of the boreholes and surface water bodies. These issues were with regard to fluoride, potassium, sodium, iron, nickel and arsenic. Aluminium was an issue in the surface water samples WELASW, SANDSW, ANDSW and MANMSW specifically. The groundwater samples that most often presented with problems were HLU, WelA, MANT, KM, and UPCell. HLU has the highest heavy metal concentrations. While some of these constituents can be attributed to the weathering of rocks and minerals in the area it was noted that land use also appeared to have an impact on the groundwater geochemistry and quality. Further research should be conducted to determine the source of heavy metals in the water samples, whether they are anthropogenic or geogenic in origin.

There was no distinct link between radon concentrations and geology or between pH, DO, EC, TDS, SAL, ORP and radon concentrations. As expected, radon concentrations in the groundwater samples were much higher, with a mean value of 16900 Bq/m^3, compared with the surface water samples that had a mean value of 134 Bq/m^3. Radon was mostly found in the surface water samples ANDSW, WelASW, SANSW and THORSW1. This along with these surface water samples having pH, TDS, ORP and DO values that occasionally overlapped with the groundwater samples, could possibly be a sign of groundwater discharge into the rivers and dams.

This study has significantly advanced the understanding of the hydrochemistry of the greater Timbavati area and highlights the complex interconnectivity of hydrology, hydrogeology, geography, and geology. The analysis of hydrogen and oxygen isotopes provided an insight into the recharge processes and water sources as well as identified that there is seasonal variation in the hydrochemistry

in the area. The detection of radon in certain surface water and groundwater samples along with the overlap in pH, TDS, DO and ORP of those samples, suggests potential groundwater-surface water interactions, showing there is interconnectivity of the hydrology and hydrogeology in the area. The characterization of both the groundwater and surface water chemistry has revealed distinct patterns and relationships between the water geochemistry and quality with the local geology and geography. Piper plots, Stiff and Schoeller diagrams identified three main groups of groundwater samples, each characterized by unique cation-anion compositions associated with a specific underlying geology. While elevated nitrate concentrations and heavy metals in specific groundwater samples highlight the impact of anthropogenic activities on the water quality. These findings have implications for water resource planning and management and highlight the need for integrated approaches to safeguard water quality and sustainability in the greater Timbavati area.

8 References

Abiye, T., Verhagen, B., Freese, C., Harris, C., Orchard, C., Van Wyk, E., Tredoux, G., Pickles, J., Kollongei, J., Xiao, L., 2013. The use of isotope hydrology to characterize and assess water resources in South (ern) Africa. WRC Report No. TT570/13, Pretoria. 211pp.

Abiye, T.A., Demlie, M.B., Mengistu, H., 2021. An overview of aquifer physiognomies and the δ18O and δ2H distribution in the South African groundwaters. Hydrology 8, 68. https://doi.org/https://doi.org/10.3390/hydrology8020068

Adepelumi, A.A., Ajayi, T.R., Ako, B.D., Ojo, A.O., 2005. Radon soil–gas as a geological mapping tool: case study from basement complex of Nigeria. Environmental geology 48, 762–770.

Alabdula'aly, A.I., 2014. Occurrence of radon in groundwater of Saudi Arabia. J Environ Radioact 138, 186–191.

Allsopp H.L., Kramers, J.D., Jones, D.L & Erlank, A.J., 1989. The age of the Umkondo Group, eastern Zimbabwe, and implications for palaeomagnetic correlations. South African journal of geology 92, 11–19.

Anhaeusser, C.R., Johnson, M.R., Thomas, R.J., 2006. Ultramafic and mafic intrusions of the Kaapvaal Craton. The Geology of South Africa. Geological Society of South Africa, Johannesburg/Council for Geoscience, Pretoria 95–134.

Appelo, C.A.J., Postma, D., 2005. Geochemistry, groundwater and pollution, 2nd ed. CRC Press, Amsterdam.

Aquaread Ltd, 2021. Instruction Manual for the AP-5000 Multiparameter Water Quality Probe and associated Aquameter, Utilities & Accessories. Aquaread water monitoring instruments.

Ashbolt, N.J., 2001. Indicators of microbial water quality. Water quality: Guidelines, standards and health.

Baloyi, R.S., Diamond, R.E., 2019. Variable water quality of domestic wells emphasizes the need for groundwater quality monitoring and protection: Stinkwater, Hammanskraal, Gauteng. Water SA 45, 216–224

Barton Jr, J.M., 1984. Timing of ore emplacement and deformation, Murchison and Sutherland greenstone belts, Kaapvaal craton, in: Gold'82: The Geology, Geochemistry and Genesis of Gold Deposits. Symposium. pp. 629–644.

Baskaran, M., 2016. Radon: A tracer for geological, geophysical and geochemical studies. Springer. https://doi.org/10.1007/978-3-319-21329-3

Brandl, G., 1985. 1:25000 Geological Series map (2330 Tzaneen). Geological Survey of South Africa.

Brandl, G., Kröner, A., 1993. Preliminary results of single zircon studies from various Archaean rocks of the Northeastern Transvaal, in: International Colloquium on Africa Geology. pp. 54–56.

Briggs, P., 2023. Weather and Climate - Kruger National Park [WWW Document]. SafariBookings Compare African Safaris: https://www.safaribookings.com/kruger/climate.

Bristow, J.W., Armstrong, R.A., Allsopp, H.L., 1982. A note on the geology and geochemistry of the Tsange Gabbros. Trans. Geol. Soc. S. Afr 85, 135–139.

Bundy, L.G., Knobeloch, L., Webendorfer, B., Jackson, G.W., Shaw, B.H., 1994. Nitrate in Wisconsin groundwater: sources and concerns: Madison, USA. US Department of Agriculture, University of Wisconsin-Extension, Cooperative Extension, Extension Publications G 3054, 1–8.

Cho, B.W., Choo, C.O., 2019. Geochemical behaviour of uranium and radon in groundwater of Jurassic granite area, Icheon, Middle Korea. Water (Basel) 11, 1278.

Cho, B.-W., Choo, C.O., Kim, M.S., Hwang, J., Yun, U., Lee, S., 2015. Spatial relationships between radon and topographical, geological, and geochemical factors and their relevance in all of South Korea. Environ Earth Sci 74, 5155–5168.

Cho, B.W., Kim, H.K., Kim, M.S., Hwang, J.H., Yoon, U., Cho, S.Y., Choo, C.O., 2019. Radon concentrations in the community groundwater system of South Korea. Environ Monit Assess 191, 1–10.

Cho, B.-W., Sung, I.-H., Cho, S.-Y., Park, S.-K., 2007. A preliminary investigation of radon concentrations in groundwater of South Korea. Journal of Soil and Groundwater Environment 12, 98–104.

Choubey, V.M., Ramola, R.C., 1997. Correlation between geology and radon levels in groundwater, soil and indoor air in Bhilangana Valley, Garhwal Himalaya, India. Environmental Geology 32, 258–262.

Clark, I., 2015. Groundwater Geochemistry and Isotopes, 1st ed. CRC Press, Boca Raton.

Clark, I.D., 1997. Tracing the hydrological cycle. Environmental isotopes in hydrogeology 35–61.

Clubley-Armstrong, A.R., 1979. The geology of the southern Kruger National Park, from west of Pretoriuskop eastward to the Lebombo Mountains and the Mocambique border. Geological Survey of South Africa (Unpublished).

Council for Geoscience, 2019, RSA 1m Shape Layer Font, 1:1000000. https://dev.jctest.co.za/geoscience-main/wp-content/uploads/2022/10/rsa1mshapelayerfonttar.zip

Craig, H., 1961. Isotopic variations in meteoric waters. Science (1979) 133, 1702–1703.

Criss, R.E., 1999. Principles of stable isotope distribution. Oxford University Press.

Cronin, A.A., Hoadley, A.W., Gibson, J., Breslin, N., Kouonto Komou, F., Haldin, L., Pedley, S., 2007. Urbanisation effects on groundwater chemical quality: findings focusing on the nitrate problem from 2 African cities reliant on on-site sanitation. J Water Health 5, 441–454.

Dansgaard, W., 1964. Stable isotopes in precipitation. Tellus 16, 436–468. https://doi.org/https://doi.org/10.1111/j.2153-3490.1964.tb00181.x

Department of Water Affairs and Forestry, 2004. Olifants Water Management Area: Internal Strategic Perspective. Prepared by GMKS, Tlou Matji and WMB on behalf of the Directorate: National Water Resource Planning. DWAF Report No P WMA 04/000/00/0304. South Africa.

Dewandel, B., Lachassagne, P., Wyns, R., Maréchal, J.-C., Krishnamurthy, N.S., 2006. A generalized 3-D geological and hydrogeological conceptual model of granite aquifers controlled by single or multiphase weathering. J Hydrol (Amst) 330, 260–284.

Diamond, R.E., 2022. Stable Isotope Hydrology, 1st ed. The Groundwater Project, Ontario.

Diamond, R.E., Harris, C., 2019. Stable isotope constraints on hydrostratigraphy and aquifer connectivity in the Table Mountain Group. South African Journal of Geology 2019 122, 317–330. https://doi.org/10.25131/sajg.122.0021

Ding, Z., Ma, J., Zhao, W., Jiang, Y., Love, A., 2013. Profiles of geochemical and isotopic signatures from the Helan Mountains to the eastern Tengger Desert, northwestern China. J Arid Environ 90, 77–87. https://doi.org/10.1016/j.jaridenv.2012.10.01

Dube, T., Shoko, C., Sibanda, M., Baloyi, M.M., Molekoa, M., Nkuna, D., Rafapa, B., Rampheri, B.M., 2020. Spatial modelling of groundwater quality across a land use and land cover gradient in Limpopo Province, South Africa. Physics and Chemistry of the Earth, Parts a/b/c 115, 102820.

Durridge Company Inc, 2022. RAD7 Electronic Radon Detector User Manual. Billerica. Durridge Company Inc.

Durridge Company Inc., 2019. Product Brief. Durridge Company Inc.

Edmunds, W.M., Kinniburgh, D.G., Moss, P.D., 1992. Trace metals in interstitial waters from sandstones: acidic inputs to shallow groundwaters. Environmental Pollution 77, 129–141.

Esan, D.T., Sridhar, M.K.C., Obed, R., Ajiboye, Y., Afolabi, O., Olubodun, B., Oni, O.M., 2020. Determination of residential soil gas radon risk indices over the lithological units of a Southwestern Nigeria University. Sci Rep 10, 7368.

ESRI, 2023. World_Imagery [basemap], Scale Not Given. https://services.arcgisonline.com/arcgis/rest/services/World_Imagery/MapServer/tile/{z}/{y}/{x}

European Space Agency Climate Change Initiative Land Cover Project, 2016. Land Use [basemap], Scale Not Given. http://2016africalandcover20m.esrin.esa.int/download.php?token=514694adc9bbe6146fdacf4f3597da3c

Fenech, C., Rock, L., Nolan, K., Tobin, J., Morrissey, A., 2012. The potential for a suite of isotope and chemical markers to differentiate sources of nitrate contamination: a review. Water Res 46, 2023–2041.

Froehlich, K., Gibson, J.J., Aggarwal, P.K., 2002. Deuterium excess in precipitation and its climatological significance.

Gat, J.R., Gonfiantini, R., 1981. Stable isotope hydrology. Deuterium and oxygen-18 in the water cycle. A monograph prepared under the aegis of the IAEA/UNESCO working group on nuclear techniques in hydrology of the international hydrological programme.

Gordon-Welsh, J.F., 1980. A gravity and magnetic profile northeast of Orpen in the Kruger National Park. Internal Report of the Geological Survey of Southern Africa (Unpublished).

Graham, J.P., Polizzotto, M.L., 2013. Pit latrines and their impacts on groundwater quality: a systematic review. Environ Health Perspect 121, 521–530. https://doi.org/10.1289/ehp.1206028

Groeneveld, D., Visser, D.L., von Gruenewaldt, G., 1970. Symposium on the Bushveld Igneous Complex and Other Layered Intrusions.

Grolander, S., 2009. Radon as a groundwater tracer in Forsmark and Laxemar. Swedish Nuclear Fuel and Waste Management Co.

Hallberg, G.R., Keeney, D.R., 1993. Nitrate. Regional ground-water quality. WM Alley.

Haller, L., McCarthy, P., O'Brien, T., Riehle, J., Stuhldreher, T., 2013. Nitrate pollution of groundwater. 2014: Alpha Water Systems Inc. Google Scholar.

Hanson, R.E., Crowley, J.L., Bowring, S.A., Ramezani, J., Gose, W.A., Dalziel, I.W.D., Pancake, J.A., Seidel, E.K., Blenkinsop, T.G., Mukwakwami, J., 2004. Coeval large-scale magmatism in the Kalahari and Laurentian cratons during Rodinia assembly. Science (1979) 304, 1126–1129.

Hanson, R.E., Gose, W.A., Crowley, J.L., Ramezani, J., Bowring, S.A., Bullen, D.S., Hall, R.P., Pancake, J.A., Mukwakwami, J., 2004. Paleoproterozoic intraplate magmatism and basin development on the Kaapvaal Craton: Age, palaeomagnetism and geochemistry of~ 1.93 to~ 1.87 Ga post-Waterberg dolerites. South African Journal of Geology 107, 233–254.

Hao, S., Li, F., Li, Y., Gu, C., Zhang, Q., Qiao, Y., Jiao, L., Zhu, N., 2019. Stable isotope evidence for identifying the recharge mechanisms of precipitation, surface water, and groundwater in the Ebinur Lake basin. Science of the Total Environment 657, 1041–1050. https://doi.org/10.1016/j.scitotenv.2018.12.102

Harkness, J.S., Swana, K., Eymold, W.K., Miller, J., Murray, R., Talma, S., Whyte, C.J., Moore, M.T., Maletic, E.L., Vengosh, A., 2018. Pre-drill groundwater geochemistry in the Karoo Basin, South Africa. Groundwater 56, 187–203. https://doi.org/10.1111/gwat.12635

Hill Laboratories, 2023. Technical note anion cation balances [WWW Document]. Hill Laboratories. [Online] Available at: chrome-extension://efaidnbmnnnibpcajpcglclefindmkaj/https://www.hill-labs.co.nz/media/hbzngknw/13213v6-technical-note-anion-cation-balances.pdf.

Hiscock, K.M., Bense, V.F., 2014. Hydrogeology: principles and practice. John Wiley & Sons.

Hoehn, E., Von Gunten, H.R., 1989. Radon in groundwater: A tool to assess infiltration from surface waters to aquifers. Water Resour Res 25, 1795–1803.

Hoehn, E., Von Gunten, H.R., Stauffer, F., Dracos, T., 1992. Radon-222 as a groundwater tracer. A laboratory study. Environ Sci Technol 26, 734–738.

Holland, M., 2011. Hydrogeological Characterisation of Crystalline Basement Aquifers within the Limpopo Province, South Africa (PhD thesis). University of Pretoria, Pretoria.

Hughes, C.E., Crawford, J., 2012. A new precipitation-weighted method for determining the meteoric water line for hydrological applications was demonstrated using Australian and global GNIP data. J Hydrol (Amst) 464, 344–351. https://doi.org/10.1016/j.jhydrol.2012.07.029

Hunt, M., Herron, E., Green, L., 2012. Chlorides in fresh water. The University of Rhode Island Watershed Watch 4.

International Atomic Energy Agency, 1983. Guidebook on nuclear techniques in hydrology. Vienna.

Irunde, R., Ijumulana, J., Ligate, F., Maity, J.P., Ahmad, A., Mtamba, J., Mtalo, F., Bhattacharya, P., 2022. Arsenic in Africa: potential sources, spatial variability, and the state of the art for arsenic removal using locally available materials. Ground Sustain Dev 18, 100746.

Jacks, G., Rajagopalan, K., Alveteg, T., Jönsson, M., 1993. Genesis of high-F groundwaters, southern India. Applied geochemistry 8, 241–244.

Jung, H., Koh, D.-C., Kim, Y.S., Jeen, S.-W., Lee, J., 2020. Stable isotopes of water and nitrate for the identification of groundwater flow paths: A review. Water (Basel) 12, 138.

Kafri, U., 2001. Radon in groundwater as a tracer to assess flow velocities: two test cases from Israel. Environmental Geology 40, 392–398.

Karim, M.D.M., 2000. Arsenic in groundwater and health problems in Bangladesh. Water Res 34, 304–310.

Keeney, D., Daniel, T.C., Shaw, B., 1980. Nitrate in Wisconsin groundwater: sources and concerns. Publication-Cooperative Extension Programs, University of Wisconsin (USA).

Keeney, D.R., 1989. Sources of nitrate to groundwater, in: Developments in Agricultural and Managed Forest Ecology. Elsevier, pp. 23–34.

Knutsson, G., Olofsson, B.O., 2002. Radon content in groundwater from drilled wells in the Stockholm region of Sweden.

Kronfeld, J., Godfrey-Smith, D.I., Johannessen, D., Zentilli, M., 2004. Uranium series isotopes in the Avon Valley, Nova Scotia. J Environ Radioact 73, 335–352.

Lachassagne, P., Dewandel, B., Wyns, R., 2014. The conceptual model of weathered hard rock aquifers and its practical applications. CRC Press Boca Raton, FL.

Lachassagne, P., Dewandel, B., Wyns, R., 2021. Hydrogeology of weathered crystalline/hard-rock aquifers—guidelines for the operational survey and management of their groundwater resources. Hydrogeol J 29, 2561–2594. https://doi.org/10.1007/s10040-021-02339-7

Lachassagne, P., Wyns, R., Dewandel, B., 2011. The fracture permeability of hard rock aquifers is due neither to tectonics, nor to unloading, but to weathering processes. Terra Nova 23, 145–161.

Lapworth, D.J., Baran, N., Stuart, M.E., Ward, R.S., 2012. Emerging organic contaminants in groundwater: a review of sources, fate and occurrence. Environmental pollution 163, 287–303.

Le Druillennec, T., Ielsch, G., Bour, O., Tarits, C., Tymen, G., Alcalde, G., Aquilina, L., 2010. Hydrogeological and geochemical control of the variations of 222Rn concentrations in a hard rock aquifer: Insights into the possible role of fracture-matrix exchanges. Applied geochemistry 25, 345–356.

Litt, B.R., Korn, L.R., Moser, F.C., Bell, C., Clare, A.K., Uptegrove, J., Key, R.M., 1992. Influence of geology on radon in groundwater supplies of the New Jersey Highlands.

Liu, Y., Yamanaka, T., 2012. Tracing groundwater recharge sources in a mountain–plain transitional area using stable isotopes and hydrochemistry. J Hydrol (Amst) 464, 116–126. https://doi.org/10.1016/j.jhydrol.2012.06.053

Mahler, R.L., Tayor, R., Porter, E., 1990. Nitrate and groundwater. University of Idaho, Cooperative Extension System, Agricultural Experiment.

Mahmoud, M.A., Abd El-Halim, E.S., Hassan, S.F., El Sayed Mohamed, T.E., 2021. Geological Controls Affecting Radon Gas Concentrations in Granitic Gneisses at Wadi Abu Rushied, Southeastern Desert, Egypt. American Journal of Sciences and Engineering Research 4, 134–144.

Masindi, V., Foteinis, S., 2021. Groundwater contamination in sub-Saharan Africa: Implications for groundwater protection in developing countries. Clean Eng Technol 2, 100038.

McCarthy, K.A., McFarland, W.D., Wilkinson, J.M., White, L.D., 1992. The dynamic relationship between groundwater and the Columbia River: using deuterium and oxygen-18 as tracers. J Hydrol (Amst) 135, 1–12.

McGill, B., Villholth, K.G., 2019. Enhancing water security in Southern Africa by tackling nitrate contamination of aquifers and unravelling links to climate change and sanitation: A case from Ramotswa, Botswana.

McGill, B.M., Altchenko, Y., Hamilton, S.K., Kenabatho, P.K., Sylvester, S.R., Villholth, K.G., 2019. Complex interactions between climate change, sanitation, and groundwater quality: a case study from Ramotswa, Botswana. Hydrogeol J 27, 997–1015. https://doi.org/10.1007/s10040-018-1901-4

McNeill, A., Unkovich, M., 2007. The nitrogen cycle in terrestrial ecosystems. Nutrient cycling in terrestrial ecosystems 10, 37–64.

Merlivat, L., Jouzel, J., 1979. Global climatic interpretation of the deuterium-oxygen 18 relationship for precipitation. J Geophys Res Oceans 84, 5029–5033.

Meteoblue, 2023a. Simulated historical climate & weather data for Orpen Rest Camp [WWW Document]. https://www.meteoblue.com/en/weather/historyclimate/climatemodelled/orpen-rest-camp_south-africa_12104318.

Meteoblue, 2023b. Simulated historical climate & weather data for Acornhoek [WWW Document]. https://www.meteoblue.com/en/weather/historyclimate/climatemodelled/acornhoek_south-africa_1023713.

Michaluk, E., 1983. The geology of parts of the eastern Transvaal lowveld between the Kruger National Park and the Drakensberg Escarpment. Explain. Notes, geol. Surv. S. Afr. (Unpublished).

Miller, R.G., Kopfler, F.C., Kelty, K.C., Stober, J.A., Ulmer, N.S., 1984. The occurrence of aluminium in drinking water. Journal-American Water Works Association 76, 84–91.

Mirzavand, M., Ghasemieh, H., Sadatinejad, S.J., Bagheri, R., 2020. An overview on source, mechanism and investigation approaches in groundwater salinization studies. International Journal of Environmental Science and Technology 17, 2463–2476. https://doi.org/10.1007/s13762-020-02647-7

Muchingami, I., Chuma, C., Gumbo, M., Hlatywayo, D., Mashingaidze, R., 2019. Approaches to groundwater exploration and resource evaluation in the crystalline basement aquifers of Zimbabwe. Hydrogeol J 27, 915–928.

Muchingami, I., Mkali, A., Vinqi, L., Pietersen, K., Xu, Y., Whitehead, R., Karsten, J., Villholth, K., Kanyerere, T., 2021. Integration of hydro geophysical and geological investigations in enhancing groundwater potential assessment in Houtriver gneiss crystalline basement formation of South Africa. Physics and Chemistry of the Earth, Parts A/B/C 123, 103009.

Otton, J.K., Gundersen, L.C.S., Schumann, R.R., 1992. The Geology of Radon. US Department of the Interior. US Geological Survey, Open Report 30.

Peng, T.-R., Huang, C.-C., Zhan, W.-J., Wang, C.-H., 2016. Assessing groundwater sources and their association with reservoir water using stable hydrogen and oxygen isotopes: a case study of the Taipei Basin, northern Taiwan. Environ Earth Sci 75, 1–13. https://doi.org/10.3390/geosciences8030084

Petersen, R.M., Nel, J.M., Strydom, T., Riddell, E., Coetsee, C., February, E., 2023. The use of stable isotopes to identify surface water–groundwater interaction in the Kruger National Park, South Africa. Water SA 49, 96–102. http://dx.doi.org/10.17159/wsa/2023.v49.i2.3992

Phungela, T.T., Maphanga, T., Chidi, B.S., Madonsela, B.S., Shale, K., 2022. The impact of wastewater treatment effluent on Crocodile River quality in Ehlanzeni District, Mpumalanga Province, South Africa. S Afr J Sci 118, 1–8.

Podgorski, J., Berg, M., 2020. Global threat of arsenic in groundwater. Science (1979) 368, 845–850.

Poujol, M., Robb, L.J., Respaut, J.-P., Anhaeusser, C.R., 1996. 3.07-2.97 Ga greenstone belt formation in the northeastern Kaapvaal Craton; implications for the origin of the Witwatersrand Basin. Economic Geology 91, 1455–1461.

Prat, O., Vercouter, T., Ansoborlo, E., Fichet, P., Perret, P., Salonen, L., Kurttio, P., 2009. Uranium speciation in drinking waters from drilled wells in Southern Finland and its links to health effects.

Putman, A.L., Fiorella, R.P., Bowen, G.J., Cai, Z., 2019. A global perspective on local meteoric water lines: Meta-analytic insight into fundamental controls and practical constraints. Water Resour Res 55, 6896–6910. https://doi.org/10.1029/2019WR025181

Robb, L.J., Brandl, G., Anhaeusser, C.R., Poujol, M., Johnson, M.R., Thomas, R.J., 2006. Archaean granitoid intrusions. The Geology of South Africa 57–94.

Rosario, A.S., Wichmann, H.E., 2006. Radon. Environmental Pollutants 120–125.

Rozanski, K., Araguás-Araguás, L., Gonfiantini, R., 1993. Isotopic patterns in modern global precipitation. Climate change in continental isotopic records 78, 1–36.

Saggerson, E.P., Logan, C.T., 1970. Distribution controls of layered and differentiated mafic intrusions in the Lebombo volcanic sub-province. Special Publication Geological Society of South Africa 1, 721–733.

Salem, Z.E.-S., Elnahrawy, A.M., Abdelrahman, K., Fnais, M.S., Abu-Alam, T., 2022. Oxygen and hydrogen stable isotopes as recharge indicators, Central Nile Delta Quaternary aquifer, Egypt. J King Saud Univ Sci 34, 101834. https://doi.org/https://doi.org/10.1016/j.jksus.2022.101834

Schutte, I.C., 1986. The general geology of the Kruger National Park. Koedoe 29, 13–37.

Self, J.R., Waskom, R.M., 2013. Nitrate in drinking water. Colorado: Colorado State University. US Department of Agriculture and Colorado counties cooperating.

Şen, Z., 2014. Practical and applied hydrogeology. Elsevier.

Shmeis, R.M.A., 2022. Nanotechnology in wastewater treatment, in: Comprehensive Analytical Chemistry. Elsevier, pp. 105–134.

Skeppström, K., Olofsson, B., 2007. Uranium and radon in groundwater. European Water 17, 51–62.

Smedley, P.L., Kinniburgh, D.G., 2002. A review of the source, behaviour and distribution of arsenic in natural waters. Applied geochemistry 17, 517–568.

South African Bureau of Standards, 2022. SANS 241 Drinking Water. SABS, Pretoria.

Tommasino, L., 2005. Radon. J Chem Educ 82, 32–44.

Tredoux, G., Engelbrecht, P., Israel, S., 2009. Nitrate in Groundwater: Why is it a hazard and how to control it? Stellenbosch.

United States Environmental Protection Agency, 2014. Basic Information about Radon in Drinking Water [WWW Document]. https://archive.epa.gov/water/archive/web/html/basicinformation-2.html.

U.S. Geological Survey, 2018. Saline Water and Salinity [WWW Document]. https://www.usgs.gov/special-topics/water-science-school/science/saline-water-and-salinity

U.S. Geological Survey Earth Explorer, 2022. Digital Elevation Model [basemap], Scale Not Given. https://ers.cr.usgs.gov/ s25_e031_1arc_v3.tif

Venter, F.J., Gertenbach, W.P.D., 1986. A cursory review of the climate and vegetation of the Kruger National Park. Koedoe 29, 139–148.

Viers, J.H., Liptzin, D., Rosenstock, T., Jensen, V.B., Hollander, A.D., 2012. Nitrogen Sources and Loading to Groundwater, California. California.

Vital, M., Grondona, S., Dimova, N., Martinez, D.E., 2022. Factors affecting the radon (222Rn) emanation from aquifer rock materials: Implications for radiological and groundwater tracer studies. Applied Radiation and Isotopes 189, 110433.

Volkert, R.A., Monteverde, D.H., Drake, A.A., 1989. Bedrock geologic map of the Stanhope quadrangle, Sussex and Morris Counties, New Jersey. US Geological Survey.

Walraven, F., 1983. The Timbavati gabbro of the eastern Transvaal Lowveld—a probable example of Hertzian fracturing. Annals of the geological survey (Pretoria) 17, 21–27.

Walraven, F., 1984. Geochemistry of the Timba Vati Gabbro of the Eastern Transvaal Lowveld, South Africa. South African Journal of Geology 87, 211–223.

Walraven, F., 1986. The Timbavati Gabbro of the Kruger National Park. Koedoe 29, 69–84.

Walraven, F., 1989. The geology of the Pilgrim's Rest area. (No Title). https://api.semanticscholar.org/CorpusID:127896541

Walraven, F., Hartzer, F.J., 1986. Sheet 2530 Barberton (1: 250 000 Geological Series). Geol. Surv. S. Afr.

Welch, A.H., Westjohn, D.B., Helsel, D.R., Wanty, R.B., 2000. Arsenic in groundwater of the United States: occurrence and geochemistry. Groundwater 38, 589–604.

West, A.G., February, E.C., Bowen, G.J., 2014. Spatial analysis of hydrogen and oxygen stable isotopes ("isoscapes") in groundwater and tap water across South Africa. J Geochem Explor 145, 213–222. https://doi.org/10.1016/j.gexplo.2014.06.009

Wetzel, R.G., 2001. Limnology: lake and river ecosystems. Gulf Professional Publishing.

Widdlson, P.E., Burt, T.P., 2008. Nitrogen Cycle. Global Ecology 2526–2533.

Wilson, M.A., Carpenter, S.R., 1999. Economic valuation of freshwater ecosystem services in the United States: 1971–1997. Ecological Applications 9, 772–783.

World Health Organization, 2004. Guidelines for drinking-water quality.

Worthington, S.R.H., Davies, G.J., Alexander Jr, E.C., 2016. Enhancement of bedrock permeability by weathering. Earth Sci Rev 160, 188–202.

Wright, E.P., 1992. The hydrogeology of crystalline basement aquifers in Africa. Geological Society, London, Special Publications 66, 1–27. https://doi.org/10.1144/GSL.SP.1992.066.01.01

Yang, N., Zhou, P., Wang, G., Zhang, B., Shi, Z., Liao, F., Li, B., Chen, X., Guo, L., Dang, X., Gu, X., 2021. Hydrochemical and isotopic interpretation of interactions between surface water and groundwater

in Delingha, Northwest China. J Hydrol (Amst) 598, 126243. https://doi.org/https://doi.org/10.1016/j.jhydrol.2021.126243

Yeh, H.-F., Lee, C.-H., Hsu, K.-C., 2011. Oxygen and hydrogen isotopes for the characteristics of groundwater recharge: a case study from the Chih-Pen Creek basin, Taiwan. Environ Earth Sci 62, 393–402. https://doi.org/10.1007/s12665-010-0534-2

Yeh, H.-F., Lee, J.-W., 2018. Stable hydrogen and oxygen isotopes for groundwater sources of Penghu Islands, Taiwan. Geosciences (Basel) 8, 84. https://doi.org/10.3390/geosciences8030084

Yeh, H.-F., Lin, H.-I., Lee, C.-H., Hsu, K.-C., Wu, C.-S., 2014. Identifying seasonal groundwater recharge using environmentally stable isotopes. Water (Basel) 6, 2849–2861.

Yun, U., Kim, T.S., Kim, H.K., Kim, M.S., Cho, S.Y., Choo, C.O., Cho, B.W., 2017. Natural radon reduction rate of the community groundwater system in South Korea. Applied Radiation and Isotopes 126, 23–25.

Yurtsever, Y., Gat, J.R., 1981. Stable isotope hydrology: deuterium and oxygen-18 in the water cycle. Vienna.

Zhou, J., Liu, G., Meng, Y., Xia, C., Chen, K., Chen, Y., 2021. Using stable isotopes as tracer to investigate hydrological condition and estimate water residence time in a plain region, Chengdu, China. Sci Rep 11, 2812.

Zhou, Z., Ansems, N., Torfs, P., 2015. A global assessment of nitrate contamination in groundwater. International Groundwater Resources Assessment Center. Internship report 4.

Zhu, S., Zhang, F., Zhang, Z., Kung, H., Yushanjiang, A., 2019. Hydrogen and Oxygen Isotope Composition and Water Quality Evaluation for Different Water Bodies in the Ebinur Lake Watershed, Northwestern China. Water (Basel) 11, 1–35. https://doi.org/10.3390/w11102067

9 APPENDIX A.

9.1 Hydrocensus form

Site Identifier:			
Owner:		Contact Details:	
Site Address:			
Weather/ Climate:			
Land Cover/ Use:			
Geology/ Soils			
Drainage/ Slope:			
Coordinates:		Instrument:	
Recorded By:		Date & Time:	
BH Use:		Last Pumping:	
Pump Type:		BH Depth:	
Pump Power:		Pump Depth	
Discharge:		Collar Height:	
Estimated Yield:		Water Level:	
Construction:		Protection:	
Water Strike:		Blow Yield:	
Sample No.			
Place Sampled:			
Sample Method:			
Sample Depth:			
Container:			
Volume:			
Visual:			
Olfactory:			
Notes			

9.2 Raw field data

TABLE 12: HYDROGEN AND OXYGEN ISOTOPE RATIOS FOR SURFACE AND GROUNDWATER SAMPLES AS WELL AS RAINWATER SAMPLES.

Sample Name	Sample Date	δD (‰)	$\delta^{18}O$(‰)
01KM	14/09/2021	-0,8	1,31
02SANSW	14/09/2021	-10,4	-1,99
03SAN	14/09/2021	-26,3	-4,74
04UPCell	14/09/2021	-22,1	-3,81
05MANT	15/09/2021	-27,7	-4,99
06A202	26/10/2021	-24,0	-4,64
07HLU	27/10/2021	-20,9	-3,92
08SANBH	27/10/2022	-10,3	-1,82
09SANSW	27/10/2021	8,3	2,75
10SAWC	27/10/2024	-20,4	-3,92
11NOU	28/10/2025	-25,7	-4,82
12SCC	28/10/2026	-25,9	-4,84
13SCC	21/02/2022	-25,8	-4,59
14A201	21/02/2022	-24,6	-4,56
15A202	21/02/2022	-23,6	-4,46
16NOR	21/02/2022	-25,0	-4,52
17SANSW	22/02/2022	-14,1	-2,17
18SAN	22/02/2022	-10,1	-1,65
19ANDSW	22/02/2022	14,5	3,43
20AND	22/02/2022	-22,7	-4,28
21Wits1	22/02/2022	-13,8	-2,94
22Wits2	22/02/2022	-18,1	-3,55
23WelfA	23/02/2022	-23,9	-4,28
24WelfSW	23/02/2022	-9,7	-1,41
25MANSW	23/02/2022	11,7	1,98
26MANM3	23/02/2022	-9,8	-1,70
27THOSW1	23/02/2022	-9,5	-2,18
28Xih	23/02/2022	-21,8	-4,11
29THORSW2	23/02/2022	12,1	2,99
30BAO1	23/02/2022	-24,8	-4,46
31WelB	24/02/2022	-22,8	-4,14
32HLU	24/02/2022	-20,6	-3,89
33KM	24/02/2022	-26,4	-4,52
34MANT	24/02/2022	-27,1	-4,68
36SAWC	25/02/2022	-19,3	-3,57
35UPCell	24/02/2022	-21,2	-3,44
37SCC	30/05/2022	-25,0	-4,53
38NOR	30/05/2022	-24,5	-4,53
39A201	30/05/2022	-24,0	-4,41
40SANSW	31/05/2022	-0,2	0,64
41SAN	31/05/2022	-9,3	-1,57

Sample Name	Sample Date	δD (‰)	δ18O(‰)
42ANDSW	31/05/2022	20,1	4,24
43AND	31/05/2022	-23,1	-4,21
44Wits1	31/05/2022	-13,4	-2,67
45Wits2	31/05/2022	-17,4	-3,42
46WelA	01/06/2022	-23,2	-4,27
47WelASW	01/06/2022	5,6	-0,02
48HLU	01/06/2022	-19,9	-3,99
49BABO	01/06/2022	-24,7	-4,49
50KM	02/06/2022	-25,1	-4,32
51MANT	02/06/2022	-27,1	-4,75
52MANSW	02/06/2022	20,6	3,60
53MANM1	02/06/2022	-10,6	-1,75
54MANM2	02/06/2022	-15,1	-2,63
55THORSW2	03/06/2022	22,7	4,82
56THORSW1	03/06/2022	-4,8	-1,75
57SAWC	03/06/2022	-17,9	-3,51
58UPCell	03/06/2022	-20,6	-3,42
59Xih	03/06/2022	-20,9	-4,05
60 SCC	29/08/2022	-26,3	-4,98
61 NOR	29/08/2022	-26,6	-5,01
62 A201	29/08/2022	-25,0	-4,90
63 A202	29/08/2022	-24,6	-4,90
64 SAN	30/08/2022	-10,8	-2,04
65 SANSW	30/08/2022	9,6	2,36
66 AND	30/08/2022	-24,0	-4,58
67 ANDSW	30/08/2022	28,3	5,65
68 WITS1	30/08/2022	-13,3	-3,06
69 WITS2	30/08/2022	-18,5	-3,88
70 WELA	31/08/2022	-25,1	-4,99
71 WELASW	31/08/2022	28,1	4,28
72 HLU	31/08/2022	-21,4	-4,46
73 THORSW	31/08/2022	-2,6	-1,58
74 XIH	31/08/2022	-21,4	-4,50
75 MANM1	01/09/2022	-4,1	-0,64
76 MANM2	01/09/2022	-10,5	-2,13
77 MANSW	01/09/2022	34,1	5,85
78 MANT	01/09/2022	-26,5	-4,73
79 KM	01/09/2022	-27,0	-4,73
80 UPCELL	02/09/2022	-21,4	-3,51
81BAO1	30/09/2022	-24,8	-4,46
82SCC	21/11/2022	-23,9	-4,50
83NOR	21/11/2022	-24,4	-4,59
84A201	21/11/2022	-24,4	-4,51
85A202	21/11/2022	-23,1	-4,27
86ANDSW	22/11/2022	37,3	7,51
87AND	22/11/2022	-22,4	-4,14

Sample Name	Sample Date	δD (‰)	δ18O(‰)
88SANSW	22/11/2022	24,4	5,16
89SAN	22/11/2022	-10,4	-1,85
90Wits1	22/11/2022	-12,7	-2,55
91Wits2	22/11/2022	-17,7	-3,33
92WelA	23/11/2022	-23,9	-4,15
93HLU	23/11/2022	-20,3	-3,81
94MANMSW	23/11/2022	41,9	7,25
95MANM2	23/11/2022	-8,8	-1,72
96KM	23/11/2022	-25,4	-4,53
97MANT	23/11/2022	-26,7	-4,81
98Xih	24/11/2022	-21,5	-4,24
99SAWC	25/11/2022	-18,3	-3,60
100UPCell	25/11/2022	-20,5	-3,43
HHWRS(Jan22)	01/2022	-14,3	-3,48
HHWRS (Feb22)	02/2022	10,1	0,12
HHWRS (Mar22)	03/2022	-24,9	-4,81
HHWRS (April 22)	04/2022	-4,7	-3,10
HHWRS May 2022	05/2022	2,1	-1,90
HHWRS (May 22)	05/2022	1,7	-2,15
HHWRS Sept 2022	09/2022	33,1	5,40
HHWRS Oct 2022	10/2022	13,5	0,79
HHWRS(Nov21)	11/2021	-7,5	-2,82
HHWRS(Dec21)	12/2021	-8,4	-2,28
MANY MTPA(Jan22)	01/2022	-16,9	-3,90
MANY Feb 2022	02/2022	5,7	-0,65
MANY Mar 2022	03/2022	-19,9	-3,97
MANY MTPA (April 22)	04/2022	-8,5	-3,73
MANY June 2022	06/2022	2,5	-1,70

TABLE 13: RAD7 RESULTS FOR SURFACE AND GROUNDWATER SAMPLES.

Sample Name	Begin Date	Begin Time	Mean Radon (Bq/m^3)	SD Radon (Bq/m^3)	High Radon (Bq/m^3)	Low Radon (Bq/m^3)
01KM	14/09/2021	15:03	42000	2890	45400	38300
02SANSW	14/09/2021	14:22	0	0	0	0
03SAN	14/09/2021	16:01	26300	1210	27200	24600
04UPCell	14/09/2021	18:43	30600	2590	33400	27500
05MANT	15/09/2021	12:32	29300	2300	31700	26400
06A2O2	26/10/2021	15:27	39800	7350	50700	34700
07HLU	27/10/2021	08:03	30400	3510	33400	26300
08SAN	27/10/2021	17:21	27700	2150	30200	25200
10SAWC	27/10/2021	18:04	12005	2060	15003	10008
11NOR	29/10/2021	16:36	28304	2571	30035	24596
12SCC	29/10/2021	18:27	18058	2107	19813	15048
13SCC	21/10/2022	15:39	2280	310	2690	1960
14A2O1	21/10/2022	16:38	28400	1300	29700	26600
15A2O2	21/02/2022	17:45	34100	1550	36300	32700
16NOR	21/02/2022	18:39	40200	2960	42500	36000
17SANSW	22/02/2022	17:53	333	252	589	0
18SAN	22/02/2022	19:17	25300	806	26100	24500
19ANDSW	22/02/2022	18:26	74	85,5	149	0
20AND	22/02/2022	20:10	4290	1420	5960	2740
21Wits1	22/02/2022	21:00	26300	2060	29200	24500
22Wits2	22/02/2022	21:56	5250	698	6120	4410
23WelA	22/02/2022	19:33	9880	1140	10500	8170
24WelASW	23/02/2022	16:06	148	210	446	0
25MANSW	23/02/2022	16:51	0	0	0	0
26MANM	23/02/2022	20:15	413	257	752	150
27THORSW1	23/02/2022	17:54	260	254	595	0
28Xih	23/02/2022	21:21	4460	424	4960	4060
29THORSW2	23/02/2022	18:43	36,8	73,6	147	0

Sample Name	Begin Date	Begin Time	Mean Radon (Bq/m^3)	SD Radon (Bq/m^3)	High Radon (Bq/m^3)	Low Radon (Bq/m^3)
30BAO1	23/02/2022	22:16	5430	724	6280	4540
31WelB	24/02/2022	09:34	857	72,7	898	748
32HLU	24/02/2022	17:04	4350	593	5110	3850
33KM	24/02/2022	18:11	11600	20400	14100	9280
34MANT	24/02/2022	19:04	12900	918	13800	11800
35UPCell	24/02/2022	20:09	19000	2240	22200	17200
36SAWC	25/02/2022	13:53	5450	831	5880	4200
37SCC	30/05/2022	15:27	1420	464	1800	748
38NOR	30/05/2022	16:19	12000	825	12900	10900
39A2O1	30/05/2022	17:52	19000	1230	19700	17100
40SANSW	31/05/2022	17:39	74,4	85,9	150	0
41SAN	31/05/2022	19:31	10600	1990	13400	8780
42ANDSW	31/05/2022	18:35	37,2	74,4	149	0
43AND	31/05/2022	20:35	11400	753	12300	10500
44Wits1	31/05/2022	21:29	12100	802	12800	11000
45Wits2	31/05/2022	22:35	3250	598	3780	2390
46WelA	01/06/2022	13:02	9550	407	10100	9230
47WelASW	01/06/2022	12:12	74	85,5	149	0
48HLU	01/06/2022	15:54	5330	941	6620	4510
49BAO1	01/06/2022	17:05	2960	838	3760	2220
50KM	02/06/2022	17:49	21100	1180	22000	19400
51MANT	02/06/2022	18:56	13400	2750	17200	10900
52MANSW	02/06/2022	16:40	0	0	0	0
53MANM	02/06/2022	20:03	188	144	301	0
54MANM2	02/06/2022	21:02	17600	805	18500	16500
55THORSW2	03/06/2022	16:15	148	209	444	0
56THORSW1	03/06/2022	17:16	522	377	1050	147
57SAWC	03/06/2022	19:16	6790	861	7600	6930
58UPCell	03/06/2022	18:07	25900	1820	27800	23400

Sample Name	Begin Date	Begin Time	Mean Radon (Bq/m^3)	SD Radon (Bq/m^3)	High Radon (Bq/m^3)	Low Radon (Bq/m^3)
59Xih	03/06/2022	20:28	8030	560	8680	7560
60SCC	29/08/2022	12:45	13200	746	14100	12300
61NOR	29/08/2022	13:21	27800	672	28800	27200
62A2O1	29/08/2022	14:11	25200	1990	27700	23200
63A2O2	29/08/2022	14:58	38700	2130	40600	36300
64SAN	30/08/2022	15:28	36300	2380	38600	33300
65SANSW	30/08/2022	14:01	150	122	299	0
66AND	30/08/2022	16:23	29000	2890	33200	26800
67ANDSW	30/08/2022	14:43	78,2	85,7	150	0
68Wits1	30/08/2022	18:12	27300	2840	30700	23700
69Wits2	30/08/2022	18:59	17200	1190	18200	15500
70WelA	31/08/2022	14:30	12600	899	13500	11500
71WelASW	31/08/2022	12:57	112	143	298	0
72HLU	31/08/2022	15:09	3150	1040	4060	1810
73THORSW	31/08/2022	13:50	74	85,5	149	0
74Xih	31/08/2022	15:59	9490	1090	10700	8470
75MANM1	01/09/2022	13:59	22700	1620	24800	21000
76MANM2	01/09/2022	14:42	22100	2380	24500	18800
77MANSW	01/09/2022	13:12	148	0,8	149	147
78MANT	01/09/2022	15:36	51400	4590	57000	46700
79KM	01/09/2022	16:26	37900	2460	40800	35700
80UPCell	02/09/2022	10:41	23700	2050	25500	21000
82SCC	21/11/2022	14:34	10400	1390	12300	8920
83NOR	21/11/2022	15:36	18600	911	19400	17400
84A2O1	21/11/2022	16:41	30800	1640	32400	28800
85A2O2	21/11/2022	17:31	24100	1970	25800	21300
86ANDSW	22/11/2022	14:38	149	122	299	0
87AND	22/11/2022	16:13	16000	1770	17700	13500
88SANSW	22/11/2022	15:29	74,4	85,9	149	0

Sample Name	Begin Date	Begin Time	Mean Radon (Bq/m^3)	SD Radon (Bq/m^3)	High Radon (Bq/m^3)	Low Radon (Bq/m^3)
89SAN	22/11/2022	17:01	20300	1350	21700	18500
90Wits2	22/11/2022	17:54	13700	1400	15200	12400
91Wits2	22/11/2022	18:51	10400	734	11400	9730
92WelA	23/11/2022	14:43	1270	30	1650	898
93HLU	23/11/2022	15:37	1230	192	1500	1040
94MANSW	23/11/2022	13:55	0	0	0	0
95MANM2	23/11/2022	16:32	5640	886	6730	4660
96KM	23/11/2022	17:19	8950	520	9430	8210
97MANT	23/11/2022	18:13	18300	1060	19700	17200
98Xih	24/11/2022	13:41	3110	338	3610	2860
99SAWC	25/11/20922	13:01	3570	875	4360	2380
100UPCell	25/11/20922	13:40	12600	1030	13500	11300

TABLE 14: AQUAPROBE READINGS FOR SURFACE WATER AND GROUNDWATER SAMPLES

Sample Name	Sample Date	Temp (ºC)	pH	DO (%)	DO (mg/l)	EC (µS/cm)	TDS (mg/l)	SAL (PSU)	ORP (mV)	NH_4 (mg/l)	NO_3 (mg/l)
01KM	14/09/2021		7,12	68,3	5,05	2251	1465	1,14	173,5		
02SANSW	14/09/2021	25	8,53	114,5	9,02	538	345	0,22	196,3		
03SAN	14/09/2021	23,5	7,26	42,7	3,4	1639	1067	0,81	195,2		
04UPCELL	14/09/2021		7,16	58,2	4,39	1631		0,8	171,8		
05MANT	15/09/2021	24,2	7,23	79,4	6,28	2508	1625	1,28	197,6		
06A2O2	26/10/2021	23,3	7,42	36,7	2,92	2296	1493	1,16	157,8	0,72	7,66
07HLU	27/10/2021	19,3	8,22	97,4	8,43	5500	3576	2,95	124,8	0,71	169,4
08SAN	27/10/2021	21,3	7,47	37	3,09	2656	1727	1,36	107,8	0,32	2,04
09SANSW	27/10/2021	20	8,69	92,2	7,99	957	622	0,4	115,7	0,2	1,59
10SAWC	27/10/2021	23,8	8,31	66,5	5,02	1541	1001	0,76	137,3	0,39	2,02
11NOR	28/10/2021	24,1	8,23	75,2	5,61	2329	1515	1,17	127,9	0,43	9,75
12SCC	28/10/2021	23,7	7,73	62,4	4,92	2141	1389	1,08	130,3	0,32	39,86
13SCC	21/02/2022	29,6	8,40	72,8	5,15	1140	741	0,54	200,1	0,49	45,75
14A2O1	21/02/2022	26,1	7,96	44,8	3,33	1151	750	0,54	101,5	0,32	19,59

Sample Name	Sample Date	Temp (°C)	pH	DO (%)	DO (mg/l)	EC (µS/cm)	TDS (mg/l)	SAL (PSU)	ORP (mV)	NH_4 (mg/l)	NO_3 (mg/l)
15A2O2	21/02/2022	26,3	7,59	50,3	3,68	1388	900	0,66	119	0,28	11,17
16NOR	21/02/2022	27,8	8,37	85,1	6,24	1194	776	0,57	182,6	0,4	16,12
17SANSW	22/02/2022	25,9	8,42	83,2	6,41	360	235	0,11	124,5	0,42	3,68
18SAN	22/02/2022	28	7,58	81,7	6	1580	1027	0,78	108,4	0,3	4,88
19ANDSW	22/02/2022	29,1	9,30	87,3	6,26	286	186	0,09	112,3	0,6	5,8
20AND	22/02/2022	26,6	8,04	94,1	7,03	1328	864	0,63	133,8	0,19	29,14
21WITS1	22/02/2022	26,3	8,32	72,2	5,36	1047	679	0,49	104,9	0,18	5,12
22WITS2	22/02/2022	26,2	8,33	68,1	5,12	999	650	0,47	137,2	0,1	5,01
23WELA	23/02/2022	25,8	7,67	53,2	4,06	2507	1628	1,28	128,2	0,55	432,5
24WELASW	23/02/2022	24,3	8,54	83,9	6,63	298	194	0,09	103,9	0,54	9,16
25MANSW	23/02/2022	27,1	9,16	98,4	7,44	222	145	0,07	95,3	0,28	6,3
26MANM	23/02/2022	29,8	7,49	37,5	2,71	1430	928	0,68	92,1	0,23	7,5
27THORSW1	23/02/2022	29,8	7,93	110,6	7,85	680	442	0,29	103,3	0,21	6,35
28XIH	23/02/2022	25	7,90	73,4	5,66	1617	1049	0,8	19,4	0,19	10,48
29THORSW2	23/02/2022	32,4		139,3	9,53	658	427	0,28	35,4	0,39	6,5
30BAO1	23/02/2022	26,1	8,40	36,2	2,7	1068	692	0,5	105,5	0,19	55,19
31WELB	24/02/2022	28,8	7,76	78	5,63	3269	2128	1,7	110,6	0,61	401,41
32HLU	24/02/2022	26,1	7,60	85,9	6,52	3193	2076	1,66	91,8	0,67	184,88
33KM	24/02/2022	26,5	7,68	64,77	3,7	2131	1385	1,08	125,1	0,75	15,01
34MANT	24/02/2022	27	7,74	81	6,07	2232	1450	1,13	97,8	0,57	10,45
35UPCELL	24/02/2022	27	7,74	54,9	4,11	1463	952	0,7	101,6	0,32	33,74
36SAWC	25/02/2022	24,6	8,31	66,8	5,24	891	579	0,37	139,5	0,11	4,01
37SCC	30/05/2022	20,1	7,54	84,4	7,2	1109	720	0,52	93,6	0,1	44,7
38NOR	30/05/2022	23,4	7,45	49,3	3,95	1199	778	0,57	93,3	0,11	9,46
39A2O1	30/05/2022	24	7,6	44,3	3,45	1195	778	0,57	63,8	0,1	13,99
40SANSW	31/05/2022	18,9	8,3	85,5	7,55	402	262	0,13	91	0,12	4,28
41SAN	31/05/2022	18,6	7,31	48,7	4,3	1516	985	0,75	67,09	0,07	3,64
42ANDSW	31/05/2022	19,6	8,33	87,7	7,57	313	203	0,1	46,6	0,19	4,87
43AND	31/05/2022	22,7	7,77	97	7,87	1329	863	0,63	81,9	0,09	19,45
44WITS1	31/05/2022	24,4	7,43	79	6,18	1055	685	0,5	35,7	0,1	4,28

Sample Name	Sample Date	Temp (°C)	pH	DO (%)	DO (mg/l)	EC (µS/cm)	TDS (mg/l)	SAL (PSU)	ORP (mV)	NH_4 (mg/l)	NO_3 (mg/l)
45WITS2	31/05/2022	20,7	7,52	86,3	7,25	1012	656	0,47	73,2	0,04	2,75
46WELA	01/06/2022	18,1	7,55	53,1	4,74	2575	1671	1,32	97,1	0,14	380,8
47WELASW	01/06/2022	16,9	8,11	91,7	8,45	383	247	0,12	85,6	0,13	10,36
48HLU	01/06/2022	14,7	7,62	86,3	8,31	3438	2234	1,78	75,3	0,14	281,8
49BAO1	01/06/2022	24,4	7,73	80,3	6,3	1068	693	0,51	77,1	0,17	40,09
50KM	02/06/2022	22,9	7,06	59,1	4,86	2047	1331	1,03	125,4	0,32	12,65
51MANT	02/06/2022	21,5	7,15	42,3	3,6	1761	1144	0,87	91	0,26	6,24
52MANSW	02/06/2022	21,9	8,72	105,1	8,9	213	139	0,07	99	0,25	4,58
53MANM	02/06/2022	18,6	7,76	91,9	8,23	1402	910	0,66	100,5	0,08	4,97
54MANM2	02/06/2022	24,7	7,28	63	5,03	1214	787	0,57	28,4	0,18	3,08
55THORSW2	03/06/2022	23,6	8,82	157,8	12,66	757	493	0,32	109,1	1,7	5,14
56THORSW1	03/06/2022	20,2	7,85	93,3	7,97	746	484	0,31	43,1	0,13	4,52
57SAWC	03/06/2022	22,2	7,44	41,1	3,43	835	542	0,35	110,5	0,06	5,29
58UPCELL	03/06/2022	25,8	7,02	56,8	4,42	1503	977	0,74	121,3	0,22	32,22
59XIH	03/06/2022	22,9	7,55	72,9	5,89	1612	1047	0,79	111,6	0,18	6,8
60SCC	29/08/2022	22,8	7,52	73,3	5,88	1252	813	0,59	70,9	0,04	72,57
61NOR	29/08/2022	24,2	7,61	81,9	6,37	1382	897	0,65	83,3	0,04	19,96
62A2O1	29/08/2022	25,4	7,35	98,5	7,47	1512	978	0,75	93,2	0,03	11,07
63A2O2	29/08/2022	25,2	7,45	35	2,65	1341	872	0,63	54,1	0,03	17,81
64SAN	30/08/2022	21,8	7,25	53,4	4,5	1718	1116	0,85	69,1	0,03	4,86
65SANSW	30/08/2022	18,2	7,72	72,2	6,49	502	326	0,21	92,2	0,03	2,17
66AND	30/08/2022	22,8	7,15	36,5	2,97	1440	936	0,68	58,3	0,03	21,46
67ANDSW	30/08/2022	17,7	8,23	96	8,7	266	172	0,08	74,7	0,06	5,78
68WITS1	30/08/2022	22,7	7,20	69	5,61	1136	737	0,54	89,4	0,01	3,12
69WITS2	30/08/2022	22	7,19	54,5	4,5	833	541	0,35	107	0,02	2,02
70WELA	31/08/2022	21,8	7,01	58,8	4,89	2797	1817	1,44	63,7	0,17	580,2
71WELASW	31/08/2022	14,6	7,51	98,3	9,56	652	423	0,27	66,9	1,09	7,31
72HLU	31/08/2022	17,5	7,24	73,1	6,63	4024	2614	2,12	89,7	0,19	471,9
73THORSW1	31/08/2022	17,1	8,28	99,2	9,06	935	608	0,39	77,8	0,02	8,09
74XIH	31/08/2022	20,9	7,63	68,4	5,77	1901	1235	0,94	-40,2	0,06	8,43

Sample Name	Sample Date	Temp (°C)	pH	DO (%)	DO (mg/l)	EC (µS/cm)	TDS (mg/l)	SAL (PSU)	ORP (mV)	NH_4 (mg/l)	NO_3 (mg/l)
75MANM1	01/09/2022	22,2	7,63	41,2	3,45	2101	1366	1,06	63,8	0,06	9,07
76MANM2	01/09/2022	24	7,31	99,4	8,06	1717	1116	0,85	68,1	0,06	4,9
77MANSW	01/09/2022	19,3	8,62	108,3	9,65	322	209	0,1	79,8	0,1	5,44
78MANT	01/09/2022	24,4	7,03	50,5	4,02	2667	1729	1,36	153,9	0,2	13,04
79KM	01/09/2022	24,9	7,22	81,6	6,44	2359	1534	1,19	194,7	0,16	17,18
80UPCELL	02/09/2022	23,9	7,14	61,3	4,9	1756	1142	0,87	140,7	0,09	51,47
82SCC	21/11/2022	25,2	7,26	67,9	5,22	1491	969	0,71	108,2	0,09	104,6
83NOR	21/11/2022	24,5	7,42	111,1	8,64	1697	1101	0,84	92,8	0,06	14,65
84A2O1	21/11/2022	25,2	7,24	48,1	3,65	1682	1093	0,83	33,3	0,06	13,99
85A2O2	21/11/2022	25,9	7,17	102,8	7,74	1841	1196	0,91	82,3	0,05	4,77
86ANDSW	22/11/2022	26,1	7,47	88,1	6,67	572	371	0,24	71,7	0,33	3,74
87AND	22/11/2022	25,5	7,18	53,6	4,06	1739	1131	0,86	55	0,09	13,37
88SANSW	22/11/2022	25,9	7,89	94,2	7,19	690	447	0,29	78,1	0,12	1,77
89SAN	22/11/2022	28,5	7,12	69,2	5,03	1978	1289	0,98	100,9	0,11	0,81
90WITS1	22/11/2022	25,9	6,97	83	6,27	1323	858	0,63	95,7	0,04	0,87
91WITS2	22/11/2022	25,6	7,15	87,7	6,68	1312	850	0,62	101,2	0,05	0,28
92WELA	23/11/2022	27,8	6,97	74,1	5,45	3412	2217	1,77	60,3	0,25	1354
93HLU	23/11/2022	25,4	7,33	94,8	7,28	4435	2882	2,34	52,8	0,27	830
94MANSW	23/11/2022	28,7	7,94	102,8	7,6	477	310	0,15	60,5	0,2	2,04
95MANM2	23/11/2022	25,7	7,41	70,7	5,47	2025	1321	1,03	61,5	0,06	1,02
96KM	23/11/2022	26,9	7,15	94,9	7,26	2791	1813	1,43	70,5	0,18	5,66
97MANT	23/11/2022	25,9	6,99	72,5	5,56	2875	1869	1,48	85,1	0,23	2,16
98XIH	24/11/2022	25,7	7,37	69,1	5,2	2208	1435	1,12	111,4	0,08	1,45
99SAWC	25/11/20922	24,9	7,31	60	4,7	1218	791	0,58	52,6	0,03	0,84
100UPCELL	25/11/20922	26,4	7,08	73,8	5,59	2012	1307	1,02	84,1	0,1	16,4

TABLE 15: RESULTS FOR WATER CHEMISTRY ANALYSIS DONE BY THE LAB.

Locality	Date	20 - pH	01 - Alk (mg $CaCO_3$/l)	02- Cl (mg/l)	03 - SO_4 (mg/l)	06 - NO_3 (mg/l)	07 - NO_2 (mg/l)	05 - NH_4 (mg/l)	04 - PO_4 (mg/l)
60SCC	29-Aug-2022	7,66	307	71,7	16,3	9,18	-0,065	0,015	0,079
61NOR	29-Aug-2022	8,06	345	151	8,51	2,36	-0,065	0,037	0,139
62A201	29-Aug-2022	8,49	343	207	4,75	1,42	-0,065	0,039	0,011
63A202	29-Aug-2022	7,54	353	166	4,39	3	-0,065	0,044	0,02
64SAN	30-Aug-2022	7,41	648	98,3	25,6	0,254	-0,065	0,056	-0,005
65SANSW	30-Aug-2022	7,59	137	42,4	4,71	0,238	-0,065	0,173	-0,005
66AND	30-Aug-2022	7,48	367	155	11,7	3,43	-0,065	-0,008	0,028
67ANDSW	30-Aug-2022	7,37	70,4	27,1	7,83	0,642	-0,065	0,281	0,052
68WITS1	30-Aug-2022	7,29	289	96,5	29,7	-0,194	0,111	0,013	-0,005
69WITS2	30-Aug-2022	7,53	384	78,3	24,7	0,394	-0,065	0,024	-0,005
70WELA	31-Aug-2022	7,73	383	461	42,8	63,8	0,078	0,113	0,019
71WELASW	31-Aug-2022	7,72	174	42,7	6,78	0,426	0,139	1,91	0,017
72HLU	31-Aug-2022	7,43	527	761	98,3	50,5	0,318	0,061	0,008
73THORSW1	31-Aug-2022	7,66	200	145	10,4	0,382	-0,065	0,094	-0,005
74Xih	31-Aug-2022	7,72	434	287	24	0,568	-0,065	0,042	-0,005
75MANM1	01-Sep-2022	7,86	611	226	13,7	0,282	-0,065	0,039	0,073
76MANM2	01-Sep-2022	7,62	612	136	19	0,385	-0,065	0,067	0,005
77MANSW	01-Sep-2022	7,75	57,9	21,2	8,57	0,648	-0,065	0,089	0,12
78MANT	01-Sep-2022	7,25	774	406	17	1,18	-0,065	0,078	0,005
79KM	01-Sep-2022	7,45	660	276	14,5	1,69	-0,065	0,034	0,011
80UPCell	02-Sep-2022	7,47	632	151	38	7,47	-0,065	0,085	0,047
81BA0	22-Sep-2022	7,37	299	81,4	20,3	6,03	0,071	0,035	0,035

TABLE 16: RESULTS FOR WATER CHEMISTRY ANALYSIS DONE BY THE LAB.

Locality	Date	08 - F (mg/l)	30 - Ca (mg/l)	30 - Mg (mg/l)	30 - Na (mg/l)	30 - K (mg/l)	31 - Fe (mg/l)	31 - Mn (mg/l)	37 - U (mg/l)
60SCC	29-Aug-2022	1,09	33,7	18,3	141	0,541	-0,004	-0,001	-0,015
61NOR	29-Aug-2022	1,45	44,2	23	164	1,38	-0,004	-0,001	-0,015
62A201	29-Aug-2022	0,954	46,3	22,9	177	0,309	-0,004	-0,001	-0,015

Locality	Date	08 - F (mg/l)	30 - Ca (mg/l)	30 - Mg (mg/l)	30 - Na (mg/l)	30 - K (mg/l)	31 - Fe (mg/l)	31 - Mn (mg/l)	37 - U (mg/l)
63A202	29-Aug-2022	1,2	43,6	16	173	0,911	-0,004	-0,001	-0,015
64SAN	30-Aug-2022	0,936	59,5	43,7	195	1,42	-0,004	-0,001	-0,015
65SANSW	30-Aug-2022	-0,263	16,5	9,22	48,1	4,46	0,075	-0,001	-0,015
66AND	30-Aug-2022	0,756	44,9	23,5	181	3,34	-0,004	-0,001	-0,015
67ANDSW	30-Aug-2022	0,285	6,45	4,07	24,6	16,9	0,15	-0,001	-0,015
68WITS1	30-Aug-2022	0,878	48,6	19,5	102	0,442	-0,004	-0,001	-0,015
69WITS2	30-Aug-2022	1,28	49,5	18,8	126	1,59	-0,004	-0,001	-0,015
70WELA	31-Aug-2022	0,364	125	93,8	224	9,3	-0,004	-0,001	-0,015
71WELASW	31-Aug-2022	0,373	24,6	10,9	27,2	31,3	1,23	-0,001	-0,015
72HLU	31-Aug-2022	0,412	192	136	314	11,7	-0,004	-0,001	-0,015
73THORSW1	31-Aug-2022	-0,263	28,3	18,3	112	0,264	-0,004	-0,001	-0,015
74Xih	31-Aug-2022	2,01	45,7	34,6	265	1,2	-0,004	-0,001	-0,015
75MANM1	01-Sep-2022	1,41	24,5	35,6	299	1,96	-0,004	-0,001	-0,015
76MANM2	01-Sep-2022	0,738	45,5	50,3	200	1,84	-0,004	0,026	-0,015
77MANSW	01-Sep-2022	-0,263	7,35	4,88	18,8	9,44	0,126	-0,001	-0,015
78MANT	01-Sep-2022	0,382	91,9	88,7	292	10,9	-0,004	-0,001	-0,015
79KM	01-Sep-2022	0,542	61	53,1	289	7,39	-0,004	-0,001	-0,015
80UPCell	02-Sep-2022	-0,263	50,9	138	70,5	5,28	-0,004	-0,001	-0,015
81BA0	22-Sep-2022	1,78	53,7	14,4	127	1,61	-0,004	0,003	-0,015

TABLE 17: RESULTS FOR WATER CHEMISTRY ANALYSIS DONE BY THE LAB.

Locality	Date	26 - BiCarb $CaCO_3$ – Cal (mg $CaCO_3$/l)	06 - TON (mg/l)	26 - BiCarb HCO_3 – Cal (HCO_3)	91 - Li (ICP-MS) (mg/l)	91 - Be (ICP-MS) (mg/l)	91 - B (ICP-MS) (mg/l)	91 - Al (ICP-MS) (mg/l)	91 - Si (ICP-MS) (mg/l)
60SCC	29-Aug-2022	305	9,23	372	0,07105	0	0,02165	0	9,56
61NOR	29-Aug-2022	341	2,4	416	0,07188	0	0,04176	0	10,3
62A201	29-Aug-2022	334	1,47	407	0,0907	0	0	0	12,8
63A202	29-Aug-2022	352	3,05	429	0,11277	0	0,00807	0	11,4
64SAN	30-Aug-2022	646	0,309	788	0,03815	0	0,15876	0	15,2

Locality	Date	26 - BiCarb $CaCO_3$ – Cal (mg $CaCO_3$/l)	06 - TON (mg/l)	26 - BiCarb HCO_3 – Cal (HCO_3)	91 - Li (ICP-MS) (mg/l)	91 - Be (ICP-MS) (mg/l)	91 - B (ICP-MS) (mg/l)	91 - Al (ICP-MS) (mg/l)	91 - Si (ICP-MS) (mg/l)
65SANSW	30-Aug-2022	137	0,282	167	0,00149	0	0	0,52186	4,62
66AND	30-Aug-2022	366	3,48	446	0,07442	0	0,06877	0	13,3
67ANDSW	30-Aug-2022	70,3	0,703	85,7	0,00133	0	0	0,48624	7,18
68WITS1	30-Aug-2022	288	0,269	352	0,07553	0	0	0	12,1
69WITS2	30-Aug-2022	383	0,443	467	0,07038	0	0	0	12,1
70WELA	31-Aug-2022	381	63,9	465	0,05228	0	0,09779	0	9,53
71WELASW	31-Aug-2022	173	0,565	211	0,00151	0	0	0,60306	2,04
72HLU	31-Aug-2022	525	50,8	641	0,08496	0	0,07515	0	14,6
73THORSW1	31-Aug-2022	199	0,441	243	0,00215	0	0	0	3,62
74Xih	31-Aug-2022	431	0,627	526	0,0641	0	0,13027	0,00757	6,99
75MANM1	01-Sep-2022	606	0,331	740	0,03299	0	0,64284	0,00397	10,3
76MANM2	01-Sep-2022	609	0,444	743	0,03792	0	0,36299	0	10,9
77MANSW	01-Sep-2022	57,6	0,694	70,3	0,00127	0	0	0,24639	4,02
78MANT	01-Sep-2022	773	1,23	943	0,09508	0	0,36402	0	10,4
79KM	01-Sep-2022	659	1,74	803	0,08878	0	0,30879	0	10,1
80UPCell	02-Sep-2022	631	7,52	769	0,02748	0	0,04701	0	15,1
81BA0	22-Sep-2022	299	6,1	364	0,02591	0,00001	0,10868	0,00313	13,9

TABLE 18: RESULTS FOR WATER CHEMISTRY ANALYSIS DONE BY THE LAB.

Locality	Date	91 - Sc (ICP-MS) (mg/l)	91 - Ti (ICP-MS) (mg/l)	91 - V (ICP-MS) (mg/l)	91 - Cr (ICP-MS) (mg/l)	91 - Mn (ICP-MS) (mg/l)	91 - Fe (ICP-MS) (mg/l)	91 - Co (ICP-MS) (mg/l)	91 - Ni (ICP-MS) (mg/l)
60SCC	29-Aug-2022	0,183	0,00037	0,00923	0,00031	-0,00007	1,01	0,00428	-0,00001
61NOR	29-Aug-2022	0,20408	-0,00001	0,01053	0,00422	-0,00007	1,37	0,00607	-0,00001
62A201	29-Aug-2022	0,27023	-0,00001	0,02102	0,00352	-0,00007	1,5	0,0065	-0,00001
63A202	29-Aug-2022	0,24569	-0,00001	0,01074	0,00173	-0,00007	1,49	0,00672	-0,00001
64SAN	30-Aug-2022	0,3351	-0,00001	0,01439	0,00448	0,00147	2,03	0,00949	-0,00001
65SANSW	30-Aug-2022	0,11731	0,00269	0,00427	0,00087	-0,00007	0,71425	0,00181	-0,00001
66AND	30-Aug-2022	0,32391	-0,00001	0,01557	0,00298	0,02496	1,55	0,00722	-0,00001

Locality	Date	91 - Sc (ICP-MS) (mg/l)	91 - Ti (ICP-MS) (mg/l)	91 - V (ICP-MS) (mg/l)	91 - Cr (ICP-MS) (mg/l)	91 - Mn (ICP-MS) (mg/l)	91 - Fe (ICP-MS) (mg/l)	91 - Co (ICP-MS) (mg/l)	91 - Ni (ICP-MS) (mg/l)
67ANDSW	30-Aug-2022	0,18651	-0,00001	0,00583	0	-0,00007	0,61383	0,00138	-0,00001
68WITS1	30-Aug-2022	0,30879	0,06527	0,00911	0	-0,00007	1,84	0,0087	-0,00001
69WITS2	30-Aug-2022	0,34121	0,04496	0,00767	0,00204	-0,00007	1,87	0,00898	-0,00001
70WELA	31-Aug-2022	0,27051	0,16238	0,03022	0,00223	-0,00007	4,9	0,02519	0,03568
71WELASW	31-Aug-2022	0,07339	0,04042	0,00634	0,00159	0,02164	1,73	0,00632	-0,00001
72HLU	31-Aug-2022	0,47564	0,34301	0,05132	0,00244	-0,00007	7,57	0,0426	0,10465
73THORSW1	31-Aug-2022	0,14666	0,0293	0,00831	0	0,01604	1,07	0,00547	-0,00001
74Xih	31-Aug-2022	0,27354	0,06626	0,01665	0,00023	0,0309	1,99	0,01057	-0,00001
75MANM1	01-Sep-2022	0,40263	-0,00001	0,03114	0,00111	-0,00007	1,05	0,00572	-0,00001
76MANM2	01-Sep-2022	0,48652	0,02237	0,02519	0,00159	0,16961	2,19	0,01279	-0,00001
77MANSW	01-Sep-2022	0,20484	0,00609	0,00776	0	-0,00007	0,68902	0,00252	-0,00001
78MANT	01-Sep-2022	0,4916	0,04609	0,0337	0,00104	-0,00007	4,38	0,02629	0,0269
79KM	01-Sep-2022	0,49805	0,00804	0,02512	0,00041	-0,00007	3,16	0,01927	0,00882
80UPCell	02-Sep-2022	0,91509	0,01916	0,02665	0,00267	-0,00007	2,74	0,01732	0,00335
81BA0	22-Sep-2022	0,00907	0,0011	0,00214	0,00631	0,00106	0,03943	0,00002	0,00106

TABLE 19: RESULTS FOR WATER CHEMISTRY ANALYSIS DONE BY THE LAB.

Locality	Date	91 - Cu (ICP-MS) (mg/l)	91 - Zn (ICP-MS) (mg/l)	91 - Ga (ICP-MS) (mg/l)	91 - Ge (ICP-MS) (mg/l)	91 - As (ICP-MS) (mg/l)	91 - Se (ICP-MS) (mg/l)	91 - Rb (ICP-MS) (mg/l)	91 - Sr (ICP-MS) (mg/l)
60SCC	29-Aug-2022	0	-0,00028	0	-0,00001	0,00253	-0,00001	0,00079	0,22611
61NOR	29-Aug-2022	0,0007	0,01383	0	-0,00001	0,00485	-0,00001	0,00148	0,29814
62A201	29-Aug-2022	0	0,00085	0	0,00001	0,00839	-0,00001	0,00033	0,29143
63A202	29-Aug-2022	0	-0,00028	0	-0,00001	0,00651	-0,00001	0,00068	0,36666
64SAN	30-Aug-2022	0,00139	-0,00028	0	0,00001	0,00567	-0,00001	0,0009	0,79344
65SANSW	30-Aug-2022	0	-0,00028	0	-0,00001	0,00141	-0,00001	0,00335	0,23805
66AND	30-Aug-2022	0	0,00534	0	-0,00001	0,00609	-0,00001	0,00057	0,45231
67ANDSW	30-Aug-2022	0	-0,00028	0	-0,00001	0,00079	-0,00001	0,00688	0,19927
68WITS1	30-Aug-2022	0	-0,00028	0	-0,00001	0,00599	-0,00001	0,0015	0,48677
69WITS2	30-Aug-2022	0	-0,00028	0	0,00002	0,00421	-0,00001	0,0011	0,48138
70WELA	31-Aug-2022	0,00108	0,00558	0	0,00017	0,05675	-0,00001	0,00246	1,86

Locality	Date	91 - Cu (ICP-MS) (mg/l)	91 - Zn (ICP-MS) (mg/l)	91 - Ga (ICP-MS) (mg/l)	91 - Ge (ICP-MS) (mg/l)	91 - As (ICP-MS) (mg/l)	91 - Se (ICP-MS) (mg/l)	91 - Rb (ICP-MS) (mg/l)	91 - Sr (ICP-MS) (mg/l)
71WELASW	31-Aug-2022	0	-0,00028	0	0,00005	0,00465	-0,00001	0,01078	0,35703
72HLU	31-Aug-2022	0,00897	0,04552	0	0,00033	0,15592	-0,00001	0,0032	2,99
73THORSW1	31-Aug-2022	0	-0,00028	0	-0,00001	0,00429	-0,00001	0,0005	0,24416
74Xih	31-Aug-2022	0	0,12941	0	0,00012	0,01459	-0,00001	0,00154	0,50727
75MANM1	01-Sep-2022	0	0,00032	0	-0,00001	0,00622	-0,00001	0,00055	0,29131
76MANM2	01-Sep-2022	0,00015	-0,00028	0	0,00004	0,00718	-0,00001	0,00066	0,42962
77MANSW	01-Sep-2022	0	-0,00028	0	-0,00001	0,00064	-0,00001	0,0024	0,11757
78MANT	01-Sep-2022	0,00227	-0,00028	0	0,0002	0,0425	-0,00001	0,00554	0,97071
79KM	01-Sep-2022	0,00364	-0,00028	0	0,00011	0,02274	-0,00001	0,00137	0,57114
80UPCell	02-Sep-2022	0	-0,00028	0	0,00014	0,0104	-0,00001	0,00449	0,39978
81BA0	22-Sep-2022	0,00057	0,00089	0	0,00001	0,00071	0,00032	0,00203	0,25145

TABLE 20: RESULTS FOR WATER CHEMISTRY ANALYSIS DONE BY THE LAB.

Locality	Date	91 - Y (ICP-MS) (mg/l)	91 - Zr (ICP-MS) (mg/l)	91 - Nb (ICP-MS) (mg/l)	91 - Mo (ICP-MS) (mg/l)	91 - Ru (ICP-MS) (mg/l)	91 - Rh (ICP-MS) (mg/l)	91 - Pd (ICP-MS) (mg/l)	91 - Ag (ICP-MS) (mg/l)
		mg/l	mg/l	mg/l	mg/l	mg/l	mg/l	mg/l	mg/l
60SCC	29-Aug-2022	0,00006	0,00007	-0,00001	0,00059	0,00017	0,00234	-0,00001	0
61NOR	29-Aug-2022	0,00008	0,00013	-0,00001	0,00067	0,00017	0,00306	-0,00001	0
62A201	29-Aug-2022	0,00016	-0,00001	-0,00001	0,00024	0,00011	0,00294	-0,00001	0
63A202	29-Aug-2022	0,00012	-0,00001	-0,00001	0,00059	0,00015	0,00381	-0,00001	0
64SAN	30-Aug-2022	0,00093	-0,00001	-0,00001	0,0005	0,00019	0,00708	-0,00001	0
65SANSW	30-Aug-2022	0,00023	0,00005	0,00002	-0,00001	0,00091	0,00254	-0,00001	0
66AND	30-Aug-2022	0,00012	-0,00001	-0,00001	0,00071	0,00017	0,00484	-0,00001	0
67ANDSW	30-Aug-2022	0,00022	0,00002	0,00001	-0,00001	0,00075	0,00209	-0,00001	0
68WITS1	30-Aug-2022	0,00015	-0,00001	-0,00001	0,00009	0,00013	0,00505	-0,00001	0
69WITS2	30-Aug-2022	0,00021	-0,00001	-0,00001	0,00025	0,00014	0,00505	-0,00001	0
70WELA	31-Aug-2022	0,00045	-0,00001	-0,00001	-0,00001	0,00028	0,01683	-0,00001	0
71WELASW	31-Aug-2022	0,00047	0,00008	0,00002	-0,00001	0,00138	0,00399	-0,00001	0
72HLU	31-Aug-2022	0,00069	-0,00001	0,00001	-0,00001	0,00047	0,02755	-0,00001	0
73THORSW1	31-Aug-2022	0,00009	-0,00001	-0,00001	-0,00001	0,00096	0,00283	-0,00001	0

Locality	Date	91 - Y (ICP-MS) (mg/l)	91 - Zr (ICP-MS) (mg/l)	91 - Nb (ICP-MS) (mg/l)	91 - Mo (ICP-MS) (mg/l)	91 - Ru (ICP-MS) (mg/l)	91 - Rh (ICP-MS) (mg/l)	91 - Pd (ICP-MS) (mg/l)	91 - Ag (ICP-MS) (mg/l)
74Xih	31-Aug-2022	0,0002	-0,00001	-0,00001	0,00045	0,00014	0,00578	-0,00001	0
75MANM1	01-Sep-2022	0,00016	-0,00001	0,00001	0,00322	0,00028	0,00333	-0,00001	0
76MANM2	01-Sep-2022	0,00022	-0,00001	-0,00001	0,00072	0,00014	0,0051	-0,00001	0
77MANSW	01-Sep-2022	0,0001	-0,00001	-0,00001	-0,00001	0,00002	0,00136	-0,00001	0
78MANT	01-Sep-2022	0,00044	-0,00001	-0,00001	-0,00001	0,00015	0,00987	-0,00001	0
79KM	01-Sep-2022	0,00023	-0,00001	-0,00001	0,00019	0,00013	0,00723	-0,00001	0
80UPCell	02-Sep-2022	0,00017	-0,00001	-0,00001	-0,00001	0,00007	0,00528	-0,00001	0
81BA0	22-Sep-2022	0,00006	0,00012	0,00018	0,01163	0,00016	0,00039	0,00004	0,00002

TABLE 21: RESULTS FOR WATER CHEMISTRY ANALYSIS DONE BY THE LAB.

Locality	Date	91 - Cd (ICP-MS) (mg/l)	91 - In (ICP-MS) (mg/l)	91 - Sn (ICP-MS) (mg/l)	91 - Sb (ICP-MS) (mg/l)	91 - Te (ICP-MS) (mg/l)	91 - Cs (ICP-MS) (mg/l)	91 - Ba (ICP-MS) (mg/l)	91 - La (ICP-MS) (mg/l)
60SCC	29-Aug-2022	0	-0,00001	-0,00001	-0,00001	-0,00001	0,00052	0,0056	-0,00001
61NOR	29-Aug-2022	0	-0,00001	-0,00001	0,00001	-0,00001	0,00345	0,04254	-0,00001
62A201	29-Aug-2022	0	-0,00001	-0,00001	0,00003	-0,00001	0,00019	0,00256	0,00006
63A202	29-Aug-2022	0	-0,00001	-0,00001	0,00005	-0,00001	0,00058	0,00781	-0,00001
64SAN	30-Aug-2022	0	-0,00001	-0,00001	0,00001	-0,00001	0,00434	0,06201	0,00002
65SANSW	30-Aug-2022	0	0,00004	0,00073	0,00059	-0,00001	0,00569	0,08223	0,00104
66AND	30-Aug-2022	0	-0,00001	-0,00001	0,00001	-0,00001	0,00182	0,02703	-0,00001
67ANDSW	30-Aug-2022	0	-0,00001	-0,00001	0,00172	-0,00001	0,00806	0,12366	0,00131
68WITS1	30-Aug-2022	0	-0,00001	-0,00001	0,00006	-0,00001	0,00499	0,07745	-0,00001
69WITS2	30-Aug-2022	0	-0,00001	-0,00001	0,0001	-0,00001	0,00451	0,07375	0,00001
70WELA	31-Aug-2022	0	-0,00001	-0,00001	0,00007	-0,00001	0,01006	0,1759	0,00007
71WELASW	31-Aug-2022	0	-0,00001	-0,00001	0,00057	-0,00001	0,01279	0,2199	0,0034
72HLU	31-Aug-2022	0	-0,00001	-0,00001	0,00005	-0,00001	0,0033	0,05886	-0,00001
73THORSW1	31-Aug-2022	0	-0,00001	-0,00001	0,00001	-0,00001	0,00403	0,07434	0,00001
74Xih	31-Aug-2022	0	-0,00001	-0,00001	-0,00001	-0,00001	0,00368	0,0658	-0,00001
75MANM1	01-Sep-2022	0	-0,00001	-0,00001	-0,00001	-0,00001	0,00136	0,02528	-0,00001
76MANM2	01-Sep-2022	0	-0,00001	-0,00001	-0,00001	-0,00001	0,00165	0,03329	0,00004
77MANSW	01-Sep-2022	0	-0,00001	-0,00001	0,00172	-0,00001	0,00289	0,05982	0,00033

Locality	Date	91 - Cd (ICP-MS) (mg/l)	91 - In (ICP-MS) (mg/l)	91 - Sn (ICP-MS) (mg/l)	91 - Sb (ICP-MS) (mg/l)	91 - Te (ICP-MS) (mg/l)	91 - Cs (ICP-MS) (mg/l)	91 - Ba (ICP-MS) (mg/l)	91 - La (ICP-MS) (mg/l)
78MANT	01-Sep-2022	0	-0,00001	-0,00001	0,00004	-0,00001	0,00362	0,07359	-0,00001
79KM	01-Sep-2022	0	-0,00001	-0,00001	-0,00001	-0,00001	0,00049	0,01051	-0,00001
80UPCell	02-Sep-2022	0	-0,00001	-0,00001	0,00002	-0,00001	0,00163	0,03386	-0,00001
81BA0	22-Sep-2022	0	-0,00001	0,00017	0,00056	-0,00001	0,00242	0,0136	0,00005

TABLE 22: RESULTS FOR WATER CHEMISTRY ANALYSIS DONE BY THE LAB.

Locality	Date	91 - Ce (ICP-MS) (mg/l)	91 - Pr (ICP-MS) (mg/l)	91 - Nd (ICP-MS) (mg/l)	91 - Sm (ICP-MS) (mg/l)	91 - Eu (ICP-MS) (mg/l)	91 - Gd (ICP-MS) (mg/l)	91 - Tb (ICP-MS) (mg/l)	91 - Dy (ICP-MS) (mg/l)
60SCC	29-Aug-2022	0	-0,00001	-0,00001	-0,00001	0,00052	-0,00001	-0,00001	0
61NOR	29-Aug-2022	0	-0,00001	0,00001	0,00259	0,00376	-0,00001	-0,00001	0
62A201	29-Aug-2022	0,00004	0,00004	0,00005	0,00003	0,00024	0,00011	0,00005	0,00009
63A202	29-Aug-2022	0	-0,00001	0,00001	0,00048	0,00067	0,00001	0,00001	0,00001
64SAN	30-Aug-2022	0,00005	0,00007	0,00017	0,00387	0,00535	0,00034	0,00017	0,00046
65SANSW	30-Aug-2022	0,00041	0,00032	0,00035	0,00026	0,00714	0,00062	0,00033	0,00036
66AND	30-Aug-2022	0	-0,00001	-0,00001	0,00154	0,00227	-0,00001	-0,00001	0
67ANDSW	30-Aug-2022	0,00049	0,00034	0,00039	0,0003	0,01057	0,00064	0,00034	0,00037
68WITS1	30-Aug-2022	0	-0,00001	-0,00001	0,00439	0,00634	-0,00001	-0,00001	0,00001
69WITS2	30-Aug-2022	0	-0,00001	-0,00001	0,00402	0,00589	0,00001	-0,00001	0,00002
70WELA	31-Aug-2022	0,00002	0,00002	0,00004	0,00981	0,01427	0,00006	0,00003	0,00004
71WELASW	31-Aug-2022	0,00137	0,00088	0,00105	0,01398	0,01938	0,00201	0,00105	0,00116
72HLU	31-Aug-2022	0	-0,00001	0,00002	0,00325	0,00488	-0,00001	-0,00001	0,00002
73THORSW1	31-Aug-2022	0,00001	-0,00001	0,00001	0,00462	0,00684	0,00003	0,00002	0,00001
74Xih	31-Aug-2022	0	-0,00001	-0,00001	0,00416	0,00618	-0,00001	-0,00001	0
75MANM1	01-Sep-2022	0	-0,00001	0,00003	0,00164	0,00241	0,00004	0,00002	0,00004
76MANM2	01-Sep-2022	0,00003	0,00003	0,00007	0,00216	0,00318	0,00015	0,00006	0,00011
77MANSW	01-Sep-2022	0,00015	0,0001	0,00015	0,00389	0,00575	0,00035	0,00019	0,00021
78MANT	01-Sep-2022	0,00001	0,00001	0,00004	0,00478	0,00729	0,00014	0,00005	0,00014
79KM	01-Sep-2022	0	-0,00001	0,00001	0,0007	0,0011	0,00001	0,00001	0,00004
80UPCell	02-Sep-2022	0	-0,00001	0,00001	0,00234	0,00361	0,00003	0,00002	0,00003
81BA0	22-Sep-2022	0,00002	0,00002	0,00001	0,00001	0,00005	0,00001	0,00001	0,00003

TABLE 23: RESULTS FOR WATER CHEMISTRY ANALYSIS DONE BY THE LAB.

Locality	Date	91 - Ho (ICP-MS) (mg/l)	91 - Er (ICP-MS) (mg/l)	91 - Tm (ICP-MS) (mg/l)	91 - Yb (ICP-MS) (mg/l)	91 - Lu (ICP-MS) (mg/l)	91 - Hf (ICP-MS) (mg/l)	91 - Ta (ICP-MS) (mg/l)	91 - W (ICP-MS) (mg/l)
60SCC	29-Aug-2022	-0,00001	0	-0,00001	-0,00001	-0,00001	-0,00001	-0,00001	-0,00001
61NOR	29-Aug-2022	-0,00001	0,00001	0,00001	-0,00001	-0,00001	-0,00001	-0,00001	-0,00001
62A201	29-Aug-2022	0,00003	0,00004	0,00002	0,00003	0,00002	0,00001	-0,00001	-0,00001
63A202	29-Aug-2022	0,00001	0,00002	0,00001	0,00001	-0,00001	-0,00001	-0,00001	-0,00001
64SAN	30-Aug-2022	0,00018	0,00031	0,00012	0,0003	0,00013	0,00009	-0,00001	-0,00001
65SANSW	30-Aug-2022	0,00014	0,00013	0,00008	0,00015	0,00008	0,00006	-0,00001	-0,00001
66AND	30-Aug-2022	-0,00001	0	0,00001	-0,00001	-0,00001	-0,00001	-0,00001	-0,00001
67ANDSW	30-Aug-2022	0,00014	0,00015	0,00009	0,00016	0,00008	0,00005	-0,00001	-0,00001
68WITS1	30-Aug-2022	-0,00001	0,00002	0,00002	0,00001	0,00001	-0,00001	-0,00001	-0,00001
69WITS2	30-Aug-2022	0,00001	0,00004	0,00003	0,00002	0,00001	-0,00001	-0,00001	-0,00001
70WELA	31-Aug-2022	0,00002	0,00003	0,00005	0,00004	0,00001	0,00001	-0,00001	-0,00001
71WELASW	31-Aug-2022	0,00041	0,00034	0,00022	0,00046	0,00021	0,00014	-0,00001	-0,00001
72HLU	31-Aug-2022	0,00001	0,00003	0,00002	0,00002	0,00001	-0,00001	-0,00001	-0,00001
73THORSW1	31-Aug-2022	0,00001	0,00001	0,00003	0,00001	0,00001	-0,00001	-0,00001	-0,00001
74Xih	31-Aug-2022	-0,00001	0,00002	0,00003	0,00002	0,00001	-0,00001	-0,00001	-0,00001
75MANM1	01-Sep-2022	0,00002	0,00004	0,00002	0,00004	0,00002	0,00001	-0,00001	-0,00001
76MANM2	01-Sep-2022	0,00004	0,00007	0,00003	0,00006	0,00003	0,00003	-0,00001	-0,00001
77MANSW	01-Sep-2022	0,00007	0,00007	0,00005	0,00009	0,00004	0,00003	-0,00001	-0,00001
78MANT	01-Sep-2022	0,00005	0,00011	0,00006	0,00015	0,00006	0,00005	-0,00001	-0,00001
79KM	01-Sep-2022	0,00002	0,00004	0,00002	0,00005	0,00002	0,00001	-0,00001	-0,00001
80UPCell	02-Sep-2022	0,00001	0,00002	0,00002	0,00003	0,00001	0,00001	-0,00001	-0,00001
81BA0	22-Sep-2022	0,00001	0,00003	0,00001	0,00002	0,00006	0,00008	-0,00001	-0,00001

TABLE 24: RESULTS FOR WATER CHEMISTRY ANALYSIS DONE BY THE LAB.

Locality	Date	91 - Re (ICP-MS) (mg/l)	91 - Os (ICP-MS) (mg/l)	91 - Ir (ICP-MS) (mg/l)	91 - Pt (ICP-MS) (mg/l)	91 - Au (ICP-MS) (mg/l)	91 - Hg (ICP-MS) (mg/l)	91 - Tl (ICP-MS) (mg/l)	91 - Pb (ICP-MS) (mg/l)
60SCC	29-Aug-2022	-0,00001	-0,00001	-0,00001	-0,00001	0	-0,00001	-0,00001	-0,00001
61NOR	29-Aug-2022	-0,00001	-0,00001	-0,00001	-0,00001	0	-0,00001	-0,00001	-0,00001
62A201	29-Aug-2022	-0,00001	-0,00001	-0,00001	-0,00001	0	-0,00001	-0,00001	-0,00001

Locality	Date	91 - Re (ICP-MS) (mg/l)	91 - Os (ICP-MS) (mg/l)	91 - Ir (ICP-MS) (mg/l)	91 - Pt (ICP-MS) (mg/l)	91 - Au (ICP-MS) (mg/l)	91 - Hg (ICP-MS) (mg/l)	91 - Tl (ICP-MS) (mg/l)	91 - Pb (ICP-MS) (mg/l)
63A202	29-Aug-2022	-0,00001	-0,00001	-0,00001	-0,00001	0	-0,00001	-0,00001	-0,00001
64SAN	30-Aug-2022	-0,00001	-0,00001	-0,00001	-0,00001	0	-0,00001	-0,00001	-0,00001
65SANSW	30-Aug-2022	-0,00001	-0,00001	-0,00001	-0,00001	0	-0,00001	-0,00001	-0,00001
66AND	30-Aug-2022	-0,00001	-0,00001	-0,00001	-0,00001	0	-0,00001	-0,00001	-0,00001
67ANDSW	30-Aug-2022	-0,00001	-0,00001	-0,00001	-0,00001	0	-0,00001	-0,00001	-0,00001
68WITS1	30-Aug-2022	-0,00001	-0,00001	-0,00001	-0,00001	0	-0,00001	-0,00001	-0,00001
69WITS2	30-Aug-2022	-0,00001	-0,00001	-0,00001	-0,00001	0	-0,00001	-0,00001	-0,00001
70WELA	31-Aug-2022	-0,00001	-0,00001	-0,00001	-0,00001	0	-0,00001	-0,00001	-0,00001
71WELASW	31-Aug-2022	-0,00001	-0,00001	-0,00001	-0,00001	0	-0,00001	-0,00001	-0,00001
72HLU	31-Aug-2022	-0,00001	-0,00001	-0,00001	-0,00001	0	-0,00001	-0,00001	-0,00001
73THORSW1	31-Aug-2022	-0,00001	0,00002	0,00002	-0,00001	0	-0,00001	-0,00001	-0,00001
74Xih	31-Aug-2022	-0,00001	-0,00001	-0,00001	-0,00001	0	-0,00001	-0,00001	-0,00001
75MANM1	01-Sep-2022	-0,00001	-0,00001	-0,00001	-0,00001	0	-0,00001	-0,00001	-0,00001
76MANM2	01-Sep-2022	-0,00001	-0,00001	-0,00001	-0,00001	0	-0,00001	-0,00001	-0,00001
77MANSW	01-Sep-2022	-0,00001	-0,00001	-0,00001	-0,00001	0	-0,00001	-0,00001	-0,00001
78MANT	01-Sep-2022	-0,00001	-0,00001	-0,00001	-0,00001	0	-0,00001	-0,00001	-0,00001
79KM	01-Sep-2022	-0,00001	-0,00001	-0,00001	-0,00001	0	-0,00001	-0,00001	-0,00001
80UPCell	02-Sep-2022	-0,00001	-0,00001	-0,00001	-0,00001	0	-0,00001	-0,00001	-0,00001
81BA0	22-Sep-2022	-0,00001	-0,00001	0,00001	-0,00001	0	-0,00001	0,00103	0,00258

TABLE 25: RESULTS FOR WATER CHEMISTRY ANALYSIS DONE BY THE LAB.

Locality	Date	91 - Bi (ICP-MS) (mg/l)	91 - Th (ICP-MS) (mg/l)	91 - U (ICP-MS) (mg/l)
60SCC	29-Aug-2022	0	-0,00001	-0,00001
61NOR	29-Aug-2022	0	-0,00001	-0,00001
62A201	29-Aug-2022	0	-0,00001	-0,00001
63A202	29-Aug-2022	0	-0,00001	-0,00001
64SAN	30-Aug-2022	0	-0,00001	-0,00001
65SANSW	30-Aug-2022	0	-0,00001	-0,00001
66AND	30-Aug-2022	0	-0,00001	-0,00001

Locality	Date	91 - Bi (ICP-MS) (mg/l)	91 - Th (ICP-MS) (mg/l)	91 - U (ICP-MS) (mg/l)
67ANDSW	30-Aug-2022	0	-0,00001	-0,00001
68WITS1	30-Aug-2022	0	-0,00001	-0,00001
69WITS2	30-Aug-2022	0	-0,00001	-0,00001
70WELA	31-Aug-2022	0	-0,00001	-0,00001
71WELASW	31-Aug-2022	0	-0,00001	-0,00001
72HLU	31-Aug-2022	0	-0,00001	-0,00001
73THORSW1	31-Aug-2022	0	-0,00001	-0,00001
74Xih	31-Aug-2022	0	-0,00001	-0,00001
75MANM1	01-Sep-2022	0	-0,00001	-0,00001
76MANM2	01-Sep-2022	0	-0,00001	-0,00001
77MANSW	01-Sep-2022	0	-0,00001	-0,00001
78MANT	01-Sep-2022	0	-0,00001	-0,00001
79KM	01-Sep-2022	0	-0,00001	-0,00001
80UPCell	02-Sep-2022	0	-0,00001	-0,00001
81BA0	22-Sep-2022	0,00001	0,0001	0,00057